INFORMATION TO USERS

This manuscript has been reproduced from the microfilm master. UMI films the text directly from the original or copy submitted. Thus, some thesis and dissertation copies are in typewriter face, while others may be from any type of computer printer.

The quality of this reproduction is dependent upon the quality of the copy submitted. Broken or indistinct print, colored or poor quality illustrations and photographs, print bleedthrough, substandard margins, and improper alignment can adversely affect reproduction.

In the unlikely event that the author did not send UMI a complete manuscript and there are missing pages, these will be noted. Also, if unauthorized copyright material had to be removed, a note will indicate the deletion.

Oversize materials (e.g., maps, drawings, charts) are reproduced by sectioning the original, beginning at the upper left-hand corner and continuing from left to right in equal sections with small overlaps.

Photographs included in the original manuscript have been reproduced xerographically in this copy. Higher quality 6" x 9" black and white photographic prints are available for any photographs or illustrations appearing in this copy for an additional charge. Contact UMI directly to order.

Bell & Howell Information and Learning
300 North Zeeb Road, Ann Arbor, MI 48106-1346 USA
800-521-0600

Nonlinear material properties shape locomotor performance in hydrozoan jellyfish

Erica B. Goldman

A dissertation submitted in partial fulfillment of the
requirements for the degree of

Doctor of Philosophy

University of Washington

2002

Program Authorized to Offer Degree: Zoology

UMI Number: 3053504

ProQuest Information and Learning Company
300 North Zeeb Road
P.O. Box 1346
Ann Arbor, MI 48106-1346

In presenting this dissertation in partial fulfillment of the requirements for the Doctoral Degree at the University of Washington, I agree that the Library shall make its copies freely available for inspection. I further agree that extensive copying of the dissertation is allowable only for scholarly purposes, consistent with "fair use" as prescribed in the U.S. Copyright Law. Requests for copying or reproduction of this dissertation may be referred to ProQuest Information and Learning, 300 North Zeeb Road, Ann Arbor, MI 48106-1346, to whom the author has granted "the right to reproduce and sell (a) copies of the manuscript in microform and/or (b) printed copies of the manuscript made from microform."

Signature: Erica Aldrich

Date: 6/13/02

University of Washington
Graduate School

This is to certify that I have examined this copy of a doctoral dissertation by

Erica B. Goldman

and have found that it is complete and satisfactory in all respects,
and that any and all revisions required by the final
examining committee have been made.

Chair of Supervisory Committee:

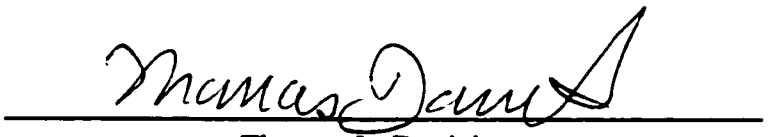

Thomas L. Daniel

Reading Committee:

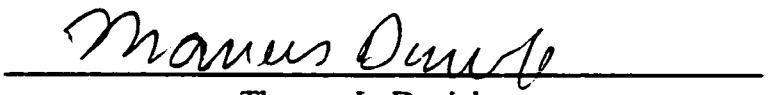

Thomas L. Daniel

Richard R. Strathmann

Daniel Grünbaum

Date: June 7, 2002

University of Washington

Abstract

Nonlinear material properties shape locomotor performance in hydrozoan jellyfish

Erica B. Goldman

Chair of the Supervisory Committee:
Professor Thomas L. Daniel
Zoology

Nonlinear mechanics and dynamics are pervasive at all levels of biological organization. Chapter 1 presents an overview of the diversity of nonlinear mechanics across various spatial scales and nonlinear dynamics over different temporal scales. This chapter sets the stage for an integrated perspective of the role of nonlinear material properties in hydrozoan locomotion.

Composite swimming behavior of hydrozoan jellyfish incorporates neuronal control, muscle forces, passive mechanics, and fluid stresses. In Chapter 2, I measure passive mechanical properties of mesoglea from *Polyorchis penicillatus* and *Mitrocoma cellularia* and find different nonlinear dependencies on strain but no interspecific difference in stiffness. Fits to stress/strain curves estimate an exponent of nonlinearity for each species which is incorporated into a simple dynamical system to model the passive mechanical properties of mesoglea. Nonlinearity yields oscillation amplitude augmentation and added frequency components that depend on its magnitude.

Coupling the frequency of muscle activation with the resonant frequency of a locomotor structure leads to large oscillation amplitudes for small periodic forces and may enable energetic savings. In Chapter 3, I explore resonant phenomena in medusa *Mitrocoma cellularia*. Experimental perturbation by manipulation of seawater viscosity tests whether emergent responses are more consistent with nonlinear or linear resonant behavior. A shift in bell position, without concurrent shifts in driving frequency, suggests that passive exploitation of strain-dependent bell stiffness may enable recovery

from perturbation. A recovery mechanism independent of neural feedback is consistent with predictions of nonlinear resonant phenomena.

In Chapter 4, a coupled fluid-solid model enables integration of aspects of locomotion to predict forward swimming velocity. Navigating a multi-dimensional parameter space, which includes bell size, shape, stiffness, and patterns of force production, maps nonlinear material properties against structural and temporal variables. Nonlinearity often enhances swimming velocity, but creates a landscape of tuning optima in which combinations of parameters contribute differentially to swimming performance. Smaller jellyfish exploit a larger set of "suitable" combinations of shape, stiffness, and muscle timing parameters than large jellyfish. Nonlinearity enhances peaks and troughs in performance and interacts with temporal patterns of force production to confer sensitivity over a fine scale, but robustness to perturbation over a longer scale.

TABLE OF CONTENTS

LIST OF FIGURES

LIST OF TABLES

ACKNOWLEDGEMENTS

It is hard to know how to begin to thank all of the people who have contributed their time and resources to this dissertation, either directly or indirectly. Everyone who has helped to shape my six wonderful years in Seattle has participated in some way to the path of my graduate experience and I thank all of you.

But, first and foremost, my research would not have been possible without the support, encouragement, and creativity of my advisor, Tom Daniel. From my first day in the Daniel lab, six years ago, Tom has helped me develop my quantitative skills and, more importantly, my confidence in my quantitative skills that were necessary to undertake and execute my dissertation research. Tom has also been incredibly supportive of all of my academic and non-academic endeavors over the years. Co-advisor Richard Strathmann and committee member Danny Grunbaum have also provided a great deal of helpful advice and support. Past and present members in the Daniel lab have also been amazing resources. Stacey Combes, Mike Tu, Mike MacPherson, Kevin Flick, Jordanna Henry, Michael Dillon, Liz Stockwell, Mark Frye, Alan Trimble, and Brian Helmuth have answered innumerable questions and made the Daniel lab a dynamic and fun place to work.

Friends Stacey Combes, Sharon Lynn, Jennifer and Paul Hohenlohe, Angela Stewart, Lesley Low, Amaya Ormazabal, Jonah Givelber, Doug Young, and Yvette Maestas have made Seattle an incredibly special place over the past six years. And finally my family, especially my father, my brother, and my husband, Joel Klein, has provided immeasurable support over the years, both emotional and practical. Without Joel's love, dedication, and willingness to digitize video and align margins, this dissertation might not have been possible. So many thanks...

DEDICATION

For my Mom, who has given me my roots and wings and whose memory will always live in my heart.

Chapter 1:

Linking nonlinear mechanics and nonlinear dynamics in biological systems

Summary:

Nonlinear mechanics and nonlinear dynamical behaviors are pervasive at all levels of biological organization. To set the stage for an analysis of the role of nonlinear mechanics in the dynamics of hydrozoan locomotion, this review presents an overview of the diversity of nonlinear mechanics across a wide range of spatial scales and nonlinear dynamics over a wide range of temporal scales. It includes a discussion of approaches to characterizing both nonlinear mechanics and nonlinear dynamics and incorporates examples that span from molecular to evolutionary scale processes. Special emphasis is given to fields that attempt to explicitly link nonlinear mechanics to their dynamical consequences, such as cardiovascular and respiratory dynamics, auditory mechanics, and intra-molecular dynamics of protein conformational changes. Ubiquity of nonlinear mechanical and dynamic processes raises questions about structural design and the evolutionary significance of nonlinearity and these broader issues are discussed.

Introduction:

From individual molecules of DNA to beating hearts to interactions between biotic and abiotic factors in complex communities, nonlinear mechanics and nonlinear dynamical behaviors permeate all levels of biological organization (Berger and Malpas, 1998; Bjornstad and Grenfell, 2001; Garcia et al., 1994; Ivanov et al., 1999; Ruesink,

1998). But nonlinearity is more than merely pervasive in biological systems; it is an essential component of dynamical signals. Nonlinearity is so central to biological patterns that the loss of nonlinear dynamical properties is often a sign of pathology. For example, nonlinear dynamics are a fundamental property of the healthy heartbeat. Cardiac rhythms decrease in nonlinear complexity with age, congestive heart failure, and just prior to atrial fibrillation, but increase in complexity with exercise (Ivanov et al., 1999; Pikkujamsa et al., 1999; Tulppo et al., 2001; Vikman et al., 1999). In the respiratory system, a similar decrease in the dynamic complexity of breathing correlates with cases of Sudden Infant Death Syndrome (SIDS) (Small et al., 1999). Although these changes in resultant signal complexity have clear physiological underpinnings, such as the loss of cells from the sinoatrial node in the heart as a function of age, it is the resultant rhythm that sets the healthy state (Pikkujamsa et al., 1999).

Given that nonlinear dynamics are not only abundant in biological systems, but essential to their functionality, exploring the diversity of nonlinear mechanics and their dynamical consequences, provides a context for understanding a wide range emergent behaviors--from enzyme kinetics to evolutionary processes. In this dissertation, I approach the mechanics and dynamics of locomotion in the hydrozoan jellyfish, one of the simplest morphologies in the animal kingdom, as an example of a nonlinear dynamical system. I attempt to establish empirical links between material and structural nonlinearities and their functional, dynamic, and hydrodynamic consequences. I sample a broad overview of nonlinear dynamics in biological systems across diverse levels of organization. From the bottom up, I survey some existing links between nonlinear

biological materials and static deformations of structures composed of these materials. From the top down, I review some examples of complex nonlinear biological signals and their existing connections to the source of their nonlinear behaviors. Finally, I examine the area of overlap between nonlinear mechanics and nonlinear dynamics, cases in which there are clear links between structural sources of nonlinearity and their dynamic consequences.

Nonlinear mechanics in biological systems: Diversity and functional significance

Nonlinear materials and structures span all levels of biological organization and often act as "springs," that store and return mechanical strain energy. Examples at the molecular, cellular, tissue, and organ levels demonstrate the key roles nonlinear mechanical properties often play in biological systems. Figure 1.1 illustrates several of these examples of materials with a nonlinear stress/strain relationship.

At the molecular level, DNA conformational interactions (Garcia et al., 1994; Klapper and Qian, 1998), protein configurations (Kharakoz, 2000; Lawrence et al., 1987), and competitive binding enzyme kinetics (Murray, 1977; Ngo and Roussel, 1997; Romashko et al., 1998) all exhibit nonlinear mechanical properties. The DNA double helix is nonlinearly elastic under normal tension, which introduces nonlinear kinematics to large-scale conformational movements (Klapper and Qian, 1998). In proteins, the energy associated with elastic deformation depends nonlinearly on compression and storage of mechanical strain energy serves as a reservoir of energy in catalytic pathways (Kharakoz, 2000).

At the cellular level, the passive mechanical properties of cell membranes, particularly of erythrocytes and neutrophils, are nonlinearly viscoelastic (Tozeren et al., 1982; Tsai et al., 1993). The surface glycocalyx of capillary endothelial cells, designed to accommodate the passage of large leukocytes, also exhibits nonlinear mechanical properties (Damiano and Stace, 2002). In muscle cells, actin can function as a "biological wire", exhibiting nonlinear inhomogeneous transmission properties (Lin and Cantiello, 1993). Stretch activation of insect fibrillar flight muscle may arise naturally as a nonlinear property of a cross-bridge interacting with a single attachment site on a thin filament. The cross-bridge stores elastic strain energy in compression and, by stretching the filaments, reduces the elastic energy required for attachment (Campbell et al., 2001; Thomas and Thornhill, 1996).

At the tissue level, many biological materials, across disparate taxa, respond nonlinearly to applied strains. Jellyfish mesoglea (Goldman, Chapter 2; DeMont and Gosline, 1988), sea cucumber dermis (Szulgit and Shadwick, 2000), mussel byssal threads (Sun et al., 2001), kelp (Johnson and Koehl, 1994), equine hoof wall (Kasapi and Gosline, 1996; Kasapi and Gosline, 1999), and dolphin vertebra (Long et al., 1997) represent only a tiny subset of the diversity of nonlinear properties of biological materials. In each case, nonlinear mechanical properties have structural significance for the organism. For example, byssal threads act like tendons, with distinct origin and insertion points, and experience large cyclic strains as waves pound the intertidal zone. Like tendons, byssal threads also exhibit strain-stiffening response at high strains, which helps to resist breakage (Figure 1.1C) (De Zee et al., 2000; Sun et al., 2001). Repeated

extension of byssal threads increases the magnitude of the nonlinear response over successive cycles, effectively increasing the thread stiffness for repetitions of the same strains (Sun et al., 2001). Giant kelp, typically found in high flow environments, also experiences repeated hydrodynamic stresses and also displays a nonlinear stress/strain relationship (Johnson and Koehl, 1994). The nonlinear mechanical properties of jellyfish mesoglea, which provides elastic energy storage and return for repeated swimming contractions, will be discussed in great detail throughout the remainder of this dissertation.

Nonlinear mechanical properties are similarly ubiquitous within individual organ systems, in invertebrate and vertebrate examples. Arteries (Figure 1.1A) (Armentano et al., 1995; Gosline and Shadwick, 1996; Imura et al., 1990; Shadwick, 1999; Zhou and Fung, 1997), cochlear membranes in the ear (Cooper and Rhode, 1995), tendon (Figure 1D) (Buchanan and Marsh, 2001; De Zee et al., 2000; Wang and Ker, 1995), and lung and diaphragm tissue (Figure 1.1B) (Boriek et al., 2000; Boriek and Rodarte, 1997; Maksym and Bates, 1997) represent a few examples of physiologically-significant materials with highly nonlinear mechanical properties.

In musculoskeletal systems, nonlinear materials act as elastic "springs", storing mechanical strain energy to power a subsequent motor response (Alexander, 1988). Tendon, ligament, and mesoglea act as muscle agonists and can reduce the energetic cost of locomotion up to 70% by passively deforming and returning elastic strain energy (Alexander and Goldspink, 1977). While nonlinearity is common feature of these musculosketal springs, it is often discussed only as a safety factor at large strains

(Wainwright et al., 1976) but is understated in predictions of the dynamic role of springs in locomotion. Estimates of a linear Young's modulus (E) from nonlinear stress/strain curves are often taken as a tangent to the curve at one point, rather than continuously throughout the physiological strain range (Alexander and Goldspink, 1977). Models of running and hopping often incorporate linear springs (a single value for a spring constant) to predict forward speeds (Farley et al., 1993). In Chapter 2, I compare the dynamics of linear and nonlinear springs and suggest that the nonlinearity of virtually all musculosketal springs may have important consequences for locomotion.

Nonlinear dynamics in biological systems

At all levels of organization, from protein to cell to organs to organ systems to populations to communities to evolutionary processes, complex signals emerge from constituent nonlinear elements. These nonlinear dynamics span a huge breadth of temporal and spatial scales. For example, the nonlinear dynamics of macromolecular conformational changes operate in the range of 10^{-12} to10^{-9} seconds, while evolutionary processes occur over geological time scales up to 10^{16} seconds. Biological molecules measure in the range of 10^{-9} meters while ecosystems can span ~10^{6} meters (Mosekilde and Mouritsen, 1995). Here, I describe some of the fundamental characteristics of nonlinear dynamical systems, survey their prominence and diversity in biological world, and discuss some of the approaches to their characterization.

General characteristics of nonlinear dynamical systems

Nonlinear systems are highly responsive to small changes, but are often dynamically robust over large time scales (Romashko et al., 1998; Chang, 2000). Periodically forced passive nonlinear structures can produce subharmonic frequencies, superharmonic frequencies, and multiple resonances (Cartwright et al., 2001). Coupled nonlinear oscillators experience mutual entrainment or frequency-locking (Chang et al., 2000). Nonlinear dynamical systems undergo cycle doublings and other types of bifurcations, such as a Hopf bifurcation in which a system's fixed point undergoes a transition to a stable periodic orbit. Figure 1.2 illustrates a mathematical example of a cycle doubling. Cycle doublings can generate chaotic behaviors which, while deterministic, are inherently unpredictable on the scale of the whole system (Bar-Yam, 1997). For example, experimentally measured cycle doubling in cardiac rhythms often precede the transition to the chaotic behavior of ventricular fibrillation (Figure 1.3, 1.4) (Weiss et al., 1999; Bar-Yam, 1997; Scheinerman, 1996). While chaotic behavior in cardiac systems can represent the healthy condition, with loss of chaos signaling a pathological one (Goldberger, 1991; Ivanov et al., 1999), the extreme chaotic behavior associated with ventricular fibrillation in the heart results in ineffective contractions (Hastings et al., 1996).

Spatio-temporal diversity of biological nonlinear dynamical systems

These features of nonlinear dynamical systems pervade all levels of biological spatio-temporal organization. Over the most rapid time scale, 10^{-12} to 10^{-9} seconds, the

dynamics of metabolic pathways are one of many examples of nonlinear dynamical systems. Cooperative binding and inhibition are common features of metabolic pathways and are inherently nonlinear (Gilchrist and Nijhout, 2001). The enzymatic pathways involved in energy metabolism can undergo large changes in activity in response to small perturbations of key effector molecules. While under certain conditions, this nonlinear response to small perturbation causes instability and chaotic behavior, it also confers sensitivity and the ability to respond rapidly to changes in cellular workload or environmental conditions (Romashko et al., 1998).

At the time scale at which organ systems operate, 10^{-2} to 10^{4} seconds, nonlinear dynamics pervade most physiological outputs. Nervous systems undergo large changes in their rhythmic properties with small changes in their inputs and these changes correlate with substantive changes in behavior (Guckenheimer et al., 1993). Encoding of a single action potential, exemplified by the cockroach tactile spine neuron, can be represented as a single-input single-output nonlinear dynamic process, in which the input includes a cascade of dynamic linear, static nonlinear, and dynamic linear components (French and Korenberg, 1989). Insect mechanoreceptors (campaniform sensillae) show similar linear and nonlinear properties of neural encoding, with a Wiener cascade model consisting of a linear filter and static nonlinearity arranged in series, accurately capturing measured spike frequencies (Dickinson, 1990). Cardiac and respiratory rhythms exhibit nonlinear dynamical components that are fundamental to their healthy state (Goldberger, 1991; Goldberger et al., 1985; Ivanov et al., 1999; Small et al., 1999). The auditory system depends on nonlinear dynamical properties such as harmonic distortion and

multiple frequency resonances in pitch perception (Cartwright et al., 2001). In visual systems, fly photoreceptors show dynamic nonlinear behavior that is evoked by a wide range of light intensities (French et al., 1993). Locust photoreceptors and pattern discrimination processes in the human visual system exhibit nonlinear mechanisms for gain adaptation (Pece et al., 1990; Wilson, 1993).

At the level of population, community, and evolutionary processes, a time scale of 10^2 to 10^{16} seconds, nonlinear dynamical systems are also highly visible. Bioconvective and locomotor dynamics in bacteria (Czirok et al., 2000; Schimz and Hildebrand, 1992), the dynamics of viral infection (Bohoeffer et al., 1997), the dynamics of social interactions within insect populations (Allen and Logan, 1992; Millor et al., 1999), predator-prey relationships and community interactions (Fussmann et al., 2000; Ruesink, 1998), and the dynamics of animal population fluctuations (Bjornstad and Grenfell, 2001; Higgins et al., 1997) are merely a few examples of nonlinear dynamical systems at this level of organization.

On an evolutionary time scale, the nonlinear relationship between genetic variation and phenotypic variation affects the emergence of dominance among alleles that control the developmental process. The nonlinear relationship between genotype and phenotype derives from the composite nonlinearities in developmental regulatory processes. Most developmental and physiological processes, like enzymatic pathways or regulatory genetic circuits, involve nonlinear processes such as negative and positive feedback, cooperativity, inhibition, or the diffusion of a signal. Since gene products mediate these regulatory processes, a nonlinear relationship between genetic and

phenotypic variation will emerge in the product of these processes. A single nonlinearity between genotype and phenotype in a simple developmental system for pattern formation can lead to emergent dominance in all parts of the mechanism (Gilchrist and Nijhout, 2001).

Approaches to characterizing nonlinear biological systems

Since the evidence for nonlinear dynamics in biological systems encompasses such a diverse spectrum of time-scales and levels of organization, and an in-depth treatment of all of these examples becomes unwieldy, an alternate organizational approach to this existing diversity is to discuss the different approaches used in their characterization. Techniques for characterizing biological systems fall into two main categories: 1) Analyzing the emergent dynamics of a system to uncover its nonlinear components (i.e. a macroscopic approach); 2) Incorporating measured nonlinear relationships in a model for a biological system to predict the appropriate behaviors (i.e. a microscopic approach).

The emergent dynamics of biological systems vary in complexity and require different analytical approaches. Experimental indications of bifurcations in biological processes are one of the simpler clues that a system exhibits nonlinearly dynamic properties. The Hopf bifurcation, in which a system's fixed point destabilizes and undergoes a transition to a stable periodic orbit, has been detected on levels of organization that range from a single cell to a system of predator/prey interactions (Bi and Yu, 1999; Scheinerman, 1996; Ospeck et al., 2001).

Hopf bifurcations are similarly apparent in predator/prey systems but are difficult to evaluate in the field. In a chemostat-controlled aquatic predator/prey system of planktonic rotifers feeding on unicellular green algae, population fluctuations experience a Hopf bifurcation at two distinct dilution rates (volume fraction of system that is replaced daily) (Fussmann et al., 2000). Populations fluctuate between an equilibrium state, a limit cycle, or extinction of the predator or both predator and prey. Dilution of the media can destabilize an equilibrium point and cause it to switch to a limit cycle (Figure 1.5). In the neighborhood of the bifurcation points, the dynamical behavior of the system changes rapidly with slight variation of environmental factors such as temperature or illumination (Fussmann et al., 2000).

Period doubling is another diagnostic feature of a nonlinear dynamical system and it is often the precursor to chaotic behavior. In addition to the example of ventricular fibrillation discussed previously, the locomotor patterns of halobacteria and defensive behaviors of honeybees are two examples of a period doubling at the level of population dynamics. Halobacteria spontaneously reverse their swimming direction every 10 to 15 seconds and respond to light stimuli by a transient perturbation of this rhythm. At first, as the stimulation frequency increases, the reversal rate follows the stimulation frequency. But soon, the reversal rate undergoes a transition to a state where short and long intervals occur alternatingly—a period doubling. This state is soon followed by the appearance of irregular interval sequences that suggest chaotic motion (Schimz and Hildebrand, 1992).

In the case of defensive behavior in honeybees, a period doubling occurs as the

result of a competitive positive feedback mechanism within the colony. When presented with two targets, the percentage of stings depends on the total number of stings. On the more highly attacked target, this results in more stings per target where there are a greater number of initial stings. This initial fluctuation is amplified as other bees are attracted to the target by the pheremones released from the original stinger seated in the target, increasing the probability of more stings on the target. This amplification generates a bifurcation and asymmetrical distribution of stings on the target. As in many nonlinear dynamical systems, the collective response of the colony is emergent and not the simple summation of multiple genetically coded individual defense responses (Millor et al., 1999).

In complex signals, like heartbeats and respiratory rhythms, it is still possible to detect features of nonlinear systems such as period doubling bifurcations, but alternate approaches are often required to fully characterize them. With the wealth of evidence that heart rate complexity is a central component of a healthy heart rhythm, techniques for measuring heart rate variability (HRV) indices draw heavily on methods from nonlinear dynamic theory. Approaches such as Detrended Fluctuation Analysis (DFA) measures the fractal components or dimensionality of the signal and Approximate Entropy (ApEn), a "complexity index", measures the overall regularity of time series data. In evaluation of cardiac function, HRV measures have become increasingly valuable in a clinical setting, along with traditional time-frequency domain approaches, to assess aspects of these complex signals that may change in the presence of pathology (Pikkujamsa et al., 1999).

In recent years, the recognition of the importance of nonlinearity and emergent complexity in the normal heartbeat has turned the physiological guiding principle of homeostasis on its head (Goldberger, 1991). So much, that clinical treatments can now exploit our understanding of the cardiac rhythm as nonlinearly dynamic to control arrhythmias. "Chaos control" is a nonlinear-dynamical control technique that has been used successfully in a clinical setting to rapidly stabilize an unstable cardiac rhythm. Chaos control takes advantage of the fact that the aperiodic dynamics of a chaotic rhythm are actually composed of an infinite number of unstable steady-state rhythms. Chaos control attempts to regularize the dynamics of a chaotic system by exploiting the dynamics of a target unstable rhythm to hold it within that rhythm. Although it is not possible to forecast a chaotic rhythm in the long-term, it is possible to make short-term dynamical predictions. Chaos control functions by exploiting this short-term predictability of chaotic rhythms. (Christini et al., 2001).

Bridging the gap: Tracking dynamic consequences of nonlinearity from mechanical sources

While both nonlinear mechanical structures and nonlinear dynamical systems are extremely common abundant in the biological world and have been well-described, there are few examples in which links between nonlinear mechanics and dynamics have been clearly established. The emergent complexity of most nonlinear dynamical systems makes a top-down approach to establishing distinct connections between nonlinear dynamics and mechanics quite difficult. In most complex nonlinear systems, collective

behaviors are not readily understood from the behavior of the parts in isolation (Bar-Yam, 1997). For example, while the decrease in heart rhythm complexity with age suggests the importance of nonlinear components of the healthy heart rhythm, it does not reveal their structural origins (Pikkujamsa et al., 1999). Pikkujamsa, et al. (1999) hypothesize that altered heart rhythm complexity stems from a loss of sinoatrial pacemaker cells and resultant changes in coupling relationships, but do not specify a distinct connection.

Generally, a bottom up approach, examining the specific dynamic consequences of a particular nonlinear structure has been a more tractable method to link nonlinear mechanics and dynamics. But both methods have their tradeoffs, as a bottom-up approach quickly becomes complicated by attempts to examine the dynamic consequences of multiple sources of nonlinearity within a complex system. Here, I discuss several examples from different fields in which a bottom-up approach links mechanical nonlinearities to their dynamic consequences.

At the molecular level, the nonlinear elastic properties of protein molecules play an important role in intra-molecular dynamics. The elastic properties of protein molecules are nonlinearly dependent on compression. This nonlinearity directly affects intra-molecular dynamic processes and this effect has been largely unexplored. As proteins deform to create cavities in the center, there is a concurrent deformation in the surrounding medium. The free energy associated with elastic deformation plays a crucial role in the kinetics of particle transfer in the interior and acts as a reservoir of energy for catalytic processes (Daniel et al., 1998). The mechanical nonlinearity in protein

molecules causes a sharp decrease in the compliance of the molecule under compression and this partially determines the behavior of proteins as a solid rather than a liquid. In addition, a protein molecule's nonlinear mechanical dependence on compression will affect any dynamic process that depends on ion diffusion. Diffusion of an ion from the solvent to the interior of a protein will depend on pressure nonmonotically. So, at low pressure diffusion is suppressed but at high pressure it is enhanced (Kharakoz, 2000).

At the tissue/structure level, arteries are one of the best-studied examples of a nonlinearly elastic biological tissue, with a clear picture of how mechanical nonlinearity affects dynamics of peripheral circulation. Like many biological tissues, artery nonlinearity derives from composite contributions of elastin and collagen fibers arranged in parallel. The initial low modulus portion of the stress/strain relationship is mainly due to elastin while the sharp increase in stiffness at high strains is due to progressive straightening of collagen. The transition region, where both elastin and collagen work to accommodate the circumferential load does occurs at physiologically relevant strains (Shadwick, 1999). But, what is the magnitude of arterial nonlinearity in a physiological range? The "degree of nonlinearity" parameter (DNL) describes the fraction of the nonlinear strain energy in the total strain energy and is one approach to such estimates. As an example, the DNL for the aorta varies from 5% to 30%, depending on the magnitude of strain experienced (Zhou and Fung, 1997). Estimates of the magnitude of nonlinearity are crucial for predicting the dynamic consequences of nonlinearity.

Shadwick (1999) argues that arteries, in both vertebrate and invertebrate circulatory systems, are actually constrained to exhibit nonlinear elastic behavior in order

to function in static and dynamic capacities. From a static perspective, he suggests that the nonlinear stress/strain behavior in arteries is the key to protecting vessels against aneurysms and 'blowout' and finds that nonlinearity is a key feature of blood vessels across diverse taxa, from crustaceans to mollusks to amphibians to fish to mammals. Specific nonlinearities vary between taxa--in terms of the shape of the stress/strain curve, the range of moduli, and histological composition. But amazingly, when stress/strain relationships from disparate taxa are normalized for mean blood pressure, they have similarly shaped stress/strain curves and all span a nearly identical range of elastic moduli (Figure 1.6A, B). Thus variance in histological composition suggests that arteries are tuned to exhibit an appropriate nonlinearity for species-specific physiological pressure ranges (Shadwick, 1999).

What are the dynamic consequences of this apparent constraint in nonlinear artery design? Passive expansion and elastic recoil of the arteries works to directly reduce the pulsatility of flow in the peripheral circulation and pulsatile flow is energetically expensive because fluid is accelerated and decelerated in each cycle. Additionally, elastic compliance prevents blood pressure from dropping when heart valves close and decreases the pressure pulse, pressure wave velocity and hydraulic impedance faced by the heart (Shadwick, 1999). The nonlinearity of blood vessel elasticity creates the dynamic phenomenon of soliton formation in arterial pulse waves, a critical feature of hemodynamic flow (Zhou and Fung, 1997). Solitons or solitary waves are localized concentrations of energy that result from linear (dispersive) and nonlinear effects (Bronski et al., 2001). Dispersion alone creates shock fronts of a propagating wave, but

the nonlinearity can compensate for the dispersion and establish a propagating and stable wave with constant velocity and shape (Vongehr, no date). The viscous properties of arteries, although a small percent of the overall vessel stiffness, dissipate strain energy to prevent these waves from resonating (Shadwick, 1999).

In the respiratory system, multiple studies have documented the nonlinear mechanical properties of both the diaphragm and lung tissue itself (Boriek et al., 2000; Boriek and Rodarte, 1997; Maksym and Bates, 1997). The passive mechanical properties (stiffness) of the diaphragm are biaxially nonlinear and anisotropic. In the direction of the muscle fibers the nonlinearity in the stress/strain relationship is weak, while in the transverse direction, the nonlinearity is strong. Both directions exhibit the J-shaped stress/strain curve common to many biological materials (Boriek et al., 2000). Elastic recoil in lung tissue at normal breathing frequencies similarly depends on the nonlinear stress/strain characteristics of the lung tissue. Like arteries, lung tissue nonlinearity derives from fibrous collagen and elastin arranged in parallel and shows the same strain-stiffening response (Maksym and Bates, 1997). Incorporating tissue nonlinearities in a complete model of airway dynamics is critical to effectively predicting observed dynamics, such as in an approach to modeling airway changes during an asthma attack. Physiological changes in airways during an asthma attack are often a consequence of inhomogeneous airway constriction, rather a response of the lung tissue. By separating the nonlinear mechanical properties of lung tissue from airway inhomogeneities in a modeling framework, the relative contribution of the nonlinear tissue properties can be evaluated in a dynamic context (Suki et al., 1997).

In the auditory system, vibration sensitivity is at the crux of the mechanics of sound perception. Since nonlinear vibrations have fundamentally different properties than linear vibrations, understanding the mechanical sources of these nonlinear vibrations becomes critical. The mechanical properties of the apical and basalar membranes of the cochlea are highly nonlinear and have been well studied. In the basal region of the cochlea, measured nonlinearities modify the sensitivity and the selectivity of the cochlear partition over a wide and physiologically relevant dynamic range. Nonlinearities in the apical portion of the cochlea are not as characterized as in the basalar region. Apical region nonlinearities exist within a physiologically relevant range, near the optimal frequency of stimulation. At these frequencies, systematic phase shifts occur in response to increasing stimulus frequency and the elicited waveforms are quite complex. These nonlinear effects give rise to two-tone interactions and harmonic distortion (Cooper and Rhode, 1995). The nonlinear mechanics of the cochlea are thus directly linked to nonlinear dynamical properties of the auditory system as a whole, such as the generation of multiple harmonic frequencies with a single frequency of stimulation (Cartwright et al., 2001).

Linking nonlinear mechanics and dynamics in hydrozoan medusae: Consequences for locomotor performance

The diversity of both nonlinear materials and nonlinear dynamical systems in the biological world inspire an attempt to combine experimental and theoretical approaches to forge a link between the two. Hydrozoan jellyfish, which represent one of the more

primitive body plans in the animal kingdom, provide an opportunity to probe the dynamic consequences of nonlinear mechanics in locomotor performance. Jellyfish are composed predominantly of mesoglea, a fibrous acellular matrix, which responds non-linearly to applied strains. Collagenous fibers in mesoglea deform during muscular contraction and mesoglea stores strain energy to power the refilling phase of the swimming contraction (Alexander, 1962; DeMont and Gosline, 1988; Gladfelter, 1972; Koehl, 1977).

In this dissertation, I combine experimental and theoretical methods in a bottom-up approach to linking the nonlinear mechanical properties of mesoglea to the dynamic consequences of nonlinearity in swimming performance. In Chapter 2, I measure the nonlinear mechanical properties of mesoglea from two hydrozoan species, *Polyorchis penicillatus* and *Mitrocoma cellularia*. I derive an estimate for the magnitude of nonlinearity for each species' mesoglea based on curve fits to an exponential model. Equipped with estimates for the mechanical nonlinearity of mesoglea, I use finite element modeling to assess the static consequences of nonlinearity in a single deformation of the bell. I then explore the dynamic consequences of a nonlinear spring in a simple dynamical system, a mass-spring system resisted by an element of damping.

In Chapter 3, I investigate a physical example of nonlinear resonant phenomena. I experimentally perturb a swimming jellyfish, *Mitrocoma cellularia*, by altering the viscosity of its surrounding medium. I evaluate the transient and long term dynamic responses to this perturbation in the context of the predictions from a nonlinear resonant system and show that jellyfish behave in a way that is consistent with these predictions.

Since the dynamic swimming behavior of a hydrozoan jellyfish derives from a complex interplay of neuronal control, muscle forces, passive mechanics, and fluid stresses, in Chapter 4, I incorporate measured nonlinear mechanical properties for mesoglea in a fluid-solid coupled model for locomotion. Using velocity as a measure of swimming performance, I directly test the effect of nonlinear mechanics of mesoglea on swimming behaviors. I explore the ways in which structural factors such as size, shape, and stiffness of the bell interact with its non-linear mechanical properties to affect tuning for swimming performance. Finally, I investigate how variation in the shape and timing of muscle forcing interacts with nonlinear mechanical properties to confer either robustness or sensitivity to variation and perturbation.

An appreciation of the suite of locomotor possibilities generated by a simple mechanical nonlinearity in the hydrozoan example, in the context of this discussion of the spectrum of nonlinear mechanics and dynamics in the biological world, raises intriguing questions about structural design and the evolutionary significance of nonlinearity. Is mechanical nonlinearity an unavoidable consequence of material construction or has it been selected for or selected against over evolutionary time? Is there an energetic saving in constructing materials with nonlinear stress/strain relationships or is nonlinearity merely a historical artifact of evolution? Do molecules, cells, animals, and physiological systems simply accommodate nonlinearity and its dynamic consequences or do they actively or passively exploit the rich dynamics of nonlinear systems? Finally, can emergent dynamical properties of nonlinear processes offload requirements for tight control from other systems? Although addressing the

evolutionary significance of nonlinearity is beyond the scope of this dissertation, these questions of design and constraint are provocative and lend an interesting context in which to investigate the dynamic significance of mesoglea's nonlinear mechanical properties to the swimming performance of hydrozoan medusae.

Notes to Chapter 1

Alexander, R. M. (1962). Visco-elastic properties of the body-wall of sea anenomes. *Journal of Experimental Biology* 39, 373-386.

Alexander, R. M. (1988). *Elastic Mechanisms in Animal Movement*. Cambridge: Cambridge University Press.

Alexander, R. M. e. and Goldspink, G. ed. (1977). *Mechanics and energetics of animal locomotion.* London: Chapman and Hall.

Allen, J. C. and Logan, J. A. (1992). Nonlinear dynamics and chaos in insect populations. *Annual Review of Entomology* 37, 455-477.

Armentano, R. L., Barra, J. G., Levenson, J., Simon, A. and Pichel, R. H. (1995). Arterial wall mechanics in conscious dogs. *Circulation Research* 76.

Bar-Yam, Y. (1997). *Dynamics of Complex Systems*. Reading: Addison-Wesley.

Berger, C. S. and Malpas, S. C. (1998). Modeling of the dynamic relationship between arterial pressure, renal sympathetic nerve activity and renal blood flow in conscious rabbits. *Journal of Experimental Biology* 201, 3425-3430.

Bi, Q. and Yu, P. (1999). Double Hopf bifurcations and chaos of a nonlinear vibration system. *Nonlinear Dynamics* 19, 313-332.

Bjornstad, O. N. and Grenfell, B. T. (2001). Noisy clockwork: Time series analysis of population fluctuations in animals. *Science* 293, 638-643.

Bohoeffer, S., May, R. M., Shaw, G. M. and Nowak, M. A. (1997). Virus dynamics and drug therapy. *Proceedings of the National Academy of Sciences* 94, 6791-6976.

Boriek, A. M., Kelly, N. G., Rodarte, J. R. and Wilson, T. A. (2000). Biaxial constitutive relations for the passive canine diaphragm. *Journal of Applied Physiology* 89, 2187-2190.

Boriek, A. M. and Rodarte, J. R. (1997). Effects of transverse fiber stiffness and central tendon on displacement and shape of a simple diaphragm model. *Journal of Applied Physiology* 82, 1626-1636.

Bronski, J. C., Segev, M. and Weinstein, M. I. (2001). Mathematical frontiers in optical solitons. *Proceedings of the National Academy of Sciences* 98, 12872-12873.

Buchanan, C. I. and Marsh, R. L. (2001). Effects of long-term exercise on the biomechanical properties of the Achilles tendon of guinea fowl. *Journal of Applied Physiology* 90, 164-171.

Campbell, K. B., Razumova, M. V., Kirkpatrick, R. D. and Slinker, B. K. (2001). Nonlinear myofilaments regulatory processes affect frequency-dependent muscle fiber stiffness. *Biophysical Journal* 81, 2278-2296.

Cartwright, J. H. E., Gonzalez, D. L. and Piro, O. (2001). Pitch perception: A dynamical-systems perspective. *Proceedings of the National Academy of Sciences* 98, 4855-4859.

Chang, H.-S., Staras, K. and Gilbey, M. P. (2000). Multiple oscillators provide metastability in rhythm generation. *Journal of Neuroscience* 20, 5135-5143.

Christini, D. J., Stein, K. M., Markowitz, S. M., Mittal, S., Slotwiner, D. J., Scheiner, M. A., Iwai, S. and Lerman, B. B. (2001). Nonlinear-dynamical arrhythmia control in humans. *Proceedings of the National Academy of Sciences* 98, 5827-5832.

Cooper, N. P. and Rhode, W. S. (1995). Nonlinear mechanics at the apex of the guinea-pig cochlea. *Hearing Research* 82, 225-243.

Czirok, A., Janosi, I. M. and Kessler, J. O. (2000). Bioconvective dynamics: Dependence on organism behaviour. *Journal of Experimental Biology* 203, 3345-3354.

Damiano, E. R. and Stace, T. M. (2002). A mechano-electrochemical model of radial deformation of the capillary glycocalyx. *Biophysical Journal* 82, 1153-1175.

Daniel, T. L., Trimble, A. C. and Chase, P. B. (1998). Compliant realignment of binding sites in muscle: Transient behavior and mechanical tuning. *Biophysical Journal* 74, 1611-1621.

De Zee, M., Bojsen-Moller, F. and Voigt, M. (2000). Dynamic viscoelastic behavior of lower extremity tendons during simulated running. *Journal of Applied Physiology* 89, 1352-1359.

DeMont, M. E. and Gosline, J. M. (1988). Mechanics of jet propulsion in the hydromedusan jellyfish *Polyorchis penicillatus*: I. Mechanical properties of the locomotor structure. *Journal of Experimental Biology* 134, 313-332.

Dickinson, M. H. (1990). Linear and nonlinear encoding properties of an identified mechanoreceptor on the fly wing measured with mechanical noise stimuli. *Journal of Experimental Biology* 151, 219-244

Farley, C. T., Glasheen, J. and McMahon, T. (1993). Running springs: Speed and animal size. *Journal of Experimental Biology* 185, 71-86.

French, A. S. and Korenberg, M. J. (1989). A nonlinear cascade model for action potential encoding in an insect sensory neuron. *Biophysical Journal* 55, 655-661.

French, A. S., Korenberg, M. J., Jarvilehto, M., Kouvalainen, E., Juusola, M. and Weckstrom, M. (1993). The dynamic nonlinear behavior of fly photoreceptors evoked by a wide range of light intensities. *Biophysical Journal* 65, 832-839.

Fussmann, G. F., Ellner, S. P., Shertzer, K. W. and Hairston, N. G. J. (2000). Crossing the Hopf bifurcation in a live predator-prey system. *Science* 290, 1358-1360.

Garcia, A. E., Soumpasis, D. M. and Jovin, T. M. (1994). Dynamics and relative stabilities of parallel and antiparallel stranded DNA duplexes. *Biophysical Journal* 66, 1742-1755.

Gilchrist, M. A. and Nijhout, H. F. (2001). Nonlinear developmental process as sources of dominance. *Genetics* 159, 423-432.

Gladfelter, W. B. (1972). Structure and function of the locomotory system of *Polyorchis montereyensis* (Cnidaria, Hydrozoa). *Helgolander wiss. Meeresunters* 23, 38-79.

Goldberger, A. L. (1991). Is the normal heartbeat chaotic or homeostatic? *News in Physiological Sciences* 6, 87-91.

Goldberger, A. L., Bhargava, V., West, B. J. and Mandell, A. J. (1985). On a mechanism of cardiac electrical stability. The fractal hypothesis. *Biophysical Journal* 48, 525-528.

Gosline, J. M. and Shadwick, R. E. (1996). The mechanical properties of fin whale arteries are explained by novel connective tissue designs. *Journal of Experimental Biology* 199, 985-997.

Guckenheimer, J., Gueron, S. and Harris-Warrick, R. M. (1993). Mapping the dynamics of a bursting neuron. *Philosophical Transactions: Biological Sciences* 341, 345-359.

Hastings, H. M., Evans, S. J., Quan, W., Chong, M. L. and Nwasokwa, O. (1996). Nonlinear dynamics in ventricular fibrillation. *Proceedings of the National Academy of Sciences* 93, 10495-10499.

Higgins, K., Hastings, A., Sarvela, J. N. and Botsford, L. W. (1997). Stochastic dynamics and deterministic skeletons: Population behavior of Dungeness Crab. *Science* 276, 1431-1435.

Imura, T., Yamamoto, K., Satoh, T., Kanamori, K., Mikami, T. and Yasuda, H. (1990). In vivo viscoelastic behavior in the human aorta. *Circulation Research* 66, 1413-1419.

Ivanov, P. C., Amaral, L. A. N., Goldberger, A. L., Havlin, S., Rosenblum, M. G., Struzik, Z. R. and Stanley, H. E. (1999). Multifractality in human heartbeat dynamics. *Nature* 399, 461-465.

Johnson, A. S. and Koehl, M. A. R. (1994). Maintenance of dynamic strain similarity and environmental stress factor in different flow habitats: Thallus allometry and material properties of a giant kelp. *Journal of Experimental Biology* 195, 381-410.

Kasapi, M. A. and Gosline, J. M. (1996). Strain-rate dependent mechanical properties of the Equine hoof wall. *Journal of Experimental Biology* 199, 1133-1146.

Kasapi, M. A. and Gosline, J. M. (1999). Micromechanics of the Equine hoof wall: Optimizing crack control and material stiffness through modulation of the properties of keratin. *Journal of Experimental Biology* 202, 377-391.

Kharakoz, D. P. (2000). Protein compressibility, dynamics, and pressure. *Biophysical Journal* 79, 511-525.

Klapper, I. and Qian, H. (1998). Remarks on discrete and continuous large-scale models of DNA dynamics. *Biophysical Journal* 74, 2504-2514.

Koehl, M. A. R. (1977). Mechanical diversity of connective tissue of the body wall of sea anenomes. *Journal of Experimental Biology* 69, 107-125.

Lawrence, A. F., McDaniel, J. C., Chang, D. B. and Birge, R. R. (1987). The nature of phonons and solitary waves in alpha-helical proteins. *Biophysical Journal* 51, 785-793.

Lin, E. C. and Cantiello, H. F. (1993). A novel method to study the electrodynamic behavior of actin filaments. Evidence for cable-like properties of actin. *Biophysical Journal* 65, 1371-1378.

Long, J. H. J., Pabst, D. A., Sheperd, W. R. and McLellan, W. A. (1997). Locomotor design of dolphin vertebral columns: Bending mechanics and morphology of *Delphinus delphis*. *Journal of Experimental Biology* 200, 65-81.

Maksym, G. N. and Bates, J. H. T. (1997). A distributed nonlinear model of lung tissue elasticity. *Journal of Applied Physiology* 82, 32-41.

Millor, J., Pham-Delegue, M., Deneubourg, J. L. and Camazine, S. (1999). Self-organized defensive behavior in honeybees. *Proceedings of the National Academy of Sciences* 96, 12611-12615.

Mosekilde, E. and Mouritsen, O. G. e. (1995). *Modelling the Dynamics of Biological Systems: Nonlinear Phenomena and Pattern Formation.* Berlin: Springer-Verlag.

Murray, J. D. (1977). *Nonlinear-differential equation models in biology.* Oxford: Clarendon Press.

Ngo, L. G. and Roussel, M. R. (1997). A new class of biochemical oscillator models based on competitive binding. *European Journal of Biochemistry* 245, 182-190.

Ospeck, M., Eguiluz, V. M. and Magnasco, M. O. (2001). Evidence of a Hopf bifurcation in frog hair cells. *Biophysical Journal* 80, 2597-2607.

Pece, A. E., French, A. S., Korenberg, M. J. and Kuster, J. E. (1990). Nonlinear mechanisms for gain adaptation in locust photoreceptors. *Biophysical Journal* 57, 733-743.

Pikkujamsa, S., Makikallio, T. H., Sourander, L. B., Raiha, I. J., Puuka, P., Skytta, J., Peng, C.-K., Goldberger, A. L. and Huikuri, H. V. (1999). Cardiac interbeat interval dynamics from childhood to senescence. *Circulation* 100, 393-399.

Romashko, D. N., Marban, E. and O'Rourke, B. (1998). Subcellular metabolic transients and mitochondrial redox waves in heart cells. *Proceedings of the National Academy of Sciences* 95, 1618-1623.

Ruesink, J. L. (1998). Variation in per capita interaction strength: Thresholds due to nonlinear dynamics and nonequilibrium conditions. *Proceedings of the National Academy of Sciences* 95, 6843-6847.

Scheinerman, E. R. (1996). *Invitation to Dynamical Systems.* Upper Saddle River: Prentice Hall.

Schimz, A. and Hildebrand, E. (1992). Nonrandom structures in the locomotor behavior of *Halobacterium*: A bifurcation route to chaos? *Proceedings of the National Academy of Sciences* 89, 457-460.

Shadwick, R. E. (1999). Mechanical design in arteries. *Journal of Experimental Biology* 202, 3305-3313.

Small, M., Judd, K., Lowe, M. and Stick, S. (1999). Is breathing in infants chaotic? Dimension estimates for respiratory patterns during quiet sleep. *Journal of Applied Physiology* 86, 359-376.

Suki, B., Yuan, H., Zhang, Q. and Lutchen, K. R. (1997). Partitioning of lung tissue response and inhoogeneous airway constriction at the airway opening. *Journal of Applied Physiology* 82, 1349-1359.

Sun, C., Vaccaro, E. and Waite, J. H. (2001). Oxidative stress and the mechanical properties of naturally occurring chimeric collagen-containing fibers. *Biophysical Journal* 81, 3590-3595.

Szulgit, G. K. and Shadwick, R. E. (2000). Dynamic mechanical characterization of a mutable collagenous tissue: Response of sea cucumber dermis to cell lysis and dermal extracts. *Journal of Experimental Biology* 203, 1539-1550.

Thomas, N. and Thornhill, R. A. (1996). Stretch activation and nonlinear elasticity of muscle cross-bridges. *Biophysical Journal* 70, 2807-2818.

Tozeren, A., Skalak, R., Sung, K. L. and Chien, S. (1982). Viscoelastic behavior of erythrocyte membrane. *Biophysical Journal* 39, 23-32.

Tsai, M. A., Frank, R. S. and Waugh, R. E. (1993). Passive mechanical behavior of human neutrophils: power-law fluid. *Biophysical Journal* 65, 2078-2088.

Tulppo, M. P., Hughson, R. L., Makikallio, T. H., Airaksinen, K. E. J., Seppanen, T. and Huikuri, H. V. (2001). Effects of exercise and passive head-up tilt on fractal and complexity properties of heart rate. *American Journal of Physiology: Heart Circulatory Physiology* 280, 1081-1087.

Vikman, S., Makikallio, T. H., Yi-Mayry, S., Pikkujamsa, S., Koivisto, A.-M., Reinikainen, P., Airaksinen, K. E. J. and Huikuri, H. V. (1999). Altered complexity and correlation properties of R-R interval dynamics before the spontaneous onset of paroxysmal atrial fibrillation. *Circulation* 100, 2079-2084.

Vongehr, S. Solitons: The Net Advance of Physics.
http://physics1.usc.edu/~vongehr/solitons_html/solitons.html

Wang, X. T. and Ker, R. F. (1995). Creep rupture of wallaby tail tendons. *Journal of Experimental Biology* 198, 831-845.

Weiss, J. N., Garfinkel, A., Karagueuzian, H. S., Qu, Z. and Chen, P.-S. (1999). Chaos and the transition to ventricular fibrillation. Circulation 99, 2819-2826.
Wilson, H. R. (1993). Nonlinear processes in visual pattern discrimination. *Proceedings of the National Academy of Sciences* 90, 9785-9790.

Zhou, J. and Fung, Y. C. (1997). The degree of nonlinearity and anisotropy of blood vessel elasticity. *Proceedings of the National Academy of Sciences* 94, 14255-14260.

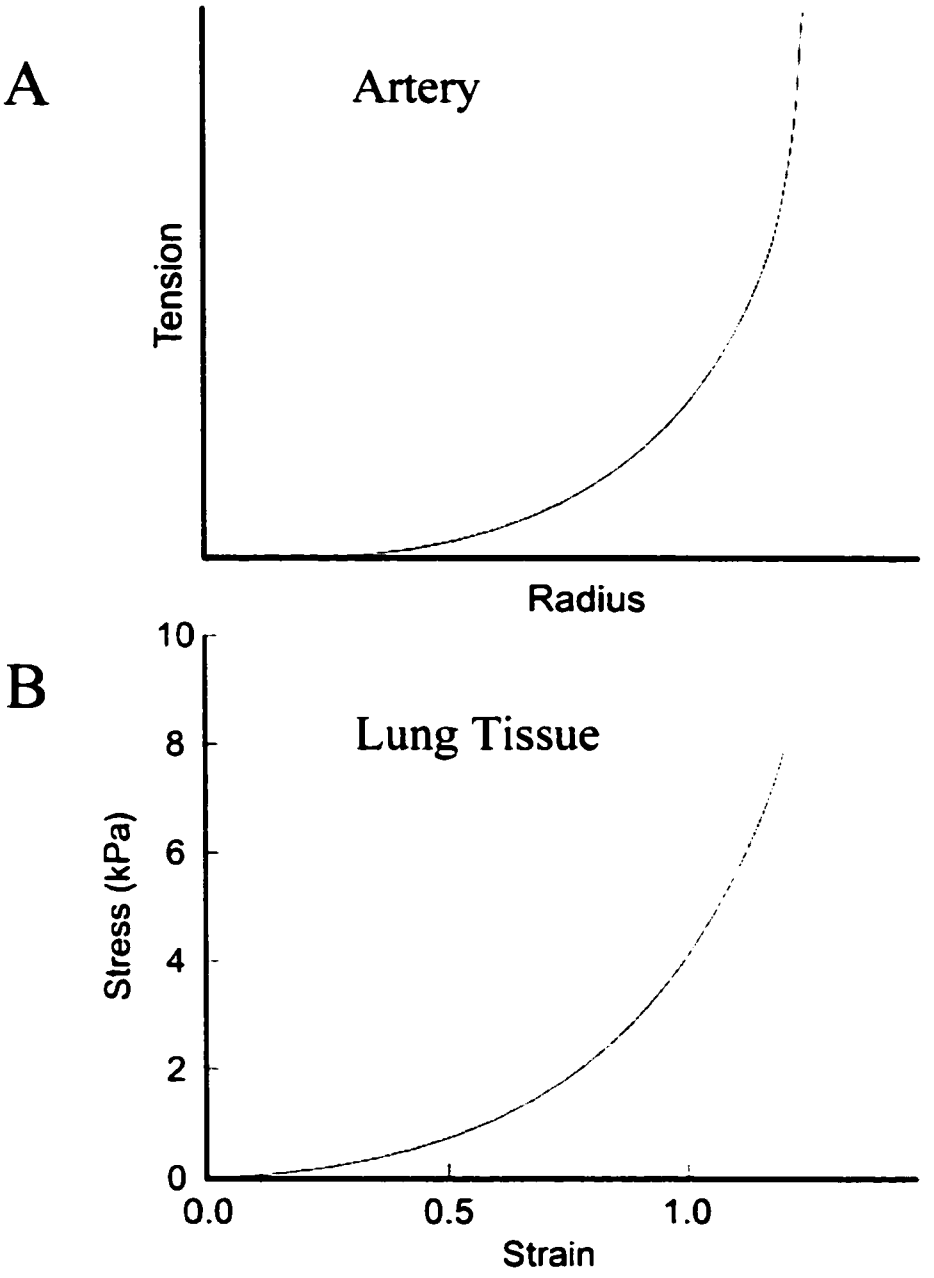

Figure 1.1A, B: Examples of nonlinear stress-strain curves from diverse biological tissues (Artery and Lung). A) Mechanical response of an artery to inflation showing the nonlinear wall tension (T) versus internal radius (R) relationship (Shadwick, 1999). B) Lung tissue stress/strain curve recorded at 0.5% of resting length extension per second (Maksym et al, 1997).

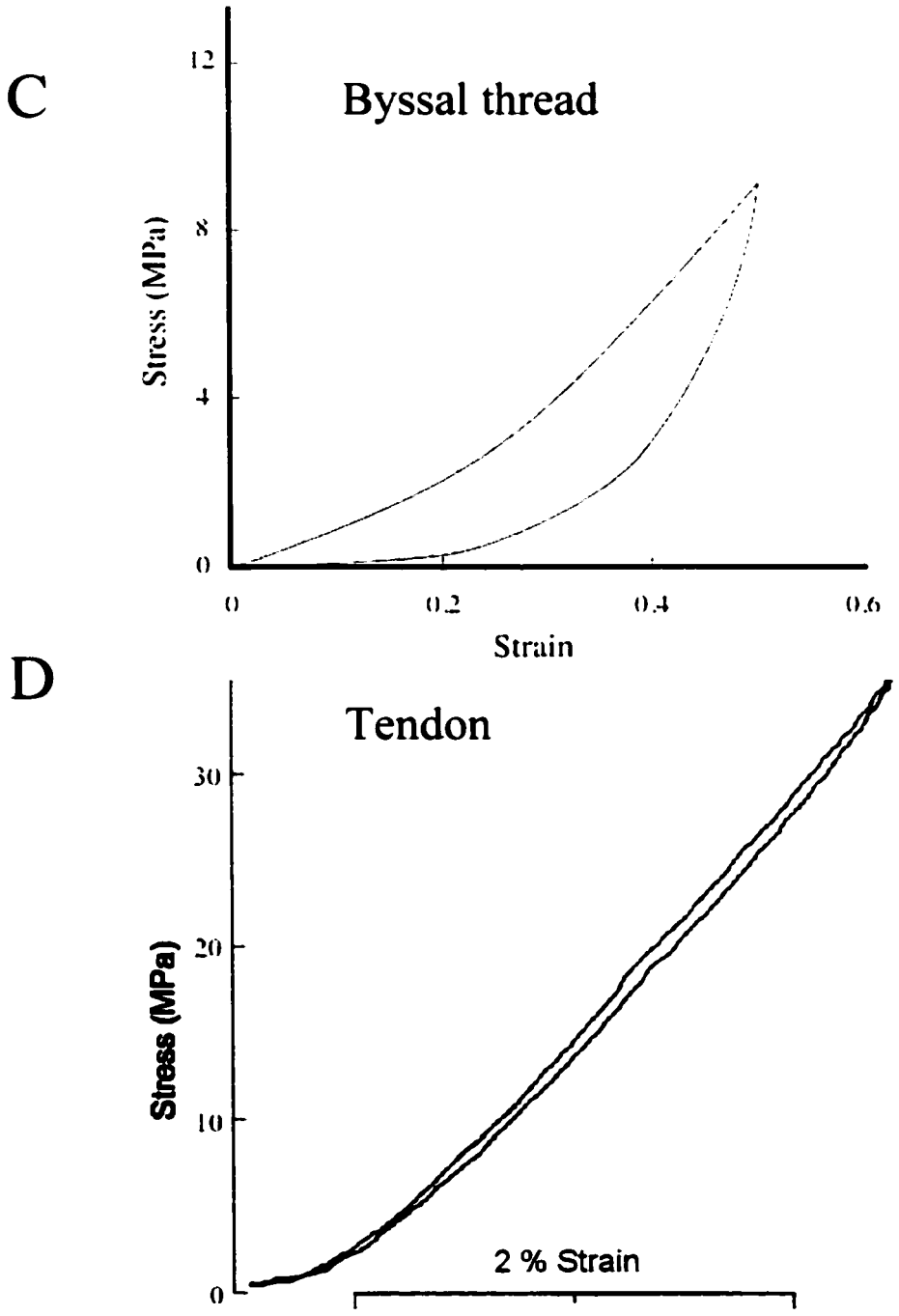

Figure 1.1C,D: Examples of nonlinear stress-strain curves from diverse biological tissues (Mussel and Tendon). C) A family of stress-strain curves for a virgin proximal mussel byssal thread (cycle 1, t = 0; cycles 2-4 each 3 min after the previous cycle) (Sun et al, 2001). D) Stress-strain plot for wallaby tail tendon recorded during sinusoidal oscillations at 1.6Hz under position control (Wang et al, 1995).

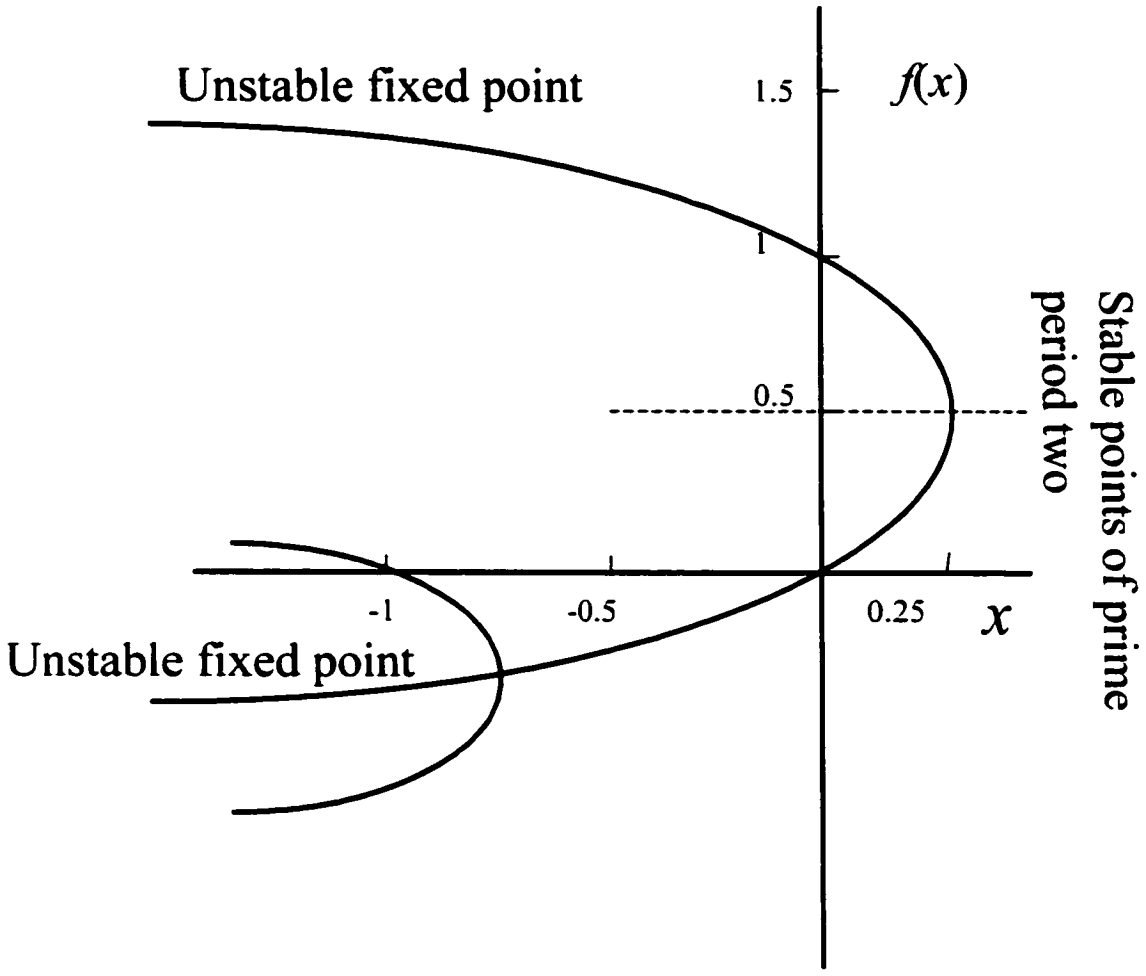

Figure 1.2: Example of a period doubling bifurcation. Bifurcation diagram for $f(x) = x^2 + a$ showing a period doubling at $a = -0.75$ (Bar-Yam, 1997).

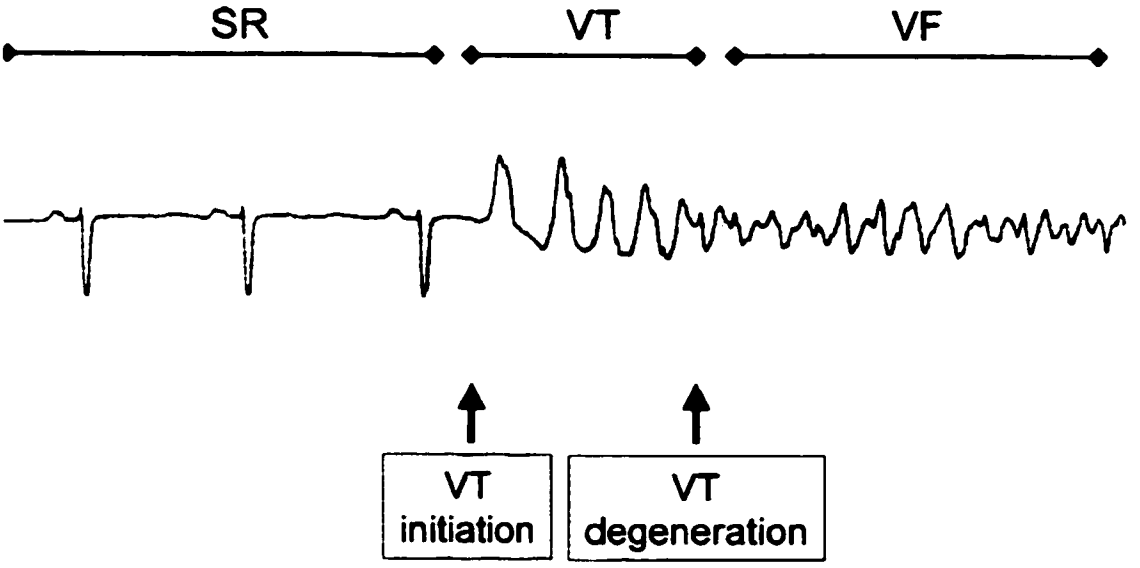

Figure 1.3: Evolution of ventricular fibrillation. Surface electrocardiogram illustrating the evolution of ventricular fibrillation (VF) from a normal sinus rhythm (SR) to ventricular tachycardia (VT) to VF. Period doubling typically occur during VT (Weiss et al, 1999).

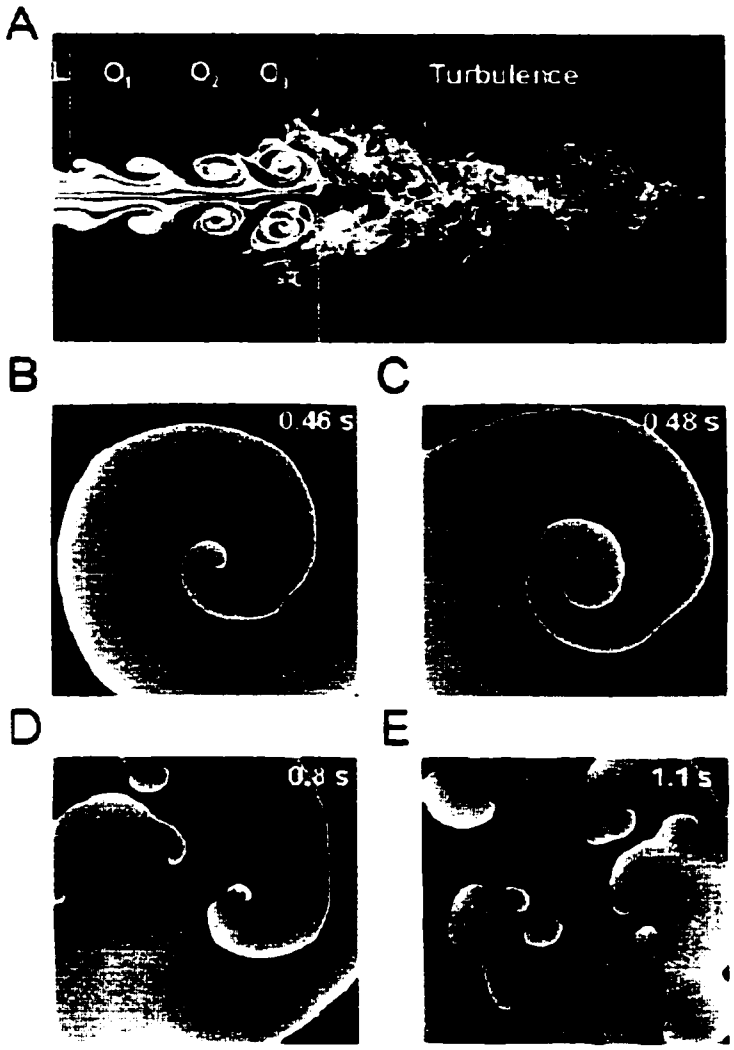

Figure 1.4: Development of turbulence in a smoke stream. A) Development of turbulence in smoke stream, illustrating a quasiperiodic(period doubling) transition to chaos. Sequence from left to right show laminar flow (L), stable vortex (first oscillation, O1), waviness in vortex walls (second oscillation, O2), even more complex oscillatory motion of vortex wall (third oscillation, O3), and abrupt transition to full turbulence (T). B through E illustrate quasiperiodic transition to chaos during spiral-wave breakup in 2D simulated cardiac tissue (300 X300 cells). Four snapshots are at times indicated after initiation of spiral wave. Oscillations increase in wavelength along spiral-wave arm (B and C), eventually leading to wave break and formation of daughter spiral waves (C and D), eventually leading to chaos (E) (Weiss et al, 1999).

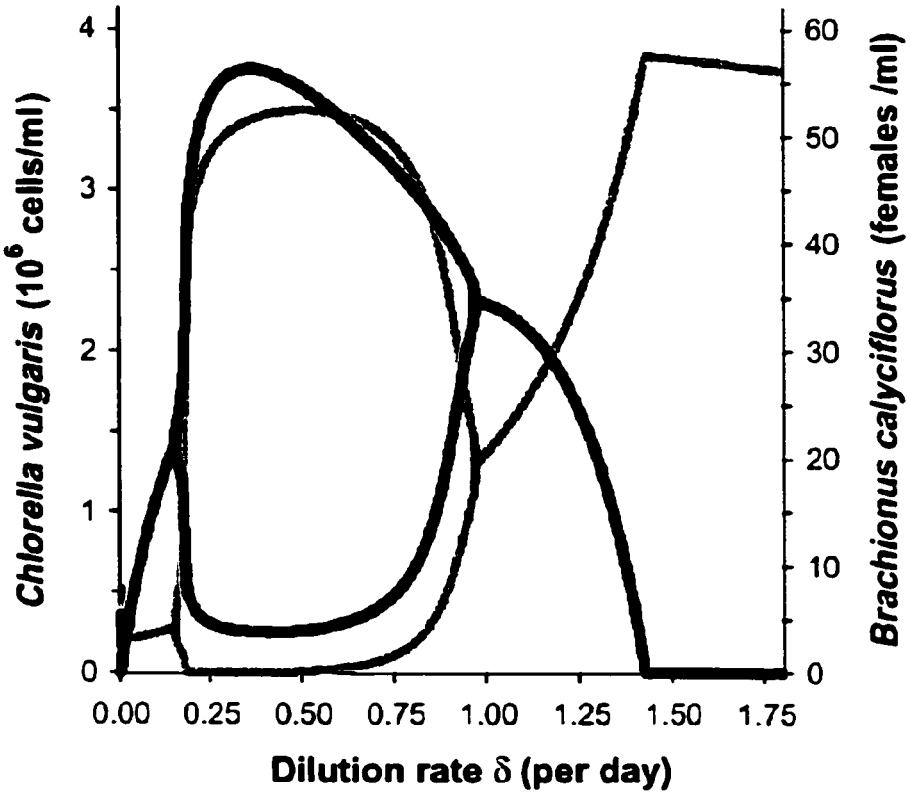

Figure 1.5: Hopf bifurcation in aquatic chemostat predator/prey system. Bifurcation diagram shows the maxima and minima of predator (*B. calyciflorus*, black line) and prey (*C. vulgaris*, gray line) concentration across a range of dilutions for a constant nutrient value (Fussman et al, 2000).

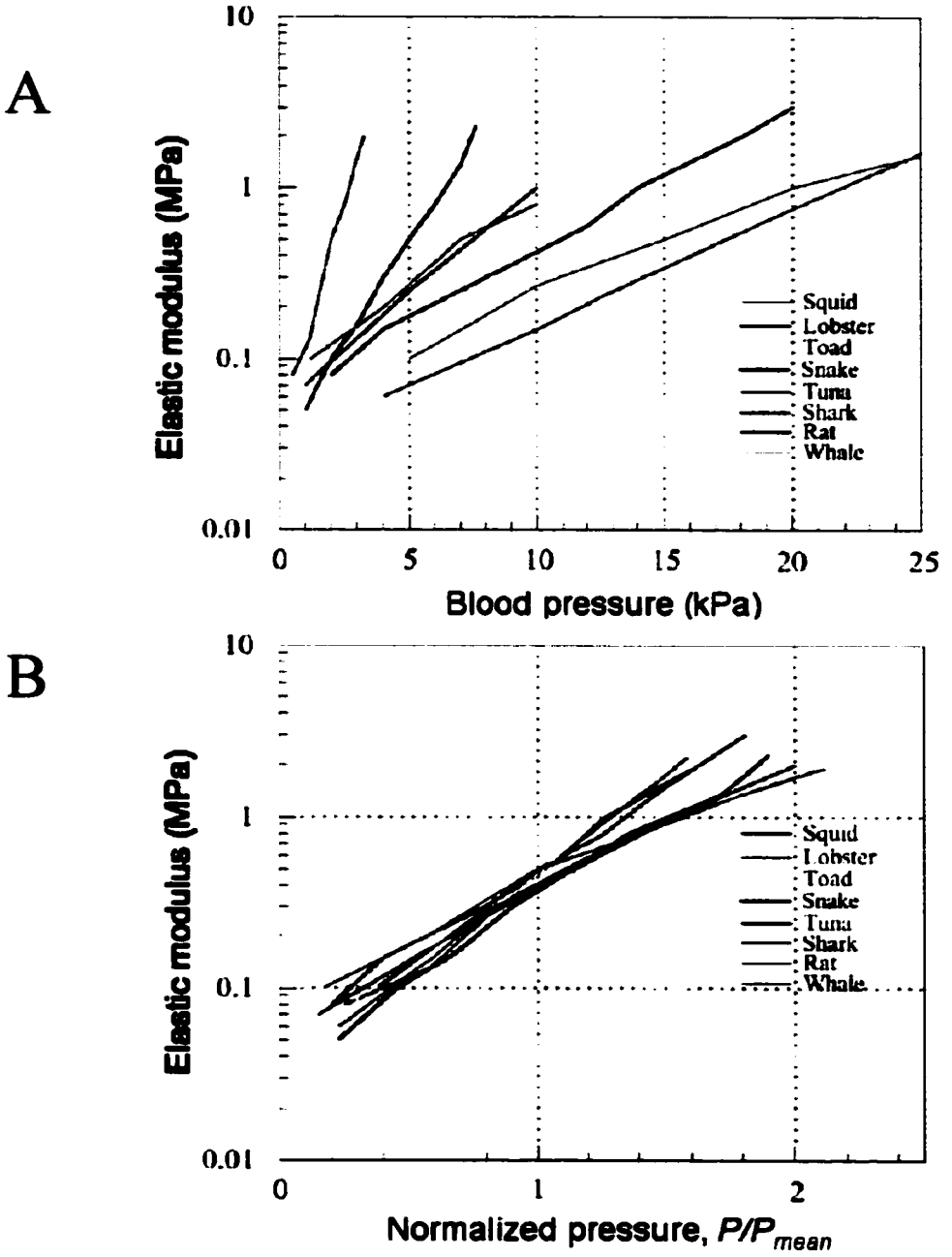

Figure 1.6A, B: Plots of aortic elastic modulus as a function of inflation pressure for a variety of species. Although substantial differences exist among the curves, in each case the aorta has nonlinear elasticity and the modulus increases dramatically with pressure. Note logarithmic scale. B) The same data as A, but plotted with pressure normalized to mean blood pressure for each species. Alignment of data from diverse taxa suggests evolutionary convergence in artery design (Shadwick, 1999).

Chapter 2:

Nonlinear materials in biological dynamical systems: Consequences for locomotion in hydrozoan medusae

Summary

Musculoskeletal springs such as tendon, ligament, and mesoglea rely on fibrous materials such a collagen and elastin to store and return mechanical strain energy. Represented in diverse taxa, these musculoskeletal springs can significantly reduce the energetic requirements for locomotion. Virtually all musculoskeletal springs exhibit a nonlinear response to an applied strain. Dynamical mechanical testing on hydrozoan mesoglea from *Polyorchis penicillatus* and *Mitrocoma cellularia* reveal different nonlinear dependencies on strain but no significant interspecific difference in stiffness. An exponential fit to measured stress/strain curves, allows determination of an exponent of nonlinearity for each species. With this estimate, a nonlinear spring is incorporated into a simple dynamical system that models the passive mechanical properties of mesoglea. Inclusion of a nonlinear spring yields oscillation amplitude augmentation over a broad range of sizes and the development of sub and superharmonic frequency components that depend on the magnitude of spring nonlinearity. Finite element modeling shows that measured nonlinear material properties can increase static deformations of the bell up to four orders of magnitude over a physiologically relevant range of applied pressures. Investigations of the role of nonlinearity in the simple system inform predictions of the role of nonlinear materials in medusan swimming performance.

Introduction

Passive skeletal "springs", elastic structures that store and return mechanical strain energy, reduce the amount of muscular work required for locomotor performance (Alexander, 1988; Alexander and Goldspink, 1977; Farley et al., 1993; Gosline and Shadwick, 1983; Pabst, 1996). Represented in diverse taxa, from jumping insects and hopping kangaroos to jetting jellyfish, squid, and scallop, energy storage and release in passive springs can reduce the metabolic costs of locomotion up to 70% (Alexander and Goldspink, 1977). Tuning these springs to optimize the amplitudes of contraction for a given energetic input depends on matching the driving force of the muscle to the natural or resonant frequency of the system. The resonant frequency in turn depends on the quantitative values of the linear and nonlinear stiffness coefficients of the system, along with its other mechanical properties. Resonance tuning may be especially important for energy conservation in invertebrate locomotion, in animals like jellyfish and scallop, where elastic energy storage and return are important components of the locomotor apparatus (DeMont, 1990; DeMont and Gosline, 1988b).

Biological materials that store and return energy are pervasive in physiological dynamic systems (Gosline and Shadwick, 1983). From DNA (Garcia et al., 1994; Klapper and Qian, 1998) and proteins (Kharakoz, 2000) to the circulatory system's arteries (Armentano et al., 1995; Gosline and Shadwick, 1996; Imura et al., 1990; Shadwick, 1999; Zhou and Fung, 1997) to the respiratory system's diaphragm (Boriek et al., 2000; Boriek and Rodarte, 1997; Maksym and Bates, 1997) to the musculoskeletal system's ligaments and tendons (Buchanan and Marsh, 2001; De Zee et al., 2000;

Wainwright et al., 1976; Wang and Ker, 1995), diverse systems rely upon elastic energy and return for various kinds of mechanical work. In all of the above examples, these biological "springs" respond nonlinearly to applied loads. Thus, by design, animals for which such materials play a role in locomotion are complex nonlinear dynamical systems and nonlinearity may have important dynamic consequences for locomotion.

Hydrozoan jellyfish, which represent one of the more primitive body plans in the animal kingdom, provide an opportunity to probe the dynamic consequences of nonlinear springs in locomotor performance. Jellyfish are composed predominantly of mesoglea, a fibrous acellular matrix, that responds nonlinearly to applied strains (Alexander, 1962; DeMont and Gosline, 1988a; Gladfelter, 1972; Koehl, 1977). Collagenous fibers in the mesoglea deform during muscular contraction, storing strain energy to power the refilling phase of the swimming contraction. The recoil phase of the contraction is entirely passive, greatly reducing the energetic expenditure that would be required by active refilling, and eliminating the need to maintain antagonistic muscle pairs (Daniel, 1995).

DeMont and Gosline (1988) assert that a nonlinear stress/strain curve might be advantageous for maximizing the force generation in a given swimming contraction. The initial low modulus region allows easy deformation during the phase of the contraction that generates high hydrodynamic thrust, while the increasing stiffness at the end of the cycle enables the storage of strain energy when the potential for hydrodynamic work is low. DeMont and Gosline's predictions about the significance of nonlinear mesoglea can be investigated and added upon in a series of both real and numerical experiments. In this study, I measure the material properties of mesoglea from two hydrozoans with

distinctly different geometries: *Polyorchis penicillatus* and *Mitrocoma cellularia* and characterize their nonlinear stress/strain relationships. I then explore the dynamic consequences of such nonlinearities with a series of numerical experiments that incorporate a nonlinear spring in a mass-spring system subject to periodic forcing. Additionally, I incorporate nonlinear materials in a finite element model of a medusan bell to examine how nonlinear materials affect the deformation and strain distribution within the bell as it undergoes a single static deformation.

Nonlinearities in material properties can lead to a variety of dynamic consequences. In this chapter, I ask what biologically significant dynamics arise in a simple dynamical system and what consequences these might have for a moving animal. Elsewhere, I account for the geometry of the jellyfish and the stresses it generates with each component of its locomotor apparatus, enabling an explicit test of the role of nonlinear mechanics in the performance a swimming jellyfish. Finally, I discuss the broader implications of my result for understanding nonlinear mechanics and nonlinear dynamics in complex biological systems.

Materials and Methods

Animals

To represent some of the geometric diversity within the *Hydrozoa* and to explore some of the consequences of morphological variation, I tested the mesoglea of two species of medusae— *Mitrocoma cellularia* and *Polyorchis penicillatus*. I collected *Mitrocoma* off the docks of Friday Harbor Laboratories in Friday Harbor, WA and

Polyorchis in the waters off the coast of Stuart Island, WA, housed them in a 10°C cold room, and fed them large brine shrimp nauplii at regular intervals.

Dynamic Materials Testing

Mechanical testing apparatus

Dynamic material testing measures a composite of mesoglea's viscous and elastic components. I used an apparatus designed to hold mesoglea, with a Ling vibrator that provides sinusoidal length oscillations on one side and is equipped with a brass force beam on the other, to measure instantaneous force and displacement as changes in voltage (Figure 2.1). A function generator supplied the sinusoidal signal to the Ling vibrator and allowed modification of driving frequency between 0.1 Hz, 1 Hz, and 10 Hz. The apparatus tracked oscillations optically through a configuration of metal flags that pass over sensors illuminated by light-emitting diodes. From calibrations, the following equations represent the behavior of the sensors:

$F = 0.0627\Delta v - .00003$ $\quad R^2 = 0.999$

LF (length displacement on force sensor) $= 0.9787\Delta v + 0.0152$ $\quad R^2 = 0.996$

$L = 0056\Delta v^3 - 0.0046\Delta v^2 + 0.119\Delta v - 0.0038$ $\quad R^2 = 0.997$

A linear equation describes the force beam side of the apparatus (F) because displacements were small and well within the linear portion of the sensor. A polynomial describes the length side of the sensor because applied length displacements exploit a larger portion of its range and the sensor exhibits nonlinear behavior at its extrema.

Standard op-amp circuitry amplified raw voltage output, which was acquired as digital input using MacLab 400 two-channel data acquisition hardware. MacLab software displayed raw voltage signals in Chart 5.3.7 which allowed signals to be converted to text files for subsequent data manipulation and calculations using a custom program written in Matlab 5.2 (Appendix A).

Experimental Protocol

At the beginning of each experiment, I weighed jellyfish in a volume of seawater to determine body mass and record morphometric measurements of bell height and inner and outer bell radius. I transferred animals to a volume of isosmolar magnesium chloride ($MgCl_2$) [67.1g/l], which replaced calcium in the seawater and acts as an anesthetic and muscle relaxant.

On a fully anesthetized animal, I excised strips of the bell in the longitudinal orientation (apex to margin). I used a finite element model of a jellyfish to verify that mesoglea experiences predominantly tensile strains in the longitudinal direction and compressive strains in the circumferential direction (Figure 2.2). I then conducted tensile longitudinal tests on strips of tissue that include mesoglea and epithelial layers with fully anesthetized muscle.

Because the particular distribution of mesoglea within the bell's geometry is species-specific, strips excised were located in regions of uniform thickness. Thus, the length of the excised strip was necessarily variable between species. I measured length, width and height of each strip and, with gel cyanoacrylate (Bondini), glued the strip to

plexiglass clamps in the orientation of excision and, once the tissue had fully adhered, submerged the entire preparation in isosmolar $MgCl_2$. The experimental preparation was maintained on a cold plate (a metal plate that conducts cold from an ice repository) causing the resultant experimental temperature to remain constant at 10°C.

I determined the original rest length by the first detectable oscillation produced in tension on the force side of the apparatus. Tissue is under tension in the intact animal, however, and the magnitude of that tension cannot be measured directly before cutting into the bell. Additionally, *in situ* tension will necessarily vary from individual to individual and will depend on factors such as the size of the animal, previous locomotor history, and nutritional state. Therefore, I defined rest length operationally as the appearance of first sinusoidal voltage changes on the force sensor and actually has a DC offset that is not precisely measurable.

In each experiment, I stretched the tissue over a range of mean tissue lengths (strains) in both ordered and randomized increments. In each case, the first set of oscillations yielded higher stress values for the same strain than did later trials, which I interpreted as tissue hysteresis. Since there were no statistical differences in measured material properties between randomized or ordered trials I conducted the remainder of the experiments in an ordered manner to minimize the wear and tear on the tissue. Ultimately, all data in repeated measures that yielded lower stress values for the same strain were excluded—essentially only counting the first recording from that strain position.

I oscillated strips of tissue over a small fixed strain amplitude, averaging 0.5 +/- .04% of the strip length, averaged over all preparations, and reconstructed the stress/strain behavior over a physiologic strain range of 3.5% in the longitudinal, apex to margin, direction. While the overall stress/strain behavior of mesoglea is nonlinear, mesoglea stress varies linearly with sinusoidal displacements of small strain amplitudes (Figure 2.3). A linear response over small amplitudes allows a piecewise linear reconstruction of the overall nonlinear curve. I oscillated tissue continuously throughout the duration of the experiment at a set driving frequency of either 1hz, 10hz or 0.1 Hz,.

I used arc length measurements extracted from video of swimming *Mitrocoma* and *Polyorchis* to determine the appropriate physiological strain range. With images digitized using NIH image 5.2, I compared total arc length between the fully contracted versus relaxed state. Although there was considerable variation from cycle to cycle and between individuals, bell arc length was on average (N = 3) 3.5% greater in the contracted than relaxed state. Thus, I estimated that a strain range of 3.5% typifies the *in situ* physiological condition, and used this value as the maximum applied strain for material property tests.

Interpretation of mechanical data

The instantaneous voltage signals from optically-tracked force beam and length tracker output, along with their calibrations, were used to create a data set of force and length measurements for a variety of fixed lengths over a physiologically relevant strain

range (up to 3.5%). These values were then converted to instantaneous stress and strain values using:

$$\sigma(t) = F(t)/A, \quad [1]$$

$$\varepsilon(t) = L(t)/L_o \quad [2]$$

where A is the cross-sectional area of the strip of tissue and L_o is its initial length.

Since the stress and strain vary sinusoidally in the experimental apparatus, their amplitude could be detected easily by a custom peak finding routine in Matlab based on sign changes of point-to-point differences of the data, which approximates the derivative. The phase between stress and strain was determined algebraically from the amplitudes of the stress and strain waves and the amplitude of the wave that is formed by their difference.

$$\varepsilon=\varepsilon_o sin\omega t \quad [3]$$

$$\sigma = \sigma_o sin(\omega t+\delta) \quad [4]$$

where ε_o is the maximum strain in each cycle, σ_o is the maximum stress in each cycle, ω is the circular frequency, and δ is the phase angle (Wainwright et al., 1976).

The total dynamic stiffness, (E^*) is given by the ratio of stress to strain amplitudes. This ratio, the total dynamic stiffness of mesoglea, represents the overall resistance to deformation and is called the complex modulus. Because it does not depend on any phase between stress and strain, it includes both elastic and viscous components of mechanical behavior. Since stress and strain are only in phase for perfectly elastic materials subject to sinusoidal loads, and mesoglea is a viscoelastic material, E^* is separated into its elastic modulus (E') and its viscous modulus (E''):

$$E' = E^*\cos\delta \quad [5]$$

$$E'' = E^*\sin\delta \quad [6]$$

$$E^* = E' + iE'' \quad [7]$$

where δ is the phase angle between the maximum stress and maximum strain (Wainwright et al., 1976). This approach enables capture of both instantaneous and time-dependent properties of the material.

Estimating the magnitude of nonlinearity

To quantify the nonlinear behavior of mesoglea, stress/strain curves were fit to a simple multiplicative exponential model, which can be written as either:

$$\sigma = a\varepsilon^x \quad [8]$$

$$\sigma = E\varepsilon|\varepsilon|^b \quad [9]$$

Both of the above formulations are used in subsequent analyses. An additive model, in which an initial strain offset is added to the exponential term, in the form $\sigma = a\varepsilon + b\varepsilon^x$, can also produce viable fits to stress/strain data. However, I chose this multiplicative model (Equation 8,9) for two reasons: 1) The stress/strain curve for mesoglea at low strains has a flat region, which is typical of most fibrous biological materials, where the material does actually approach zero stress until reaching a tension that is operationally defined as rest length and 2) Precise determination of a small initial offset is experimentally intractable.

A Nelder-Mead simplex minimization routine in Matlab estimates the coefficients a and x for a given data set (Table 2.1). In a linear material, $\sigma = a\varepsilon$ and $x = 1$. Any case

in which the best fit for $\sigma = a\varepsilon^x$ generates a parameter set where $x \neq 1$, describes a nonlinear material.

Experimental results

Over a strain range of 3.25% on longitudinal strips of mesoglea, complex modulus, E^*, that ranges from 8043 +/- 1556 to 17,505 +/- 4149 in *Mitrocoma* and from 9806 +/- 2041 to 21,328 +/- 5322 in *Polyorchis* (Figure 2.4). While the mean E* of mesoglea from *Polyorchis* is consistently stiffer than that from *Mitrocoma*, the difference between the two species is not statistically significant ($p = 0.86$, repeated measures ANOVA, StatView 5.0.1).

At an average strain of 3.25%, the stress (σ) for an applied strain in the mesoglea of *Mitrocoma* is 542 +/-187 where in *Polyorchis* 766 +/- 155 (Figure 2.5). The stress values for *Mitrocoma* and *Polyorchis* are not significantly different from one another ($p = 0.74$, repeated measures ANOVA, StatView 5.0.1).

In both *Mitrocoma* and *Polyorchis*, mesoglea exhibits a nonlinear stress/strain relationship. The predominant nonlinearity in mesoglea is in the elastic component of the complex modulus. When E^* is decomposed into its elastic modulus E' and its viscous modulus E'', for a driving frequency of 1Hz which is at or near the swimming frequency of an average-sized *Polyorchis* and *Mitrocoma*, storage modulus E' constitutes 99.7% of E^* in *Polyorchis* and 99.8% of E^* in *Mitrocoma*. At a driving frequency of 10 Hz, E' constitutes 98.7% of E* in *Polyorchis* and 98.6% of E* in *Mitrocoma*. At 0.1 Hz E' is 99.7% of E* in *Mitrocoma*. On average, regardless of oscillatory frequency, the

loss modulus, E'' is less than 2% of the complex modulus E*. Curve fits to data from individual animals yield an error estimate for the exponent x of +/- 0.10 S.E.

Preliminary experiments on a third species, *Aequorea victoria*, yield similar mesoglea stiffness values as *Mitrocoma* and *Polyorchis* and also show a pronounced nonlinearity. I measured material properties for *Aequorea* over a 30% strain range and determined a nonlinear exponent of x=2.2. Discussion of *Aequorea* is not included in this paper because its material properties were measured over a much larger range of strains and is therefore not directly comparable to measurements made on *Mitrocoma* and *Polyorchis*.

Finite element modeling: Structural effects of nonlinear materials

Model development

Because analytic solutions to stress and strain distributions of complex geometric structures are intractable, I used a finite element model to ask how incorporating nonlinear materials in the bell structure affects a single static deformation or contraction.

Morphometric measurements of bell radius, height, and apex thickness from *Polyorchis* guide the creation of a 3-dimensional finite element geometry to represent each species. Using four-noded elements with non-zero thickness ("thick shell elements") in finite element code MARC (MARC Analysis Research Corporation), each bell is meshed into 200 elements divided into 10 rows. This element type a) allows computations of principal stresses in all axes, b) is simpler to use than elements with eight or more nodes, and c) is appropriate when the radius of curvature of the geometry

as a whole is large relative to the thickness of the structural elements, which is certainly the case for the jellyfish shapes examined (though not necessarily true for all hydrozoans) (Daniel et al., 1997). Boundary conditions are 1) fixed center at the top of the bell with no displacement or rotation in x, y, z direction and 2) face pressure loads (Pa) on the bottom 6 rows, on the elements surrounding the subumbrellar cavity to simulate muscle contraction (Figure 2.6A). The bell apex (top four rows) is thicker than the rest of the bell and decreases in thickness with distance away from the top (Figure 2.6B). The geometric specifications for the two species are specified in Table 2.2.

Estimates of linear material properties are based on the linear fit to measured stress/strain data in Figure 2.5 that conserves the same average slope of the nonlinear stress/strain relationship. For *Polyorchis*, the linear Young's modulus (E) is 24000 Pa. But, to examine the effect of nonlinear material properties on static bell deformations, it is necessary to construct finite element geometries with both linear and nonlinear material properties. To apply a nonlinear material to the bell geometry, I use an Ogden material (sensu (Fu and Ogden, 2001) that is described with empirically determined coefficients to characterize the nonlinear elastic properties of mesoglea, a characteristic method for describing tissues like mesoglea with a strain stiffening response. While there are a host of models that characterize the behavior of nonlinear materials, I focused on the Ogden model because it is one of the more general models used to describe biological materials.

The Ogden model is derived from an energy function for the strain-dependent work (W) according to the formulation used in the finite element software I employ (MSC software) for a unidirectional extension.

$$W = \sum_{n=1}^{2} \frac{\mu_n}{\alpha_n} J^{\frac{-\alpha_n}{3}} (\lambda^{\alpha_n} - 1) + 4.5K(J^{-1/3} - 1)^2 \qquad [10]$$

where λ is the strain invariant in the test direction, expressed as L/Lo = ε+1, J is the Jacobian measuring dilatancy (the determinant of the deformation gradient), K is the bulk modulus of the material, μ_1 and μ_2 are moduli of the material and α_1 and α_2 are their exponents.

To determine the Ogden coeffiecients for measured stress/strain data from *Polyorchis*, I use measured fits to Equation 8 ($\sigma = 89\varepsilon^{1.8}$) to fit the Ogden coefficients for a uniaxial test using MARC's built in data-fitting algorithm. Resultant Ogden coefficients are shown in Table 2.3.

Finite element model simulations and results

Constructing a medusan bell with nonlinear material sharply reduced the amount of force/pressure required to deform the bell to a physiological displacement, with nonlinearity exerting a large effect (Figure 2.7, 2.8).

For a bell composed of linear material, deformation increased linearly with increasing pressure, but did not achieve physiologically realistic bell deformations at physiologically relevant pressures. In the linear case, more than ~1000Pa was required to deform the bell ~1%. In contrast, medusan bells constructed with nonlinear material

properties reached deformations up to 15% at bell pressures of 1.5 Pa, which correspond to the low end of the range of pressures experienced during a jet cycle (Daniel, 1995). For perspective, any actual bell contraction can range from ~15-50% and varies depending on the kind of locomotor behavior being exhibited (i.e. forward translation v. turning) (Gladfelter, 1972).

In comparison to the linear case, a bell composed of nonlinear material experienced deformations four orders of magnitude greater for equivalent pressure forces. These deformations increased nonlinearly in response to applied pressures (Figure 2.8). Finite element results are consistent with expectations from the measured material properties. A relatively high nonlinear exponent makes the bell effectively stiffer at large displacements, but easier to deform at small displacements where the heel of the stress/strain curve produces a low modulus region.

Exploring a simple dynamical system

To explore the dynamic consequences of material nonlinearities, in the absence of geometric arguments, I analyze the response of a damped mass spring system subject to periodic forcing.

$$\sigma(t) = M\frac{d^2\varepsilon}{dt^2} + D\frac{d\varepsilon}{dt} + E\varepsilon|\varepsilon|^b \qquad [11]$$

where stress (σ = force/area) is a periodic forcing function of a given frequency (ω), such that $\sigma(t) = -\cos\omega t$. Coefficients M (scaled mass), D (scaled damping), and E (Young's

modulus of stiffness) are all scaled by the area and length (i.e. M = (mass * length (L)) / area).

Solution characteristics that may contribute dynamically to a swimming jellyfish are changes in duration and amplitude of transient oscillations, oscillation amplitude, peak number/cycle, mean signal position, and the Fourier coefficients with varying values of the nonlinear exponent. I account for all Fourier coefficients in which the amplitude coefficients are greater than 1/10 the primary frequency component (1 Hz), the average swimming frequency for jellyfish of an intermediate size across a range of species. The nonlinear exponent *b* (Equation 9) modulates the simulated stress/strain response of mesoglea. When b = 0, the simulated material described is linear. Any non-zero value of b connotes a nonlinear material and the magnitude of b describes the strength of the nonlinearity.

To retain the overall modulus range with a changing nonlinear exponent, it is necessary to scale the mean slope of the stress/strain curve based on the linear slope of our measured data for *Polyorchis*. Varying *x* in Equation 8 without simultaneously modifying the scalar *a*, the mean slope of curve would change with an increase in the nonlinear exponent (Figure 2.9A) and thus *a* must be scaled so that the mean slope of the function remains constant (Figure 2.9B). The scaling relationship for *a* derives from an expression for the mean slope based on Hooke's Law, in which F = kx:

$$\frac{dF}{dx} = K$$

$$F = ax^n$$

$$dF = anx^{n-1}dx$$

$$\overline{K} = \frac{1}{x_{max}} \int_0^{x_{max}} anx^{n-1}dx$$

$$\overline{K} = anx^{n-1} \qquad [12]$$

From the linear slope of the stress/strain curve and Equation 12 above, it is possible to then select values for a, in Equation 8. So, as the magnitude of the nonlinear exponent (x) changes, a mean slope is preserved that is equivalent to the mean slope of the curve fits to the measured stress/strain curves for *Polyorchis* and the work required to displace to x_{max} is constant.

Armed with the appropriate scaling relationships, I used custom written Matlab code to solve the mass-spring system [11] numerically. I used built-in ode-solver ODE23s for stiff differential equations with adaptive time stepping to a maximum time of 10 seconds and removed the transient portion of the solution, defined observationally as the first 2.5 seconds of the solution, from steady state analyses.

Estimates for the scaled effective mass (M) (mass of the spring + entrained fluid) and scaled damping (D) were taken from DeMont and Gosline's (1988c) measurements for the medusa *Polyorchis penicillatus*. To explore size-related dynamic phenomena, I varied M for three different values of D over both a coarsely and finely sampled parameter space. For the case of coarse sampling, scaled mass (M) varies from 0.005 to 1

kg/m (in increments of 0.05 kg/m) for three values of the damping coefficient (D = 0.5, 0.1, and 0.2 Ns/m^2). For fine sampling, scaled mass (M) varies from .005 to .05 kg/m (in increments of .002 kg/m) for three values of the damping coefficient (D = 0.05, 0.1, and 0.2 Ns/m^2). The nonlinear exponent (*b*) varies in each case from 0 to 2, which effectively spans the range from a linear stress/strain relationship to a cubic nonlinearity.

Since there are no jellyfish-specific geometric arguments intrinsic to this numeric experiment, I acknowledge that this is only one of many parameter spaces that may be relevant to a swimming medusa. This is merely an attempt to show some of the dynamic possibilities that result from the addition of a nonlinear term to a simple system, not to extensively map the complete parameter space. In a following chapter, incorporating this basic dynamic system in a model that more accurately describes a swimming jellyfish, parameter choices can be matched to actual measurements along with the rich body of published data on hydrozoan medusae.

Numerical experiment results

I used a multi-tiered approach to explore the effect of a nonlinear exponent on the dynamic output of the mass-spring system [11], from the level of an individual signal output to the level an entire parameter space. By comparing the linear case (b = 0) to the measured exponents from the mesoglea of *Polyorchis* (b = 0.8) and *Mitrocoma* (b=0.2), it is possible to make a qualitative assessment of the solution and to determine what metrics to monitor in widening the scope of this exploration.

Even a subtle increase in the nonlinear exponent has measurable dynamic effects. In the transition from an exponent of b = 0 to b = 0.2 (*Mitrocoma)*, for a fixed mass and damping, there is an increase in the amplitude of oscillation of nearly three-fold (Figure 2.10A). In addition, prominent superharmonic frequencies appear, appearing as additional peaks on the signal. A Fourier transform confirms this observation. For b = 0.2, there are small peaks at 3 and 5 Hz in addition to the dominant peak at the driving frequency of 1Hz (Figure 2.10B). Adding the solution for the measured nonlinear exponent for *Polyorchis* (b = 0.8), makes these trends even more pronounced. Oscillation amplitude increases to 20x the linear case (b = 0) and the superharmonic peaks become quite prominent (Figure 2.11A). A Fourier transform detects a large peak at the driving frequency (1 Hz) and clear peaks at 3 and 5 Hz (Figure 2.11B).

In systematically varying the magnitude of the nonlinear exponent from b =0 to b=2 for a fixed mass and three different values for the damping coefficient, frequency and amplitude coefficients of a Fourier transform reveal additional effects of nonlinearity. Across all nonlinear values for b, from linear to cubic, the amplitude coefficients of the Fourier transform at the driving frequency (1Hz) increase monotonically with an increasing nonlinear exponent. Interestingly, a superharmonic frequency appears at 3 Hz immediately with an increase in the nonlinear exponent (b=0.2) but subsequently disappears at high values of *b* (*b* > 1.2) (Figure 2.12). Similarly, a third frequency at 5 Hz appears at low/intermediate values of *b* (b = 0.2 to b =~0.6 – depending on the magnitude of the damping coefficient). As the damping

decreases, there are additional peaks at 0.33 Hz for intermediate/high nonlinear values for b (b = 1 to b =1.6).

Since most jellyfish swim in bouts rather than continuously, transient phenomena might play a role in locomotor behavior. The transient portion of the solution to the mass-spring system shows qualitative differences for different values for the nonlinear exponent. In one example, with fixed mass and damping, that at (b =0.2-*Mitrocoma*), oscillation amplitude in the transient portion of the signal is larger than for b = 0. But, at b = 0.8 (*Polyorchis*), the transient is barely distinguishable from the rest of the signal (Figure 2.13). Nonlinear effects on transient oscillations may be something that plays a role in the startup of a locomotor bout.

Oscillation amplitude

Oscillation amplitude is highly sensitive to the nonlinearity of the spring. Over the coarsely sampled range of the scaled spring mass (M), (0.005 to 1 kg/m) there is a rapid increase in oscillation amplitude with an increasing nonlinear exponent (*b*) when the mass of the spring is low (Figure 2.14A). At this end of the range, the highest amplitude of oscillation clearly correlates with highest nonlinear exponent. Focusing on a finely sampled view of this part of the range, (0.005 to .05 kg/m) reveals that this trend toward increasing amplitude with increasing values for the nonlinear exponent (*b*) is remarkably insensitive to mass, except at the lowest value for the scaled damping coefficient (D). But, as the mass of the spring increases, oscillation amplitude becomes sensitive to both nonlinearity and mass. Amplitude increases at intermediate values for

the nonlinear exponent (*b*) and remains low for both small and large values of *b* (Figure 2.14B). As mass increases, the region of increased oscillation amplitude shifts toward lower and lower values of the nonlinear exponent (*b*). Not surprisingly, this pattern is more pronounced at low values of damping (D) and less apparent at high values.

Peaks per cycle

Quantifying the number of peaks per cycles determines whether superharmonic frequencies are detectable on a cycle by cycle basis and enables an evaluation of how their presence relates to the value of the nonlinear exponent (*b*). Over a coarsely sampled range of scaled mass (M), additional peaks are only prominent for very small mass values at intermediate levels of nonlinearity (Figure 2.15A). In a closer look at this part of the range, additional peaks are most apparent in the range of nonlinear exponents that encompasses the measured values for *Mitrocoma* (b = 0.2) and *Polyorchis* (b=0.8) (Figure 2.15B). As the mass increases, the band of values for *b* that have an increased number of additional peaks shrinks, encompassing an ever-decreasing range of exponents. There is a pronounced rise in the number of superharmonic peaks at weakly nonlinear values for *b* (0.2 – 0.4) at the lowest level of damping, D = 0.05 (Ns/m^2).

Cycle position

There is no global trend between mass, the value of the nonlinear exponent (*b*), and the mean cycle position (offset from zero) over a coarsely sampled range of masses (Figure 2.16A). However, several discrete islands are apparent, in which the mean bell

position shifts in the positive direction. This occurs sporadically over this whole range of masses, predominantly at intermediate to high values for the nonlinear exponent and intermediate to low values of damping. Figure 2.16B shows a close up view of one of these islands at a high value for *b*. With low value of D (D = 0.05 Ns/m^2), there is a region in which a shift in mean cycle position in the negative direction is directly adjacent to a shift in mean cycle position in the positive direction. This suggests either that there is an unstable region of parameter space, where subtle variations in M and the nonlinearity of the spring (*b*) cause dramatic dynamic effects, or marked sensitivity to initial conditions that become apparent under conditions of low damping.

Fourier components

A survey of the Fourier components of the solution over a range of nonlinear exponents and masses illustrates the wide range of dynamic possibilities in nonlinear systems. Nonlinear values for b (b>0) yield frequency peaks with higher amplitude coefficients than for b = 0 and often reveal peaks at sub and superharmonic frequencies (Figure 2.12). Here, I survey just the number of peaks, but do not compare the amplitude differences between linear and nonlinear cases, and survey a broader swath of parameter space. A linear system (b = 0) has only a single frequency peak (Figure 2.13, Figure 2.17B). In certain instances, a second peak appeared at b=0 at low values of damping and high values for mass, where the transient oscillations lasted longer and had not been fully excluded from the analysis. Across the range of nonlinear exponents, there are numerous regions with two, three, and four peaks at various values for mass and

damping (Figure 2.17A). Focusing in on the lowest part of the mass range, the linear case (b =0) has only one frequency peak throughout the range. For intermediate nonlinear values for b, there is a discrete region of multiple frequency peaks (>2) (Figure 2.17B). That region of multiple peaks at high nonlinearities spreads to cover a greater part of the range as the damping decreases.

Discussion

Since *Polyorchis penicillatus* and *Mitrocoma cellularia* are structurally dissimilar and have distinct locomotor behaviors, the measured conformity in their material properties is surprising. *Polyorchis* is prolate in shape and swims forward with directed movements at velocities of ~2-5 cm/s (Kinematic measurements presented in Chapter 4). *Mitrocoma,* on the other hand, is oblate and has a more variable swimming kinematic than *Polyorchis*. *Mitrocoma* alternates between directed movements at equivalent speeds as *Polyorchis* and a 'dog paddle' gait, in which repeated contractions of the bell do not generate forward translatory movements. As *Mitrocoma* swims, there appears to be greater bending in the tissue than in *Polyorchis*.

Recent experimental and theoretical work by Colin and Costello (2002) explores the hydrodynamic and ecological consequences of such 'gaits' or variation in propulsive modes of swimming. Prolate species, such as *Polyorchis*, develop clearly defined jet structures in their wake while oblate species, such as *Mitrocoma* do not produce defined jets but instead produced prominent vortices at the bell margin. As a result of this

difference in swimming kinematic, swimming plays different roles in foraging in oblate versus prolate medusae (Colin and Costello, 2002).

In light of these differences in overall swimming kinematics in *Polyorchis* and *Mitrocoma*, observed similarity in the material properties of mesoglea has intriguing evolutionary implications for design and constraint. Mesoglea from *Polyorchis* and *Mitrocoma* does not have different moduli, E*, but does have a different nonlinear response to an applied strain. Measured nonlinear exponents of b = 0.2 in *Mitrocoma* and b=0.8 for *Polyorchis* incorporated in the solution to the simple dynamical system in Equation 11 indicate that there can be large dynamic consequences resulting from a change in exponent of this magnitude. In terms of oscillation amplitude alone, there is a ten-fold increase between an exponent of b = 0.2 and b =0.8 (Figure 2.11).

While there is no direct link between a simple dynamical system that describes only the passive mechanical properties of the bell and an estimate of swimming performance in a jellyfish, these results provide a strong incentive to couple geometric arguments and fluid dynamics to produce a model that does account for the different components of the locomotor apparatus. An amplitude increase of the magnitude observed in the simple dynamical system suggests that a fluid-solid coupled model might predict greater swimming velocities with an increasing magnitude of nonlinear exponent. Superharmonic and subharmonic frequency components observed with the addition of a nonlinear spring to Equation 11 may interact with the forces of muscle contraction to produce different tuning optima across varying bell size and shape.

Incorporating these measured exponents in a finite element model that evaluates static bell deformations yields a similar result. Across a physiological range of deformations, a bell constructed with nonlinear material properties exhibits deformations that are roughly four orders of magnitude larger than a bell composed of linear material properties. Easy deformation at small strains supports the idea suggested by DeMont and Gosline (1988), in which the initial low modulus region allows easy deformation during the phase of the contraction that generates high hydrodynamic thrust.

Nonlinear springs may provide a way of circumventing a constraint in material construction, since the magnitude of the complex modulus of stiffness, E*, does not seem to be subject to much interspecific variation if compared point by point across the experimental strain range. However, collagen fiber density and distribution does vary between hydrozoan species and probably throughout ontogeny within a single species (Bouillon and Coppois, 1977; Gladfelter, 1972). While not demonstrated directly in these experiments, variation in the density and arrangement of collagen fibers within the extracellular matrix may play an important role in determining the nonlinearity of the material. If the nonlinearity of the material affects dynamic performance to such a large extent, this may be a mechanism for effectively changing mechanical properties through ontogeny.

Numerical experiments with a nonlinear spring in the simple dynamical system [11] also raise the issue of how resonance is manifested in nonlinear dynamical systems. From this preliminary exploration of a large parameter space, encompassing a wide range of masses, there are regions that are differentially sensitive with respect to amplitude

augmentation to changes in the nonlinear exponent. As M varies, the effective resonant frequency of the system is also changing, since the resonant frequency is defined, in part, by mass ($\omega = (k/m)^{1/2}$). But, mesoglea has a strain-dependent spring constant so the resonant frequency actually changes as the mass moves. In regions of parameter space where amplitude augmentation is highest, at the low end of the range of masses, the system is being driven closer to its resonant or natural frequency than in regions where there is no obvious amplitude augmentation. Resonance phenomena are important in many biological systems and hydrozoan locomotion is likely no exception (DeMont and Gosline, 1988b). But resonance is difficult to define for nonlinear systems and it is not immediately intuitive how to assess its dynamic role in locomotion. I address the question of resonant phenomena in nonlinear dynamical systems more fully in the next chapter.

Notes to Chapter 2

Alexander, R. M. (1962). Visco-elastic properties of the body-wall of sea anenomes. *Journal of Experimental Biology* 39, 373-386.

Alexander, R. M. (1988). *Elastic Mechanisms in Animal Movement.* Cambridge: Cambridge University Press.

Alexander, R. M. e. and Goldspink, G. ed. (1977). *Mechanics and energetics of animal locomotion.* London: Chapman and Hall.

Armentano, R. L., Barra, J. G., Levenson, J., Simon, A. and Pichel, R. H. (1995). Arterial wall mechanics in conscious dogs. *Circulation Research* 76.

Boriek, A. M., Kelly, N. G., Rodarte, J. R. and Wilson, T. A. (2000). Biaxial constitutive relations for the passive canine diaphragm. *Journal of Applied Physiology* 89, 2187-2190.

Boriek, A. M. and Rodarte, J. R. (1997). Effects of transverse fiber stiffness and central tendon on displacement and shape of a simple diaphragm model. *Journal of Applied Physiology* 82, 1626-1636.

Bouillon, J. and Coppois, G. (1977). Etude comparative de la mesoglee des cnidaires. *Cahiers de Biologie Marine* 18, 339-368.

Buchanan, C. I. and Marsh, R. L. (2001). Effects of long-term exercise on the biomechanical properties of the Achilles tendon of guinea fowl. *Journal of Applied Physiology* 90, 164-171.

Colin, S. P. and Costello, J. H. (2002). Morphology, swimming performance and propulsive mode of six co-occurring hydromedusae. *Journal of Experimental Biology* 205, 427-437.

Daniel, T. L. (1995). Invertebrate swimming: Integrating internal and external mechanics. In *Biological Fluid Dynamics*, eds. C. P. Ellington and T. J. Pedley), pp. 61-89: Society for Experimental Biology.

Daniel, T. L., Helmuth, B. S., Saunders, W. B. and Ward, P. D. (1997). Septal complexity in ammonoid cephalopods increased mechanical risk and limited depth. *Paleobiology* 23, 470-481.

De Zee, M., Bojsen-Moller, F. and Voigt, M. (2000). Dynamic viscoelastic behavior of lower extremity tendons during simulated running. *Journal of Applied Physiology* 89, 1352-1359.

DeMont, M. E. (1990). Tuned oscillations in the swimming scallop *Pecten maximus*. *Canadian Journal of Zoology* 68, 786-791.

DeMont, M. E. and Gosline, J. M. (1988a). Mechanics of jet propulsion in the hydromedusan jellyfish *Polyorchis penicillatus*: I. Mechanical properties of the locomotor structure. *Journal of Experimental Biology* 134, 313-332.

DeMont, M. E. and Gosline, J. M. (1988b). Mechanics of jet propulsion in the hydromedusan jellyfish *Polyorchis penicillatus*: III. A natural resonating bell; The presence and importance of a resonant phenomenon in the locomotor structure. *Journal of Experimental Biology* 134, 347-361.

Farley, C. T., Glasheen, J. and McMahon, T. (1993). Running springs: Speed and animal size. *Journal of Experimental Biology* 185, 71-86.

Fu, Y. B. and Ogden, R. W. (2001). *Nonlinear Elasticity: Theory and Applications*. Cambridge: Cambridge University Press.

Garcia, A. E., Soumpasis, D. M. and Jovin, T. M. (1994). Dynamics and relative stabilities of parallel and antiparallel stranded DNA duplexes. *Biophysical Journal* 66, 1742-1755.

Gladfelter, W. B. (1972). Structure and function of the locomotory system of *Polyorchis montereyensis* (Cnidaria, Hydrozoa). *Helgolander wiss. Meeresunters* 23, 38-79.

Gosline, J. M. and Shadwick, R. E. (1983). The role of elastic energy storage mechanisms in swimming: an analysis of mantle elasticity in escape jetting in the squid, *Loligo opalescens*. *Canadian Journal of Zoology* 61, 1421-1431.

Gosline, J. M. and Shadwick, R. E. (1996). The mechanical properties of fin whale arteries are explained by novel connective tissue designs. *Journal of Experimental Biology* 199, 985-997.

Imura, T., Yamamoto, K., Satoh, T., Kanamori, K., Mikami, T. and Yasuda, H. (1990). In vivo viscoelastic behavior in the human aorta. *Circulation Research* 66, 1413-1419.

Kharakoz, D. P. (2000). Protein compressibility, dynamics, and pressure. *Biophysical Journal* 79, 511-525.

Klapper, I. and Qian, H. (1998). Remarks on discrete and continuous large-scale models of DNA dynamics. *Biophysical Journal* 74, 2504-2514.

Koehl, M. A. R. (1977). Mechanical diversity of connective tissue of the body wall of sea anenomes. *Journal of Experimental Biology* 69, 107-125.

Maksym, G. N. and Bates, J. H. T. (1997). A distributed nonlinear model of lung tissue elasticity. *Journal of Applied Physiology* 82, 32-41.

Pabst, D. A. (1996). Springs in swimming animals. *American Zoologist* 36, 723-735.

Shadwick, R. E. (1999). Mechanical design in arteries. *Journal of Experimental Biology* 202, 3305-3313.

Wainwright, S. A., Biggs, W. D., Currey, J. D. and Gosline, J. M. (1976). *Mechanical Design of Organisms*. Princeton: Princeton University Press.

Wang, X. T. and Ker, R. F. (1995). Creep rupture of wallaby tail tendons. *Journal of Experimental Biology* 198, 831-845.

Zhou, J. and Fung, Y. C. (1997). The degree of nonlinearity and anisotropy of blood vessel elasticity. *Proceedings of the National Academy of Sciences* 94, 14255-14260.

Table 2.1: Coefficients determined to describe the magnitude of mesoglea's nonlinearity derived from Equation 8.

	a	**x**
Polyorchis	89	1.8
Mitrocoma	110	1.2

Table 2.2: Geometric parameters for finite element model of *Polyorchis penicillatus*. See also Figure 2.6A, B.

	Polyorchis
Radius (cm)	1.5
Height (cm)	3.0
Bell thickness (cm)	0.5 bottom 6 rows
Apex thickness (cm)	1.0 top 3 rows 0.7 fourth row

Table 2.3: Ogden coefficients for the material properties of *Polyorchis* determined by a model fit to experimental data.

Ogden Coefficients	***Polyorchis***
Bulk Modulus (K)	2592.48
μ_1	5.0925E-8
α_1	39.7191
μ_2	.0121471
α_2	85.3694

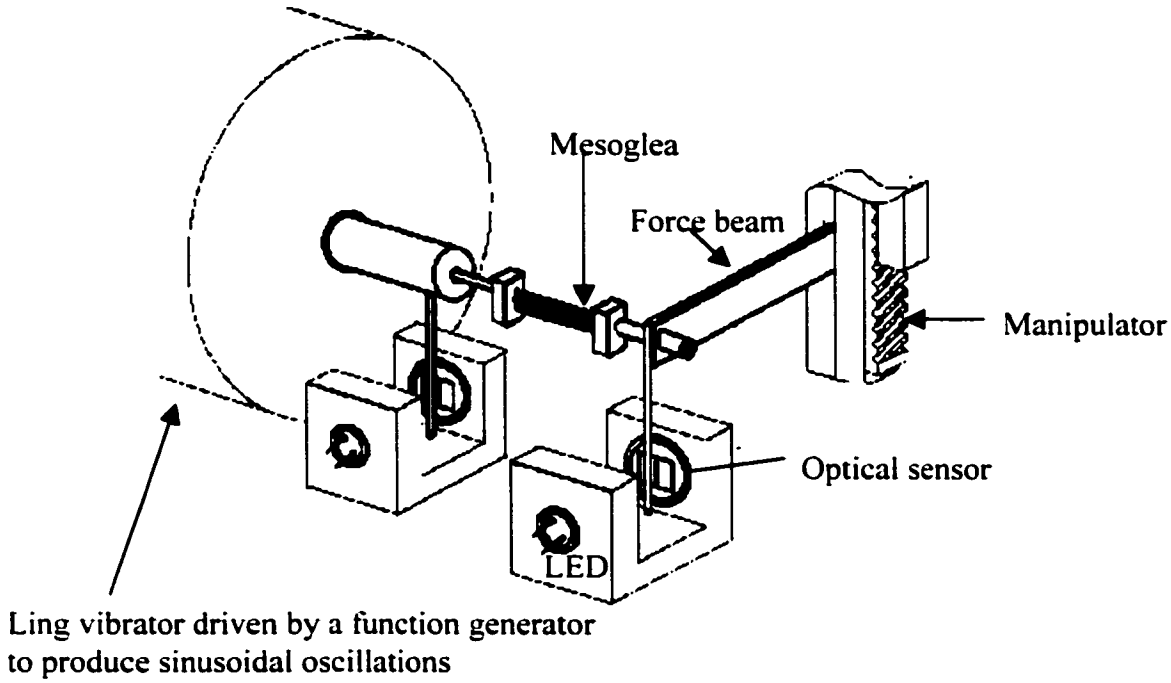

Figure 2.1- Mechanical testing apparatus: Apparatus used for dynamic measurements of material properties of mesoglea. On the left side of the apparatus, a ling vibrator provides sinusoidal oscillations of fixed small strain amplitude. An LED illuminates an optical sensor as a needle attached to the ling vibrator moves across its face. On the opposite side, a thin brass beam acts as a strain gauge and another optical sensor tracks the beam's displacement. Strips of mesoglea are glued between the clamps and the preparation is submerged in cold isosmolar MgCl2. (Figure adapted from Tu, 2000).

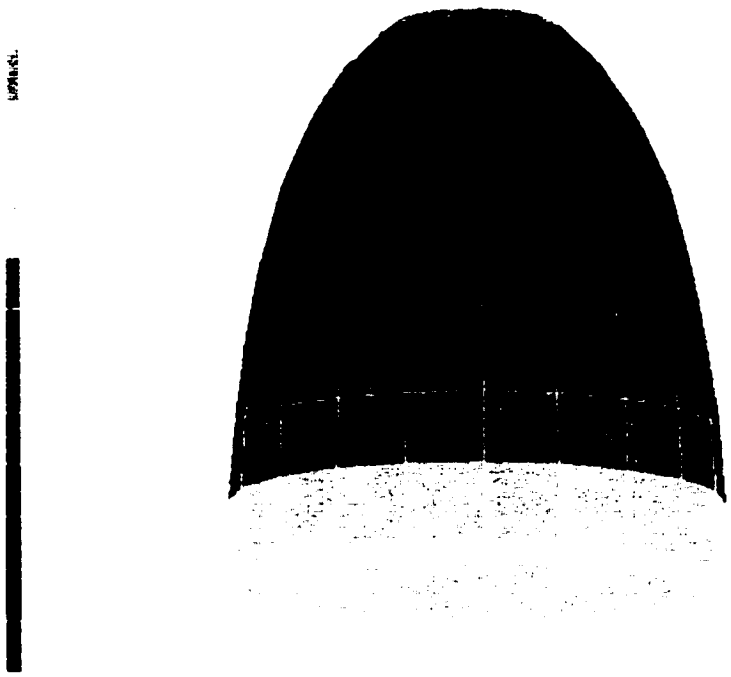

Figure 2.2-Mesoglea experiences tensile strains in the longitudinal direction: As the bell contracts there are tensile strains experienced in the longitudinal direction and compressive strains in the circumferential direction. Warm colors correspond with regions of high equivalent elastic strain with a bell pressure force applied that corresponds to physiologically relevant pressures. If a strip is cut from apex to margin and stretched in tension, applied strain will correspond with physiological strains.

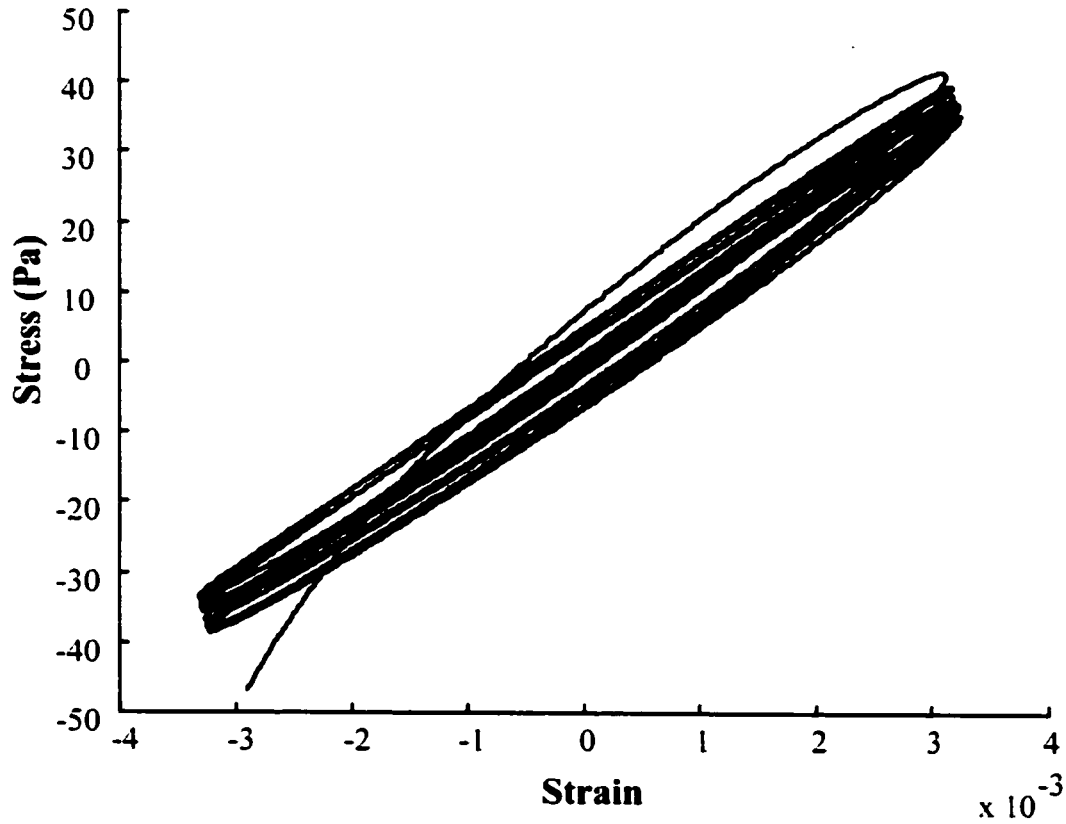

Figure 2.3– Piecewise linear behavior of mesoglea: Applied small fixed strain amplitudes, ~0.5% of strip length, show linear behavior over this range. Oscillating strips of mesoglea over small fixed strain amplitudes over a range of set strain positions allows for a piecewise linear reconstruction of the overall nonlinear behavior of the material.

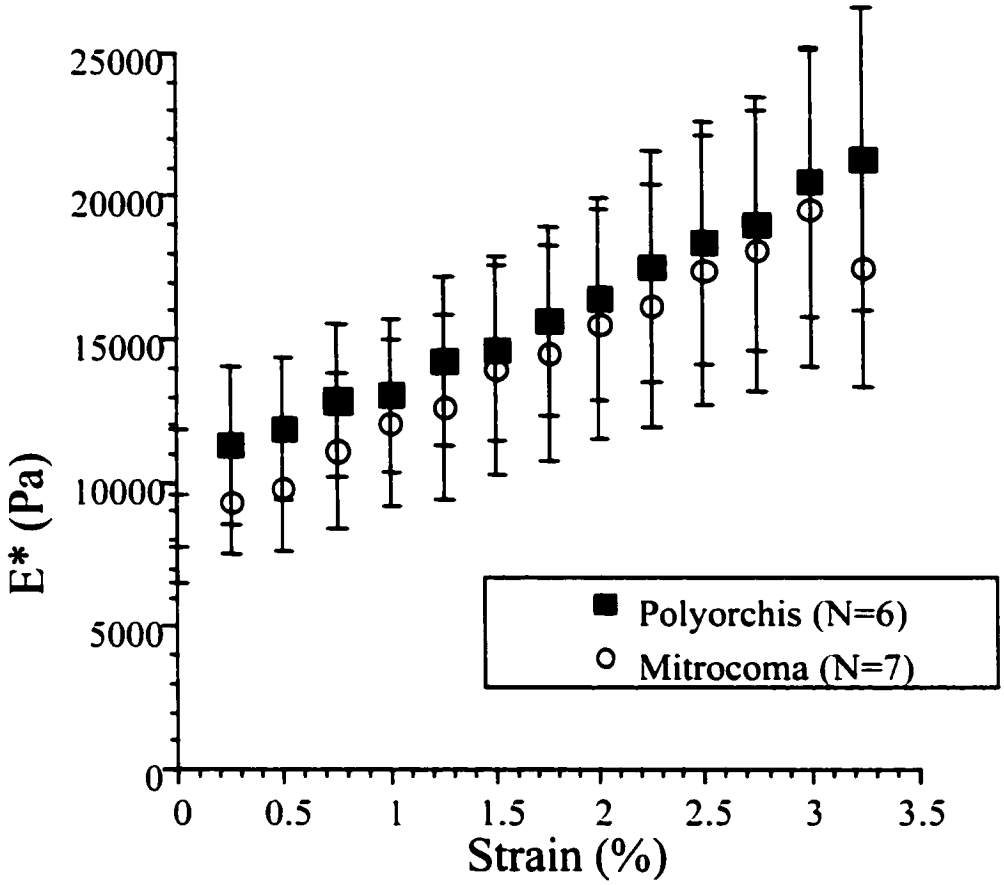

Figure 2.4- Strain-dependent complex modulus (E*) for *Polyorchis* and *Mitrocoma*: The dynamic modulus of stiffness, E*, plotted over the experimental range of strains. At each strain position (DL/L) strips of tissue are oscillated over small fixed strain amplitudes. Note that the mesoglea from *Polyorchis* and *Mitrocoma* show remarkably similar responses to applied strains. Although *Polyorchis* is consistently stiffer, there is no statistically significant difference between the two species. For both species, stiffness (E*) is strain dependent, indicating a nonlinear relationship between stress and strain.

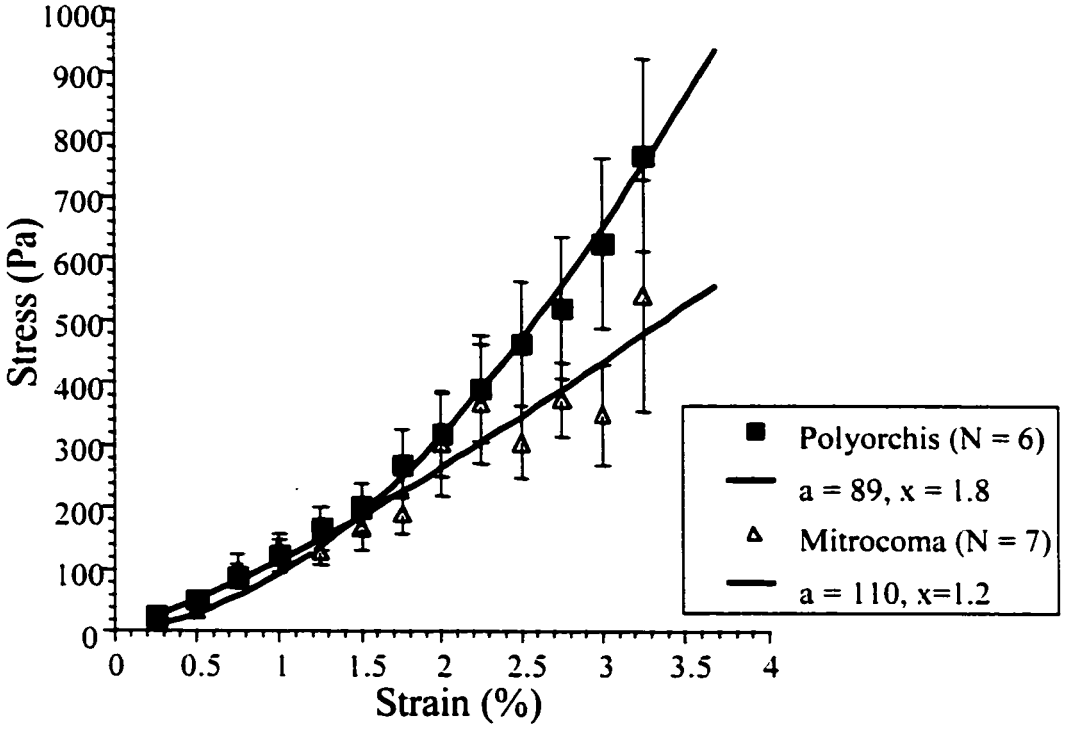

Figure 2.5-Stress-strain relationship of mesoglea for *Polyorchis* and *Mitrocoma*: The mesoglea of *Polyorchis* and *Mitrocoma* both exhibit nonlinear stress/strain relationships. Although there is no significant difference between the stress magnitude of these curves, the two species have different exponents of nonlinearity. For *Mitrocoma* the best fit to the equation $s=ae^x$ is x = 1.2 and for Polyorchis x = 1.8.

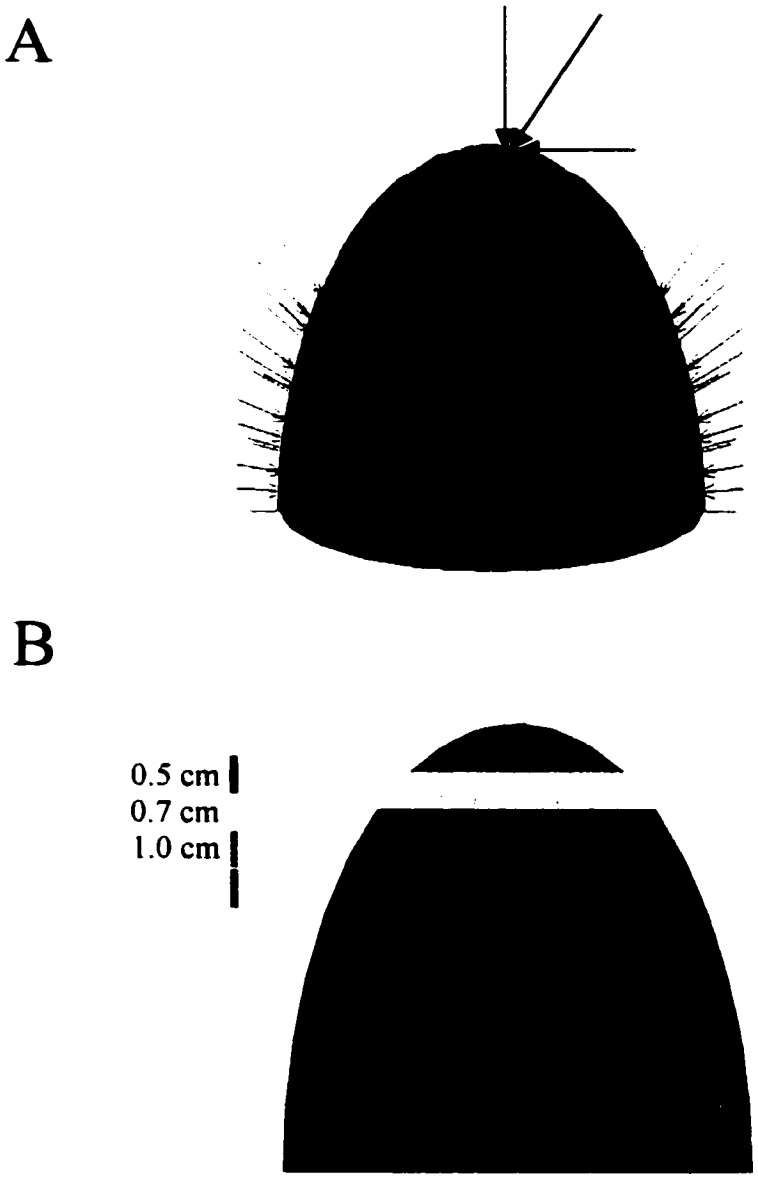

Figure 2.6 A, B: Boundary conditions for finite element model of *Polyorchis*. A) In an finite element model of a medusan bell, boundary conditions fix the bell apex to prohibit rotation and displacement (green arrows) and apply a pressure stress normal to the bell that simulates contraction of the circumferential muscles (red arrows). B) Rows 1-3 (from the top) are 1 cm (green), row 4 is 0.7 cm (yellow), and the bottom six rows are 0.5 cm (blue).

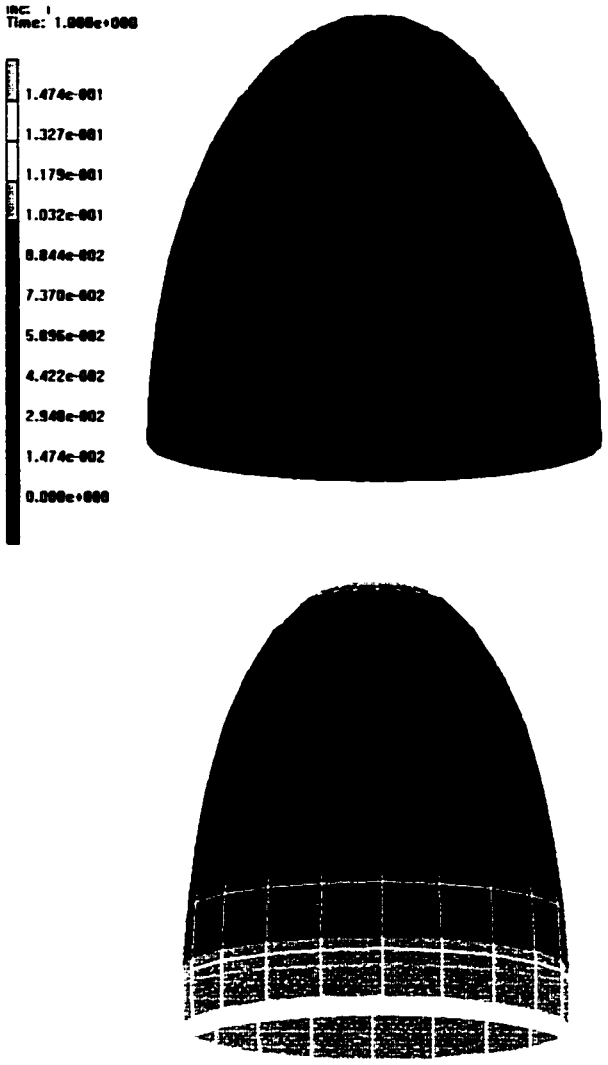

Figure 2. 7: Comparison of linear and nonlinear finite element models for the geometry of *Polyorchis*. Higher strains (with the same applied pressure stress) are seen in the nonlinear bell than the linear bell, consistent with greater bell deformations. Regions of highest strain (yellow) are concentrated towards the bottom of the bell.

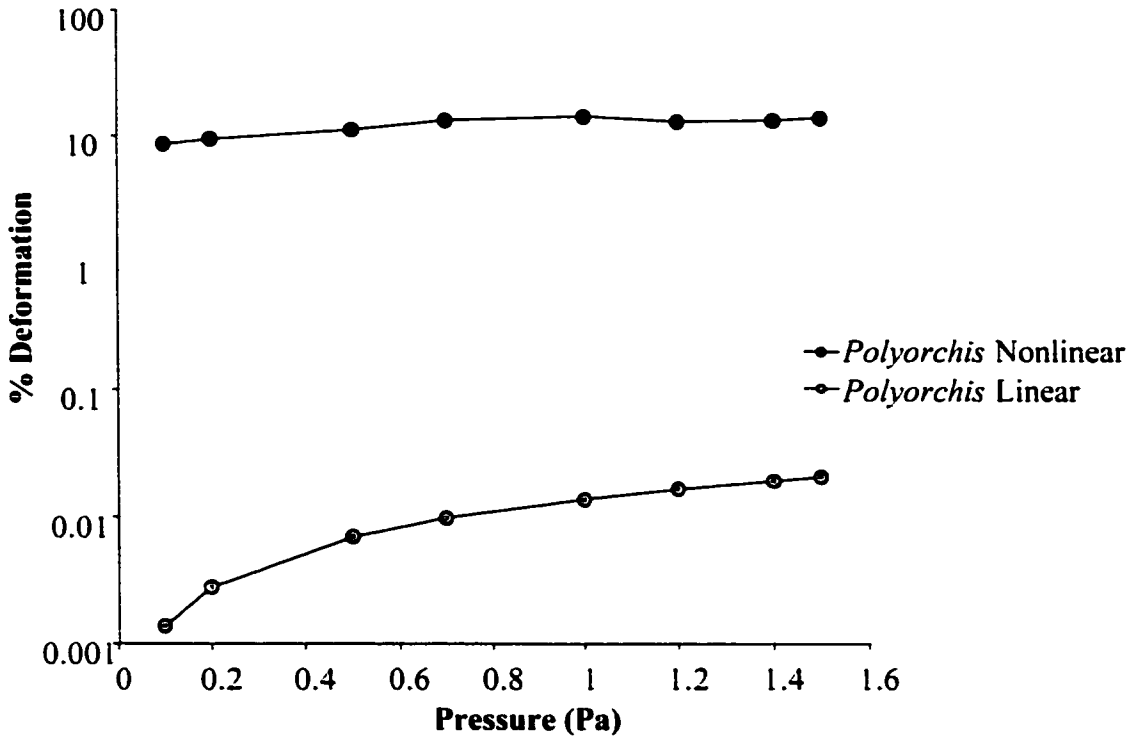

Figure 2.8: Comparison of bell deformations with linear and nonlinear material properties in *Polyorchis*. Finite element model for *Polyorchis* created with nonlinear materials analogous to measured exponent ($x = 1.8$) allows a test of the role of nonlinear material properties in a single static deformation of the bell. The linear example is scaled to the same mean slope of the nonlinear relationship. Nonlinear materials allow greater deformations of the bell for smaller applied pressures, showing a four order of magnitude difference.

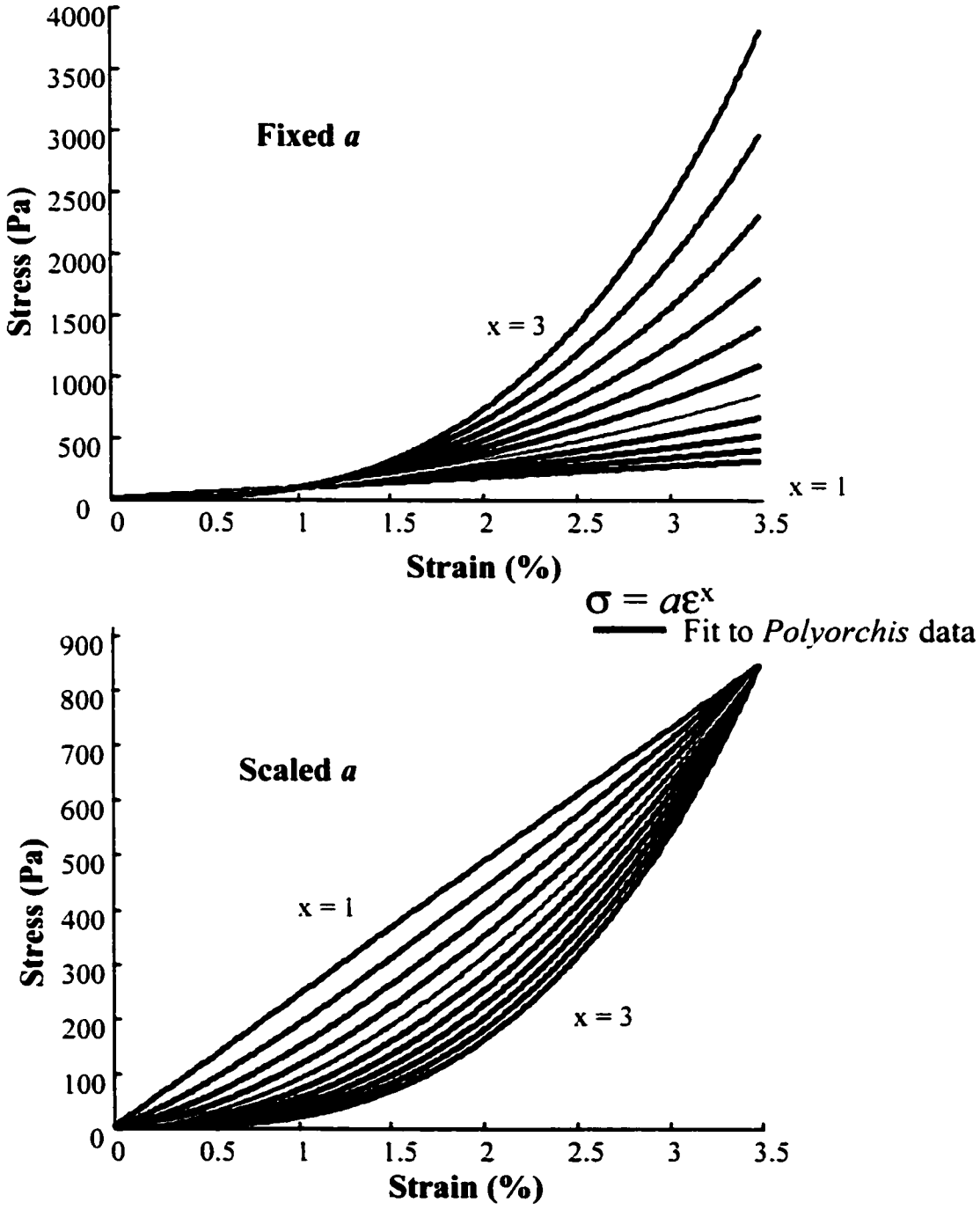

Figure 2.9-Scaling conserves mean modulus in numerical experiments with a nonlinear spring: As the magnitude the nonlinearity (x in this case) increases in the equation $\sigma = a\varepsilon^x$, a is scaled in order to maintain a constant mean slope. Note that in the absence of this scaling the stresses will far exceed the range measured for *Polyorchis* or *Mitrocoma* at strains well within the range of interest.

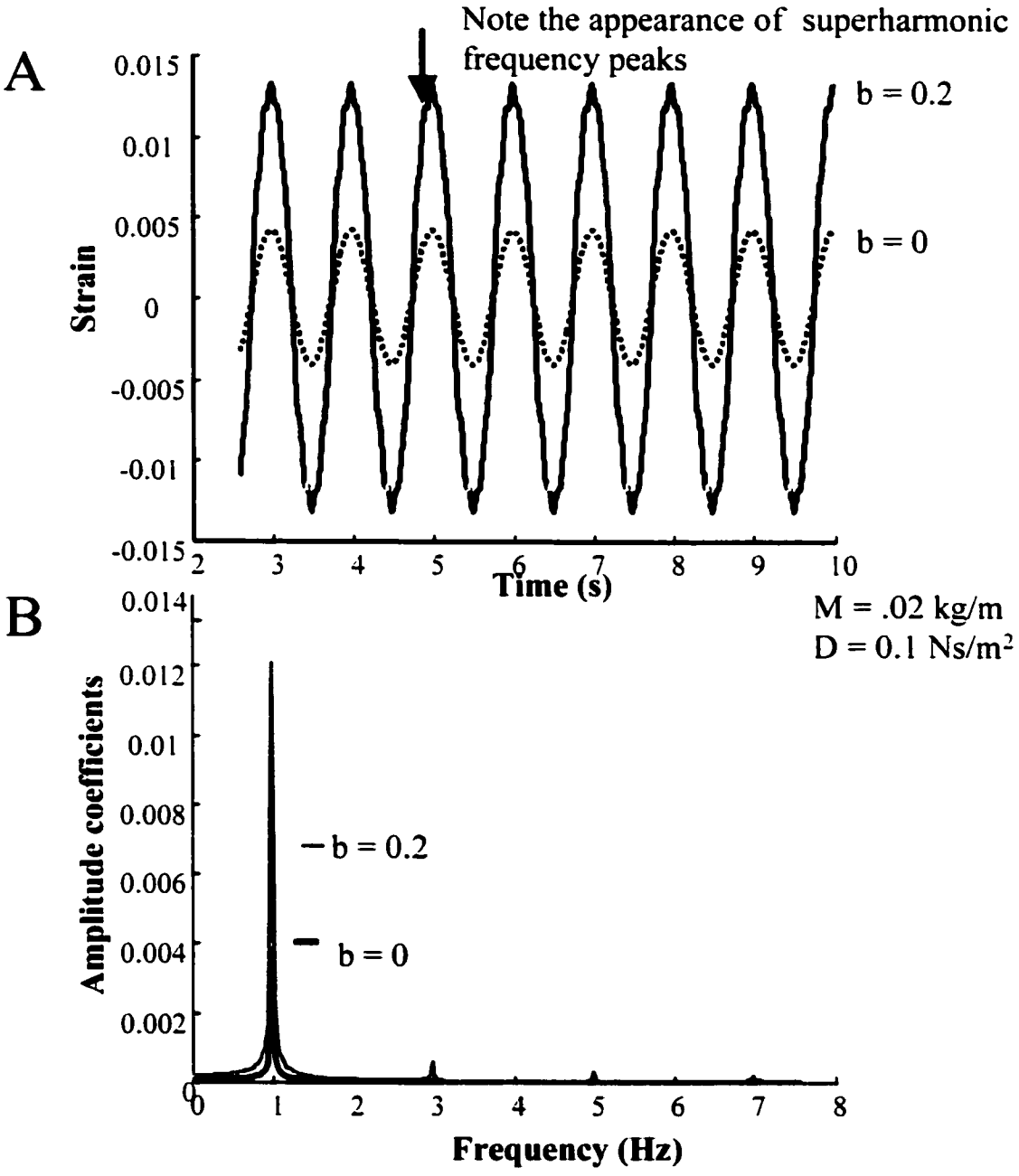

Figure 2.10-Comparison of linear and weakly nonlinear spring-mass systems: A) A weak nonlinearity (b = 0.2) such as that found in *Mitrocoma* increases the oscillation amplitude three-fold over the linear response (b =0) in the solution to equation 8. This nonlinearity also introduces a detectable secondary peak in the oscillation output. B) A Fourier transform quantifies the findings in 7a, showing a three-fold increase in amplitude at the driving frequency and a small secondary frequency component at 3 Hz.

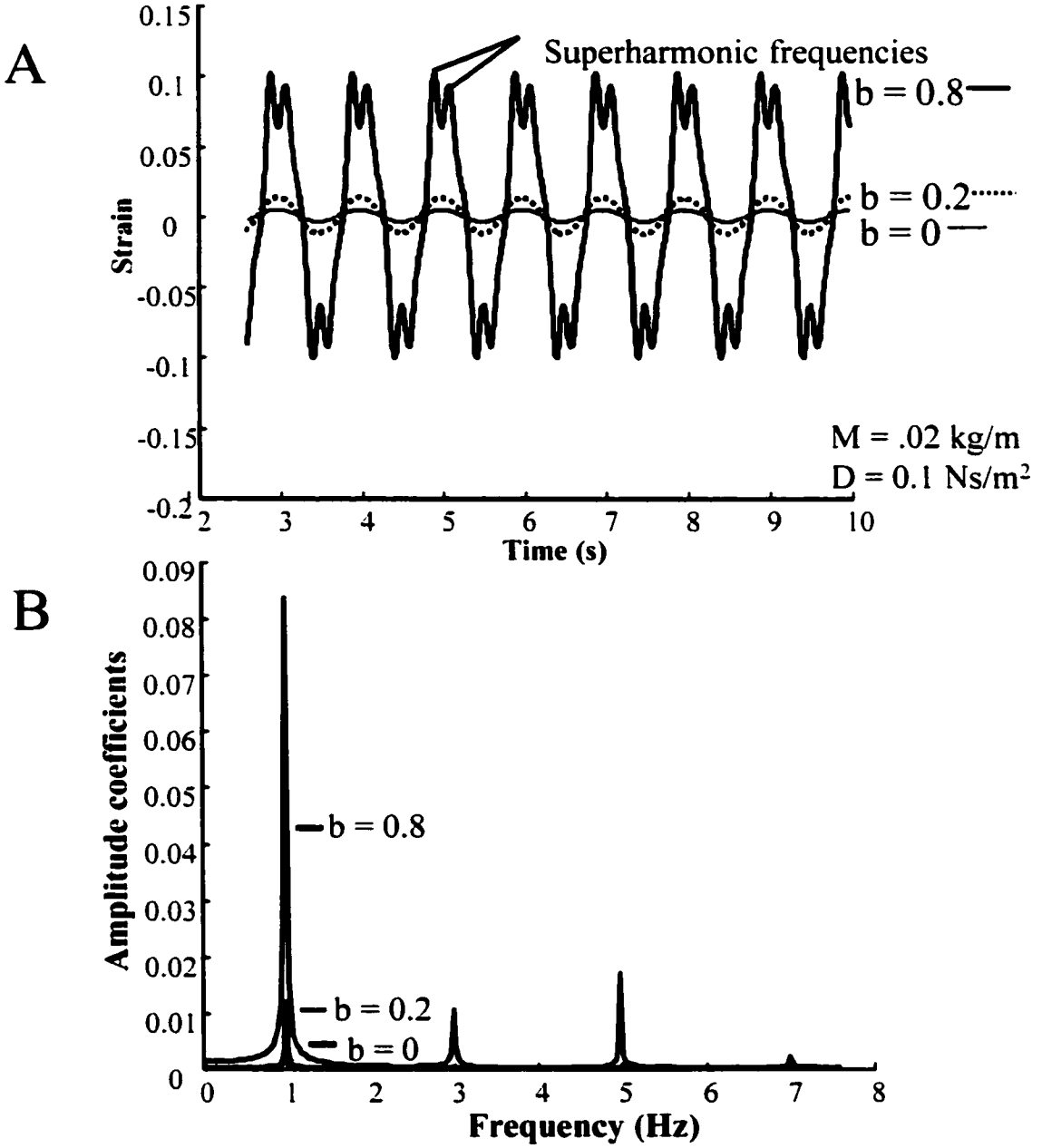

Figure 2.11 - Further comparison of linear and nonlinear spring-mass systems: A) With the addition of a third value for the nonlinear exponent equivalent to the measured exponent for *Polyorchis*, b = 0.8, oscillation amplitudes jump to almost 20x the oscillation amplitude in the linear case (*b* =0). Superharmonic peaks are extremely pronounced at this value for *b*. B) Fourier transform comparison of linear and nonlinear spring-mass systems: The Fourier transforms of these signals confirm a large amplitude augmentation at the driving frequency (1Hz) with a larger nonlinear exponent and reveals pronounced superharmonic frequencies at 3 and 5 Hz.

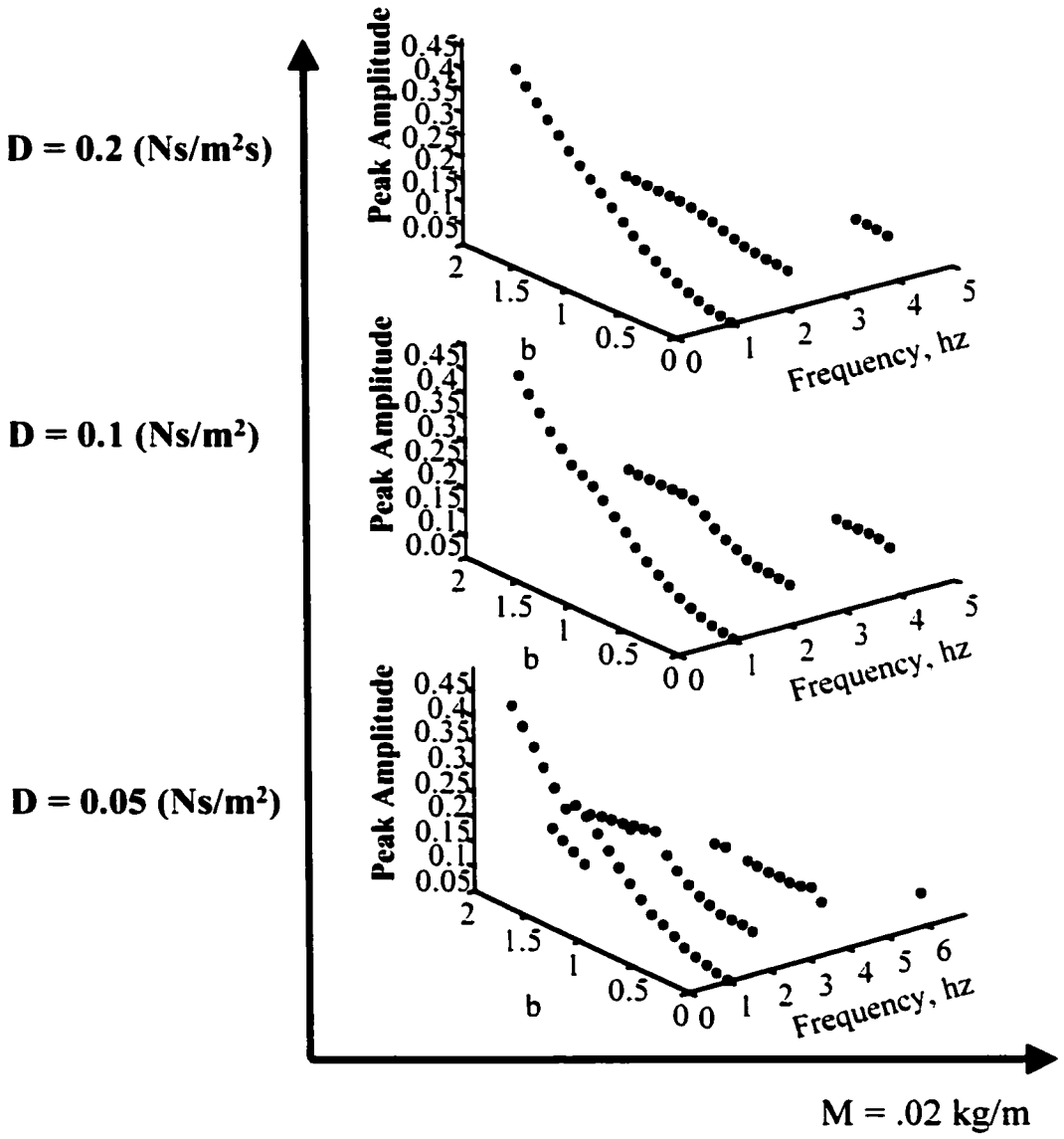

Figure 2.12- Fourier transform comparison of linear and weakly nonlinear spring-mass systems across a range of nonlinearities: Across a range of values for *b*, from the linear case *b* =0 to the cubic nonlinearity *b* =2, Fourier transforms show a monotonic increase in the peak amplitude at the driving frequency. Harmonics at 3 and 5 Hz are present for some values of *b* and, at low values for damping, a subharmonic frequency is also present for intermediate to high values for *b*.

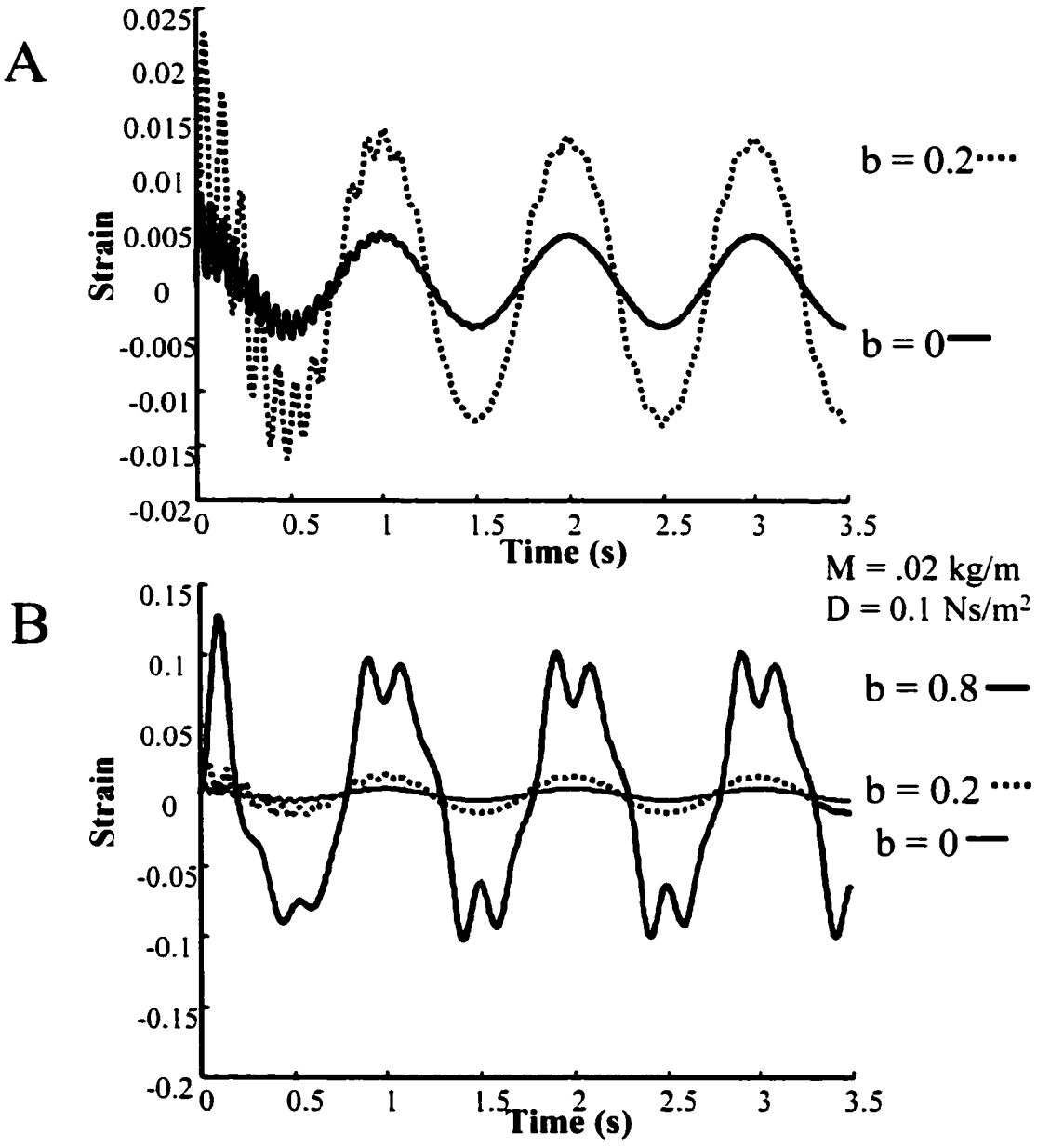

Figure 2.13-Transient oscillations in a nonlinear spring-mass system: A) Transient oscillations are more pronounced for the weakly nonlinear value of b =0.2 (*Mitrocoma*) but persist for the same amount of time as in the linear case. B) Transients are less pronounced in the case of $b = 0.8$ (*Polyorchis*) and, after the initial jump, subsequent cycles rapidly assume their steady state appearance.

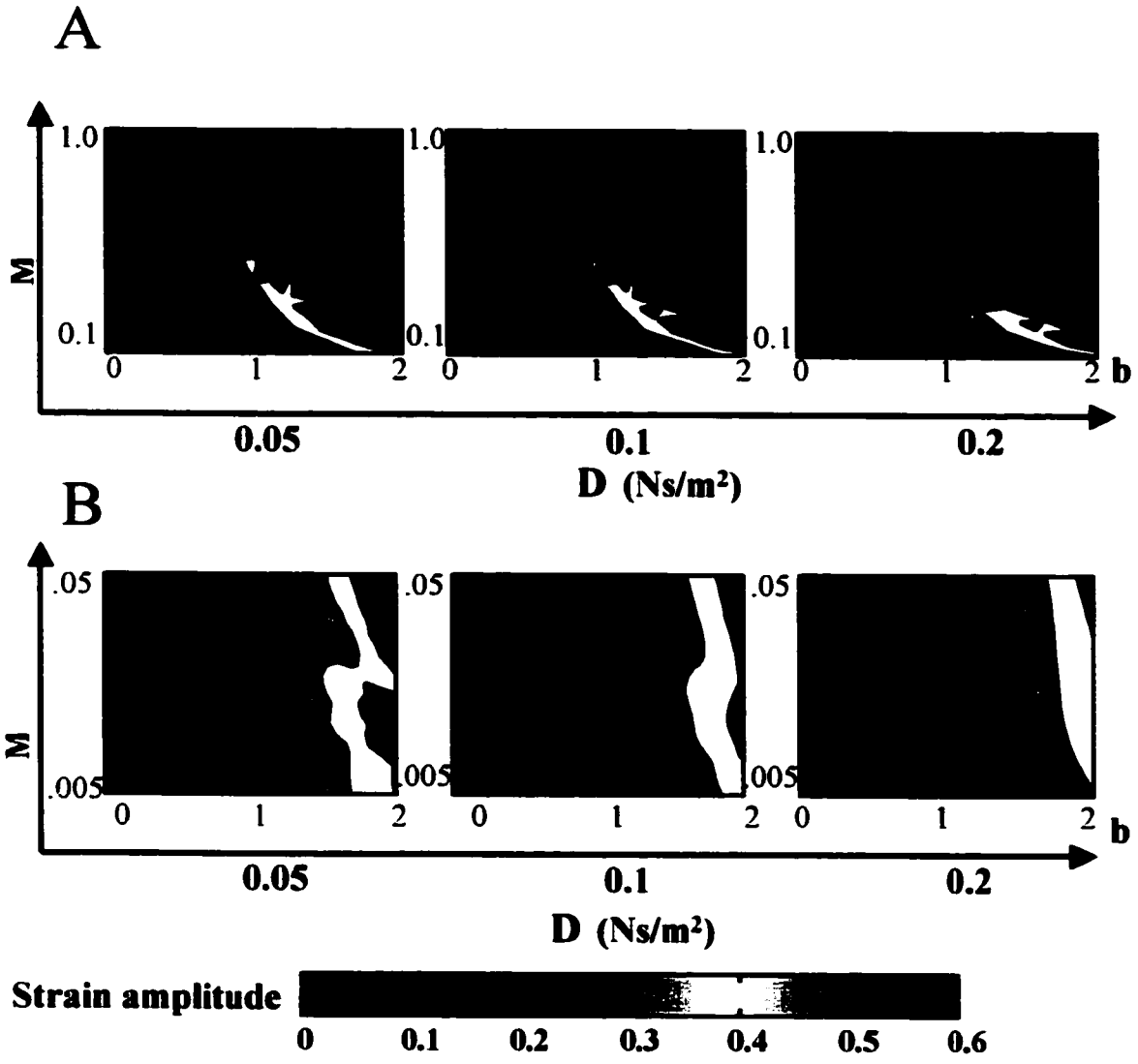

Figure 2.14 A,B—Oscillation amplitude variation with scaled spring mass (M) across a range of nonlinearities: A) Sampling a broad range of scaled mass values (M), oscillation amplitude increases with increasing nonlinearity at the low end of the range. This effect can be seen clearly in the plots below (B) which show a finely-sampled portion of this range. As the mass of the spring increases, the region of parameter space in which amplitude augmentation occurs narrows and shifts toward intermediate values for *b*, with high values for *b* showing no discernable amplitude increase.

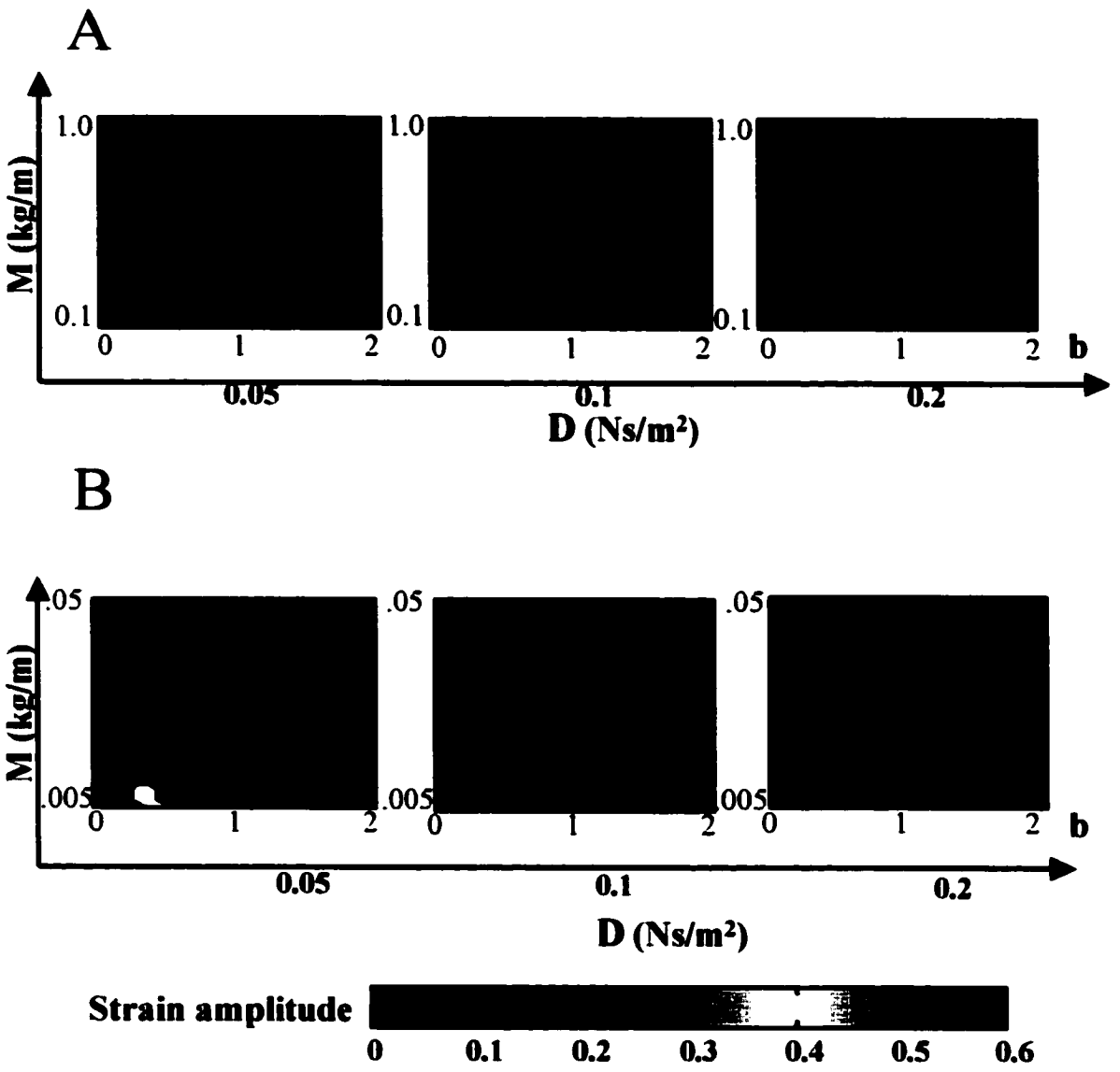

Figure 2.15 A, B-Peak variation per cycle across a range of mass values and nonlinearities: These plots show the number of peaks per cycle for a range of masses and nonlinear exponents. A) Across a broad range of mass values, there are few noticeable effects of mass or nonlinearity on the number of peaks/cycle. However, focusing closely on the low end of the mass range (B), there is a region at intermediate values for the *b* in which there is a clear increase in number of peaks per cycle which is also sensitive to the damping in the system.

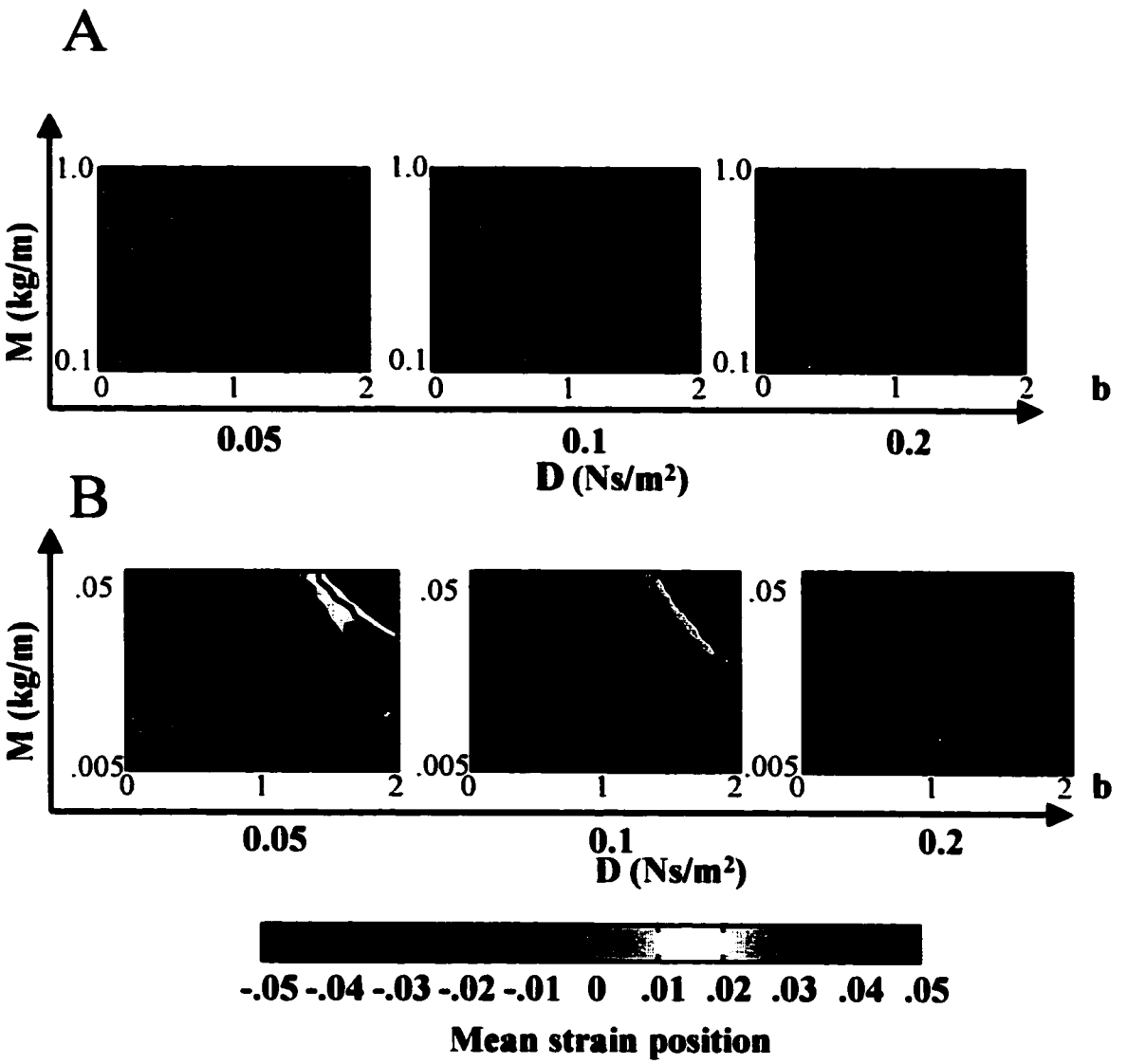

Figure 2.16 A, B-Variation in mean strain position across a range of mass values and nonlinearities: A) Mean strain position changes sporadically throughout a range of masses and nonlinear exponents. Focusing closely on the low end of the mass range (B), shifts in signal position in both the positive and negative position that occur at high values for the nonlinear exponent and low values of damping.

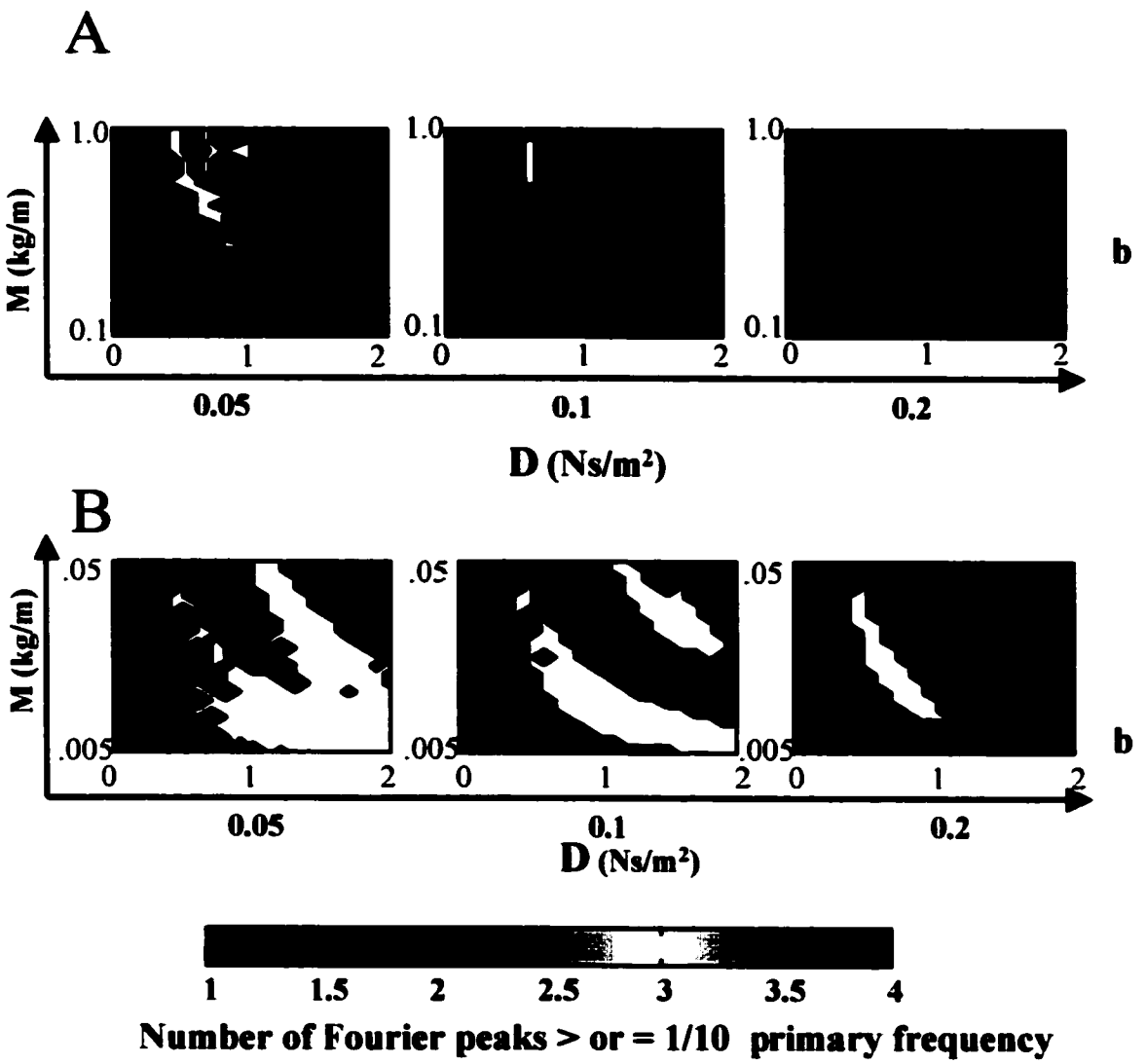

Figure 2.17 A, B -Fourier components across a range of mass values and nonlinearities: Fourier frequency components are more numerous at nonlinear values of *b* than for *b* =0. The number of peaks present is highly sensitive to the damping in the system.

Chapter 3:

A passive shift in mean bell position suggests that nonlinear resonance enables recovery from a hydrodynamic perturbation in the hydrozoan medusa *Mitrocoma cellularia*

Summary

Coupling the frequency of muscle activation with the resonant frequency of a locomotor structure leads to large oscillation amplitudes for small periodic forces and may enable considerable energetic savings for animals that range from invertebrates to mammals. Resonance tuning for the hydrozoan medusa *Polyorchis penicillatus* may reduce the energetic requirement for each cycle by 24-37% (DeMont and Gosline, 1988c). But, the nonlinear stress-strain relationship for mesoglea and for bell pressure-volume dynamics suggests that medusan dynamics may be more consistent with features of nonlinear resonant phenomena than with linear resonant phenomena. Many nonlinear systems have more that one resonant frequency and exhibit amplitude augmentation over a wider range of driving frequencies. Experimental perturbation of hydrozoan *Mitrocoma cellularia*, through manipulation of seawater viscosity, tests whether emergent responses are more consistent with nonlinear or linear resonant behavior because predicted responses to an increase in external damping differ between linear and nonlinear systems. A resultant shift in bell position (mean bell diameter), in which greater forces may be available for small displacements, without a concurrent shift in

driving frequency, suggests that passive exploitation of strain-dependent bell stiffness may enable recovery from perturbation. A recovery mechanism that does not rely on neural feedback is consistent with predictions of nonlinear resonant phenomena.

Introduction

When the periodic driving force of a physical system matches its natural or resonant frequency, the amplitude of oscillation is disproportionately large for repeated applications of a small force (DeMont and Gosline, 1988c). In the design of structures such as bridges, driving the system at its resonant frequency is a practice to be avoided—the collapse of "Galloping Gertie" (the Tacoma Narrows Bridge) during a windstorm in 1940 being a strong case in point. But, in the design of biological dynamical systems, tuning the driving force of muscular contraction to exploit the natural frequency of its passive structures can confer significant energetic savings, allowing an increase in oscillation amplitude with no additional input of mechanical work (Timoshenko et al., 1974).

Terrestrial animals such as hopping kangaroos and galloping quadrupeds derive energetic savings from muscular activation at or near their resonant frequencies, with elastic energy stored and returned in tendons—which act as mechanical springs (Farley et al., 1993). Running humans can also optimize performance with compliant running surfaces that can be fabricated such that the relationship between stride frequency and elastic energy storage and recoil is optimized (McMahon and Greene, 1979). Additionally, a wide range of birds and mammals couple the resonant frequency of their

respiratory system to the resonant frequency of the locomotor system (locomotor/respiratory entrainment) to minimize any phase interference between locomotor and ventilatory cycles and economize the work of both sets of muscles (Nassar et al., 2001).

In swimming animals, such as scallops and jellyfish, materials such as hinge ligament and mesoglea store and return elastic strain energy and act as muscle agonists (DeMont, 1990; DeMont and Gosline, 1988b). In both animals, the frequency of muscle activation is at or near the resonant frequency of their mechanical springs (DeMont and Gosline, 1988c). For the jellyfish *Polyorchis penicillatus*, a simple model of the bell as a damped harmonic oscillator suggests that swimming at the resonant frequency of the locomotor apparatus would yield an increase in oscillation amplitude of 40% and a reduction in the energetic requirement of a single cycle by 24-37% (DeMont and Gosline, 1988c).

Biological materials that act as elastic springs in locomotion, such as tendon and mesoglea, have nonlinear stress/strain relationships with characteristic strain-stiffening or J-shaped curves (Alexander, 1962; De Zee et al., 2000; DeMont and Gosline, 1988a; Gladfelter, 1972; Koehl, 1977). Such materials show dynamic motions responding to periodic forces that significantly differ from simple linear systems. A nonlinear spring does not have a single resonant frequency (ω), defined as $\sqrt{\frac{k}{m}}$, where k is the spring constant and m is the mass of the spring, because k depends on the displacement of the spring. As in a linear system, resonance in a nonlinear system results in a substantial

increase in oscillation amplitude for a given frequency of excitation, but may occur at various intervals of the excitation frequency (Schmidt and Tondl, 1986).

Both linear and nonlinear systems are sensitive to damping. In a linear system, an increase in damping reduces the oscillation amplitude and causes the resonant frequency of the system to shift to a lower value (Timoshenko et al., 1974). For a linear system that is tuned to its resonant frequency, a shift in the driving frequency would be required in order to recapture resonant tuning. In a nonlinear system, an increase in damping would transiently decrease the oscillation amplitude. But, the existence of multiple resonant frequencies introduces the possibility that a passive shift in oscillation position could exploit a different range of resonant frequencies.

Here, I explore the effect of damping in the context of nonlinear resonance using hydrozoan jellyfish *Mitrocoma cellularia* as a physical example of a nonlinear mass-spring system. I examine *Mitrocoma*'s response to a hydrodynamic perturbation that increases the damping in the system, an abrupt increase in the viscosity of seawater, to assess whether its dynamic response is more consistent with predictions of a linear or nonlinear resonant system. This manipulation attempts to distinguish between two scenarios: 1) If the medusan bell operates as a linear resonant system, one might expect either an unrecoverable decrease in oscillation amplitude or a shift in driving frequency of the bell to match the single shifted resonant frequency. While bell frequency changes over ontogeny, rapid changes in bell frequency are uncommon due to the unique neuromusculature of hydrozoan myoepithelial cells (Spencer and Satterlie, 1981). 2) If the medusan bell operates as a nonlinear resonant system, continuous variation in the

spring constant as a function of bell position (mean diameter) might enable a recovery of normal oscillation amplitude without a change in the driving frequency of contraction. Alteration of seawater viscosity represents physical challenge to the medusa that will probe its dynamic response to perturbation.

Materials and Methods:

I collected representative medusae of the species *Mitrocoma cellularia* off the docks at Friday Harbor Laboratories in Friday Harbor, WA and maintained them in individual beakers in a flow table, at the temperature of ambient seawater.

In a temperature controlled ten-gallon glass tank, I filmed each medusa with a single Sony CCD analog camera from a frontal view for twenty minutes under each of three treatments: 1) Baseline; which described as each medusa's pre-treatment swimming in unmanipulated 0.22 μm filtered seawater, with each medusa serving as its own control; 2) Acute; which described the first detectable bell contractions after transfer to 50% more viscous seawater (methods for altering seawater viscosity are described below. (3) Steady state; which described medusan swimming behavior after remaining in the altered viscosity seawater for a minimum of two hours. After each sequence of treatments, I returned each medusa to normal seawater to determine if normal swimming behavior was recovered after the viscosity treatment.

Manipulation of seawater viscosity

I increased seawater viscosity by 50% by adding polyvinyl pyrrolidone (PVP; MW 360,000; Sigma Chemical Co.). PVP is an appropriate agent for manipulating viscosity as it is 1) Newtonian; 2) Not toxic (Podolsky and Emlet, 1993); and 3) Does not significantly alter the osmolarity of the solution.

An acute 50% change in viscosity was sufficient to perturb the animal's normal swimming kinematic without falling outside of the range of environmentally realistic seawater viscosities. Over a temperature range of 0°C to 30°C, at a constant salinity of $30^{o}/_{oo}$, the viscosity of seawater varies ~75% (Dorsey, 1940). This sudden change in viscosity, however, decoupled from a concurrent change in temperature, constitutes a physical challenge to the animal and was not an attempt to mirror viscosity changes across an environmental gradient. A concentration of 3.9 g/L PVP was required to raise the viscosity of seawater by 50% (Figure 3.1).

I used a falling ball viscometer (Gilmont Instruments, GV-2100) to measure changes in seawater viscosity. A viscometer converts the measured descent time of a stainless steel ball to absolute viscosity (μ) in centipoises (cp) (10^{-2}*g/cm*s) by the following relationship.

$$\mu = K(\rho_b - \rho)t$$

where ρ_b is the density of the stainless steel ball, ρ is the density of the liquid, t is the descent time of the ball through the liquid in minutes, and K is the viscometer constant. K is determined by measuring the time of descent for a liquid of known viscosity most

similar to the unknown solution and substituting in equation 1 above. To calculate K, I used seawater precisely maintained at 10°C, which has a known viscosity of $\mu = 1.38$ cp (Dorsey, 1940). The descent time (t), in all viscosity determinations, was the average time of ten trials.

Video analysis

For video clips of each of the baseline, acute, and steady state treatments, I identified usable bouts of swimming behavior, where there were at least four sequential rhythmic contractions in which there was no rotation of the animal out of the film plane. Bout sequences were stored digitally (Adobe Premiere 5.0, Quick Time Pro). Video clips were then hand-digitized using a routine written in Matlab 5.0 by M.S. Tu, which tracks coordinates in successive images. I measured the maximum bell diameter in each frame of each clip, defined as the two points on the perimeter of the bell opening which were furthest away from each other and approximately opposite each other on the bell.

To correct for any translation in plane of motion toward and away from the camera, I measured the distance between the bell apex and the manubrium (~1/3 total bell height) as a metric that does not change with the contraction of the bell. If there were any variations in this distance within or between clips for a given individual, bell distance measures were corrected according to the smallest value for the apex-manubrium distance, when the distance between the camera and the jellyfish was maximum and the potential effects of parallax minimized. Responses to treatment effects were then evaluated for each individual against its own baseline swimming

behavior, to avoid any potential effects of size variation between individuals.

A custom written routine in Matlab (Appendix B) converted coordinates to bell diameters for each frame digitized. To find the maxima and minima of each cycle, I used a third order Butterworth filter to eliminate noise introduced by digitizing error. As each cycle within a bout did not necessarily have an identical period, I found the cycle with the smallest period and then resampled the other cycles using a cubic spline to give the same number of time steps in each cycle. The resulting bell diameters were then averaged at each time point to produce a "composite cycle" for each clip.

From this composite cycle, I tracked the maximum and minimum of bell diameter (the average maximum and average minimum of the original filtered signal), the amplitude of diameter changes, and the mean bell diameter (position). I calculate average contraction frequency of each clip from the average time (period) between cycle peaks. For each temporal set of diameters, I use a Fourier transform to compare the signal composition between baseline and treatment conditions.

Results:

Bell amplitude

Bell swimming amplitude decreases significantly as an acute response to increased seawater viscosity (Wilcoxin Signed Rank test, $p = 0.018$, Statview 5.0.1). But, at steady state (recovered), there is no significant difference from the baseline amplitude (Wilcoxin Signed Rank test, $p = 0.398$, Statview 5.0.1) (Figure 3.2).

Bell frequency

Bell frequency does not change significantly as an acute response to increased seawater viscosity, although there is a trend towards a slight increase in frequency (Wilcoxin Signed Rank test, $p = 0.24$, Statview 5.0.1). If it really exists, this increase is likely to be the result of transient errors in muscle timing induced by the perturbation, rather than a true frequency shift. At steady state, bell frequency is nearly identical to baseline frequency (Wilcoxin Signed Rank test, $p = 0.735$, Statview 5.0.1) (Figure 3.3). A Fourier analysis of these data confirms that there is no difference between the basic harmonic bell frequency in a perturbed v. unperturbed state.

Bell position

Mean bell position, measured as the mean bell diameter, does not change significantly as an acute response to increased seawater viscosity (Wilcoxin Signed Rank test, $p = 0.735$, Statview 5.0.1) nor as a steady state long-term response (Wilcoxin Signed Rank test, $p = 0.612$, Statview 5.0.1) (Figure 3.4). However, a closer look at these data reveals that under both acute and steady state conditions the mean bell position of each individual medusa does shift in either the positive or negative direction in relation to the baseline (Figure 3.5, 3.6). This shift away from baseline position is more apparent under acute than steady state conditions and is slightly stronger in the positive direction (with the mean bell position enlarged from its baseline condition). An alternate model to statistically validate this finding is still pending. A shift of this magnitude, in either the

positive or negative direction, could enable a medusa to resist a perturbation by passively exploiting the bell's nonlinear response to an applied strain.

Discussion

In response to the hydrodynamic perturbation of increased seawater viscosity, medusae of the species *Mitrocoma cellularia*, respond with a transient, but recoverable, decrease in bell amplitude, no frequency shift, and no overall change in the mean position of the bell, but some treatment-induced variation. Medusae provide a simple example of a nonlinear resonant system (DeMont and Gosline, 1988c; Pabst, 1996) and these results inform a qualitative assessment whether the response is more consistent with linear v. nonlinear resonant behavior.

In a linear resonant system, where there is a single spring constant, k, that describes the whole system, the resonant frequency, $\omega = \sqrt{\frac{k}{m}}$, is weakly dependent on increased damping (Timoshenko et al., 1974). An increase in seawater viscosity, which increases the damping in the system, would cause a decrease in bell amplitude. Recovery of normal oscillation amplitude would require neural feedback, resulting in a change in the frequency, duration, or strength of muscular contraction. Such a shift in frequency or contraction duration was not observed in response to altered seawater viscosity. While the strength of muscular contraction could not be compared between baseline and

treatment conditions, such real-time muscle force modulation is not consistent with the anatomy of hydrozoan myoepithelial cells (Spencer and Satterlie, 1981).

The nonlinear nature of medusa may afford a mechanism for recovery that does not necessitate neural feedback and merely exploits the passive mechanical properties of the bell. In a nonlinear relationship between force and displacement (x), spring constant k varies with x. Thus, over a range of displacements, there are multiple spring constants and thus multiple frequencies. As the range grows smaller, the resonant behavior will approach that of a linear system, although not necessarily with the same spring constant of a system scaled to the same mean slope across the entire range (Figure 3.7A).

Extending this argument to the swimming medusa, merely modifying the range over which it contracts (a shift in mean bell position) would result in a shift in the resonant frequencies of the system (Figure 3.7B). In light of the strain-stiffening or J-shaped curve that describes both the material properties of mesoglea and the pressure-volume relationship of the bell as a whole (DeMont and Gosline, 1988b), a shift in mean bell position, in either the positive or negative direction, would move the bell into a steeper region of the curve, with larger values for the spring constant k. The magnitude of change in the effective spring constant of the bell with a shift in mean bell position would depend on the particular strength of nonlinearity. A stiffer spring, sufficiently deformed by muscular contraction, might be able to provide the elastic recoil necessary to overcome the increased viscosity of the medium and restore the bell to its normal swimming amplitude.

In nonlinear systems, the presence of multiple regions of amplitude augmentation for a range of excitation frequencies allows resonance tuning between the driving frequency and natural frequencies to be somewhat less constrained. In a linear resonant system, amplitude augmentation only occurs when the driving frequency closely matches the natural frequency of the system. A nonlinear system, in contrast, has multiple resonant frequencies and can exhibit amplitude augmentation for driving frequencies close to the natural frequencies of the system or, if the excitation frequency contains several components, for driving frequencies far from any natural frequency of the system. Thus, even without modulation of the driving frequency of the bell, a shift in mean bell position that changes the range of resonant frequencies over which the jellyfish is operating is consistent with the possibility of tuning between the driving frequency and resonant frequencies of the system.

Experimental evidence indicating a lack of permanent shift in the driving frequency of the bell in response to increased viscosity, in conjunction with an apparent recovery of a normal oscillation amplitude, suggests that the medusan bell is not consistent with the dynamics of a linear resonant system. A shift in mean bell position offers an appealing explanation for the apparent recovery of the medusa through concepts that are in keeping with nonlinear resonant phenomena, but does not provide a definitive link all the way from the level of neural control to hydrodynamics. Such a link would require a detailed study that includes the nervous system, muscles, and fluid dynamics connected by an integrated theoretical framework.

Perturbation of a swimming medusa by an experimental manipulation of seawater viscosity presents an example of what dynamics might emerge under various types of perturbations. In conjunction with the theoretical experiment presented in Chapter 2, incorporating nonlinear spring in a simple dynamical system (Equation 3.7), I show that nonlinearity offers a suite of dynamic possibilities not available to linear systems. Insights from the simpler cases, presented in this chapter and in Chapter 2, will inform Chapter 4, which incorporates material nonlinearities in a full model of a swimming jellyfish to explore the consequences of nonlinearity in terms of swimming velocity as a metric of medusan swimming performance.

Notes to Chapter 3

Alexander, R. M. (1962). Visco-elastic properties of the body-wall of sea anenomes. *Journal of Experimental Biology* 39, 373-386.

De Zee, M., Bojsen-Moller, F. and Voigt, M. (2000). Dynamic viscoelastic behavior of lower extremity tendons during simulated running. *Journal of Applied Physiology* 89, 1352-1359.

DeMont, M. E. (1990). Tuned oscillations in the swimming scallop *Pecten maximus*. *Canadian Journal of Zoology* 68, 786-791.

DeMont, M. E. and Gosline, J. M. (1988a). Mechanics of jet propulsion in the hydromedusan jellyfish *Polyorchis penicillatus*: I. Mechanical properties of the locomotor structure. *Journal of Experimental Biology* 134, 313-332.

DeMont, M. E. and Gosline, J. M. (1988b). Mechanics of jet propulsion in the hydromedusan jellyfish *Polyorchis penicillatus*: II. Energetics of the jet cycle. *Journal of Experimental Biology* 134, 333-345.

DeMont, M. E. and Gosline, J. M. (1988c). Mechanics of jet propulsion in the hydromedusan jellyfish *Polyorchis penicillatus*: III. A natural resonating bell; The presence and importance of a resonant phenomenon in the locomotor structure. *Journal of Experimental Biology* 134, 347-361.

Dorsey, N. E. (1940). *Properites of Ordinary Water Substance*: Litton Educational Publishing, Inc.

Farley, C. T., Glasheen, J. and McMahon, T. (1993). Running springs: Speed and animal size. *Journal of Experimental Biology* 185, 71-86.

Gladfelter, W. B. (1972). Structure and function of the locomotory system of *Polyorchis montereyensis* (Cnidaria, Hydrozoa). *Helgolander wiss. Meeresunters* 23, 38-79.

Koehl, M. A. R. (1977). Mechanical diversity of connective tissue of the body wall of sea anenomes. *Journal of Experimental Biology* 69, 107-125.

McMahon, T. A. and Greene, P. R. (1979). The influence of track compliance on running. *Journal of Biomechanics* 12, 893-904.

Nassar, P. N., Jackson, A. C. and Carrier, D. R. (2001). Entraining the natural frequencies of running and breathing in guinea fowl (*Numida meleagris*). *Journal of Experimental Biology* 204, 1641-1651.

Pabst, D. A. (1996). Springs in swimming animals. *American Zoologist* 36, 723-735.

Podolsky, R. D. and Emlet, R. B. (1993). Separating the effects of temperature and viscosity on swimming and water movement by sand dollar larvae (*Dendraster excentricus*). *Journal of Experimental Biology* 176, 207-221.

Schmidt, G. and Tondl, A. (1986). *Non-Linear Vibrations.* Cambridge: Cambridge University Press.

Spencer, A. N. and Satterlie, R. A. (1981). The action potential and contraction in subumbrellar swimming muscle of *Polyorchis penicillatus* (Hydromedusae). *Journal of Comparative Physiology A.* 144, 401-407.

Timoshenko, S., Young, D. H. and Weaver, W. J. (1974). *Vibration Problems in Engineering.* New York: John Wiley & Sons.

Table 3.1: Parameters used in calculating seawater viscosity with a falling ball viscometer

K	0.231
ρ (g/ml) at 10°C	1.025
ρ_b (g/ml)	8.02

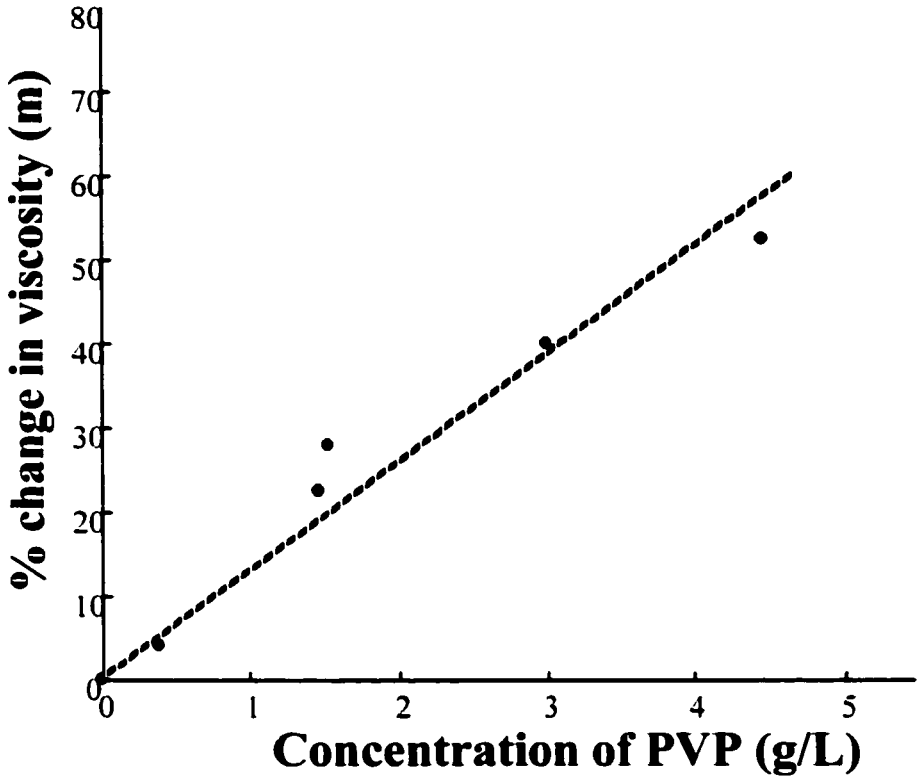

Figure 3.1: Percent change in viscosity as a result of PVP addition. This calibration was applied to determine amount of PVP to add to the ten-gallon tank. Serial dilutions with 0.22 mm filtered seawater were followed by precise measurements of resultant viscosity with a falling ball viscometer (Gilmont Instruments, GV-2100) to achieve desired viscosity change.

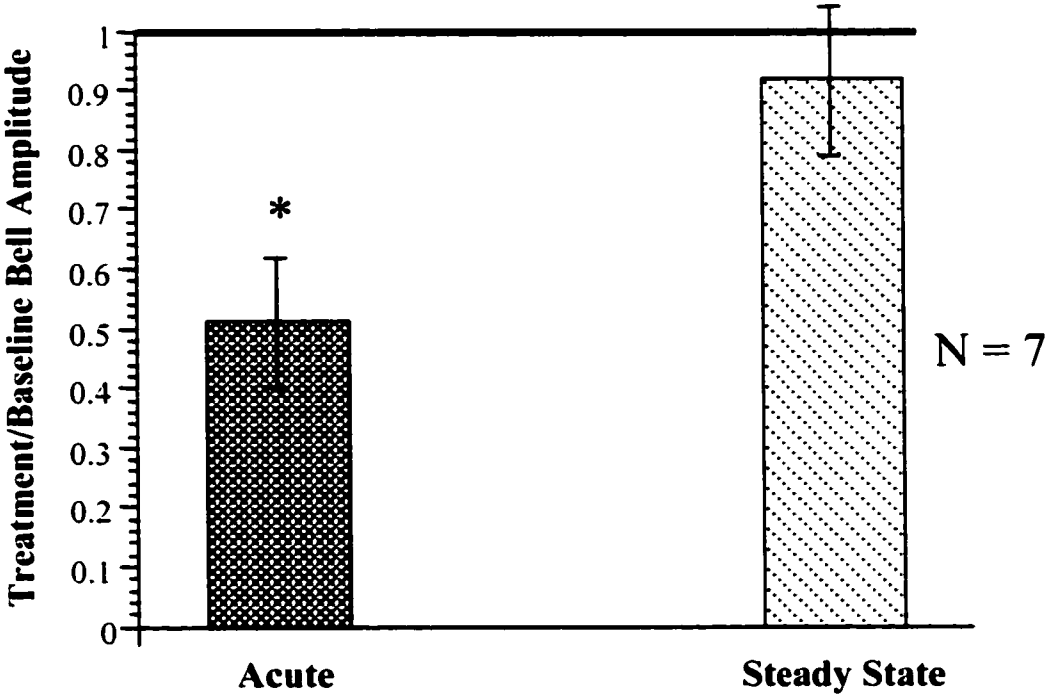

Figure 3.2: Effect of change in seawater viscosity on bell amplitude. A 50% increase in seawater viscosity causes a significant decrease in bell amplitude in an acute response, followed by a return to near-baseline bell amplitude in the steady state response (Wilcoxin Signed Rank test, $p = 0.018$, Statview 5.1.2). Error bars are S.E. Treatment response is scaled to the baseline bell amplitude of a given individual. Y-axis reports the fraction of the baseline amplitude with a ratio of 1 indicating no change.

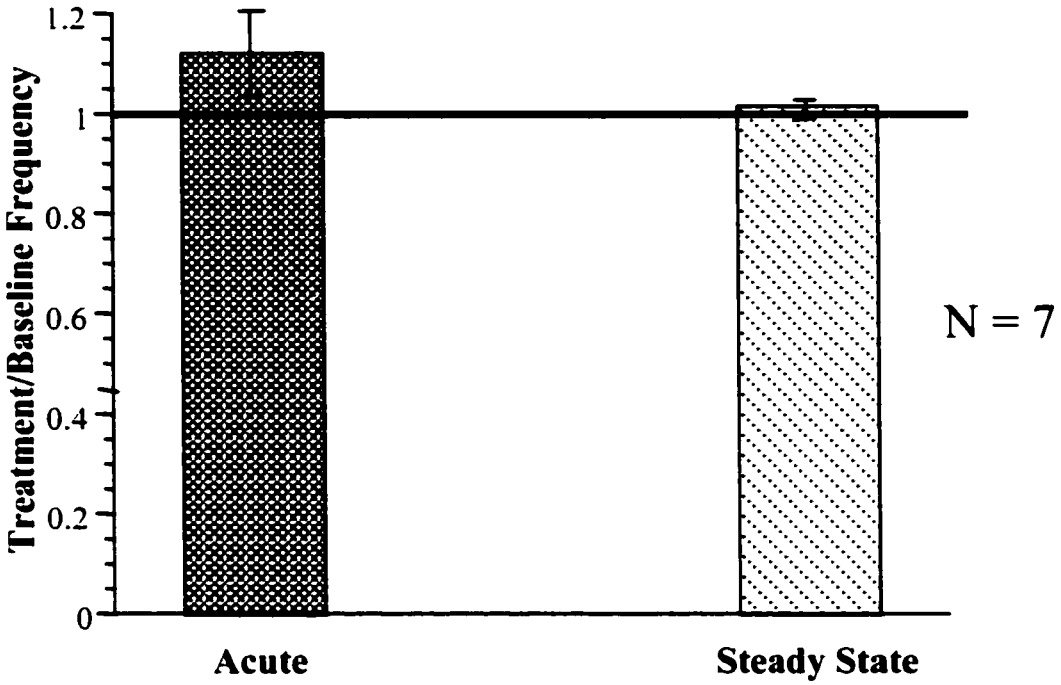

Figure 3.3: Effect of change in seawater viscosity on contraction frequency. A 50% increase in seawater viscosity leads to no significant difference from baseline bell frequency, although there is a trend toward increasing frequency in an acute treatment response. Error bars are S.E. At steady state, bell frequency is nearly identical to the baseline frequency of each individual. Treatment response is scaled to the baseline frequency of a given individual. Y-axis reports the fraction of the baseline frequency with a ratio of 1 indicating no change.

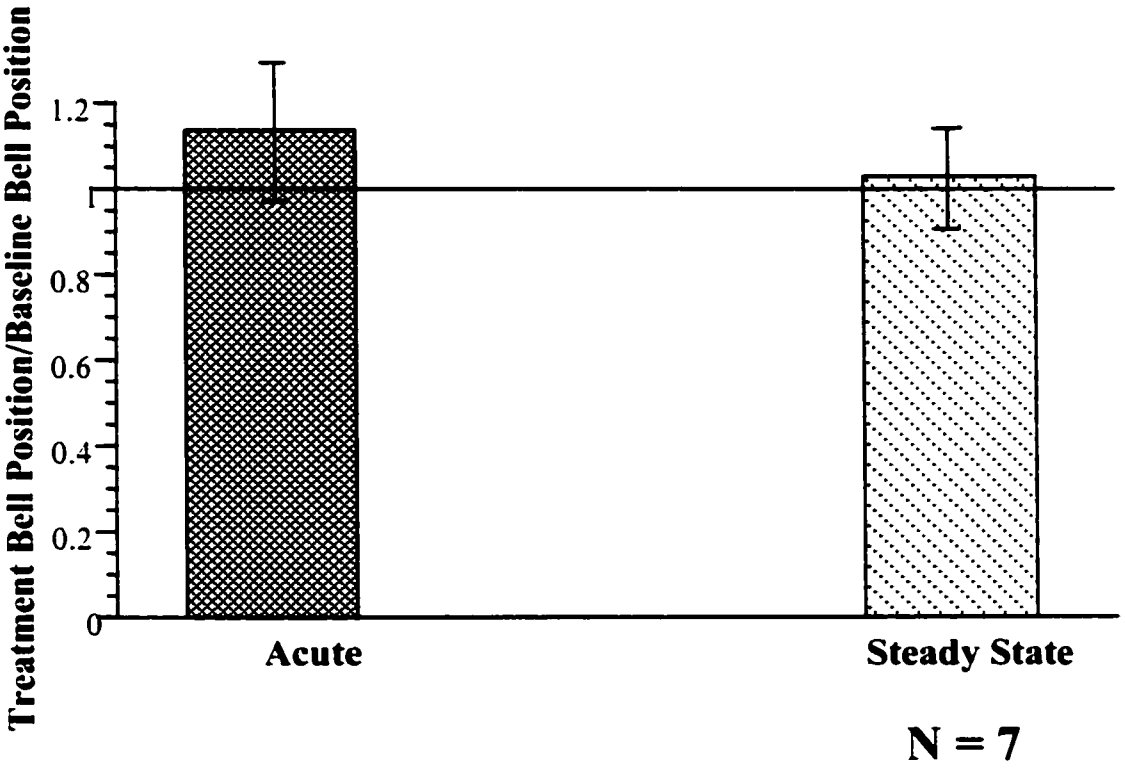

Figure 3.4: Effect of change in seawater viscosity on mean bell position. A 50% increase in seawater viscosity leads to no significant difference in mean bell position. Error bars are S.E. But, in the acute response to treatment, there is a trend toward a positive shift in bell position, with a large amount of variation. Treatment response is scaled to the baseline position of a given individual. Y-axis reports the fraction of the baseline position with a ratio of 1 indicating no change.

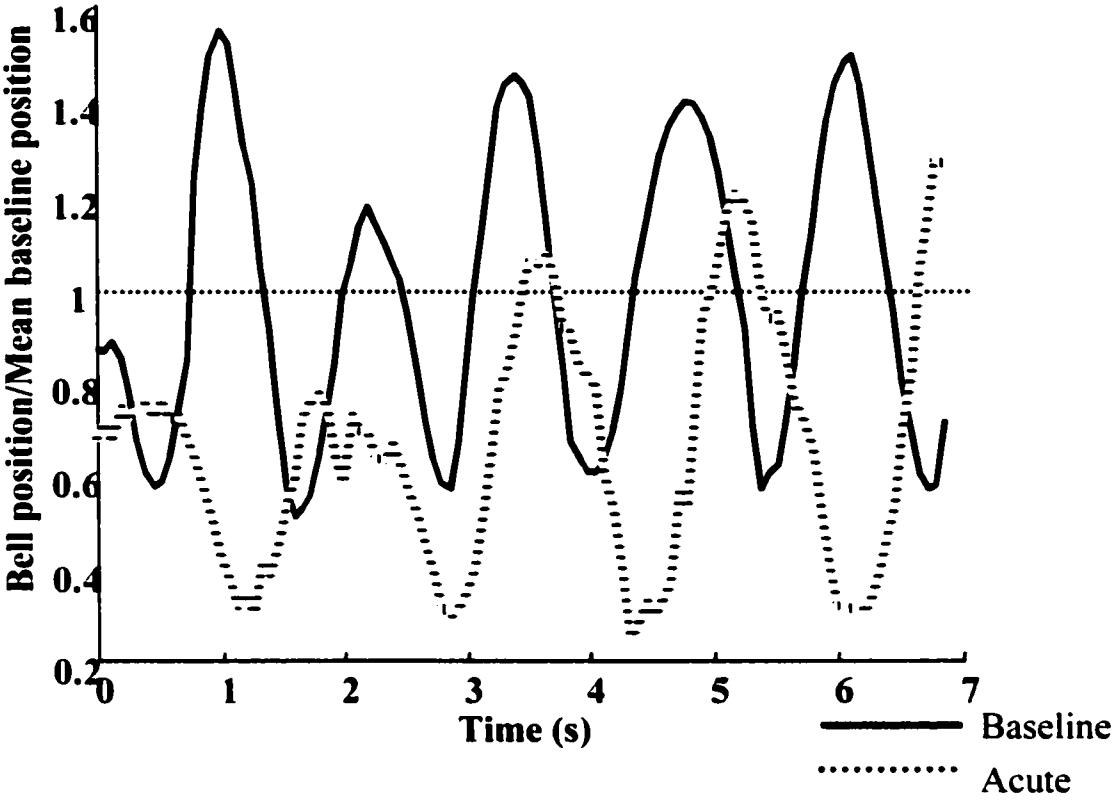

Figure 3.5: Example of increased viscosity on mean bell position. Sample digitized sequence showing a decrease in mean bell position between baseline and an acute response to a 50% increase in seawater viscosity. Treatment signal is scaled to the mean of the baseline sequence.

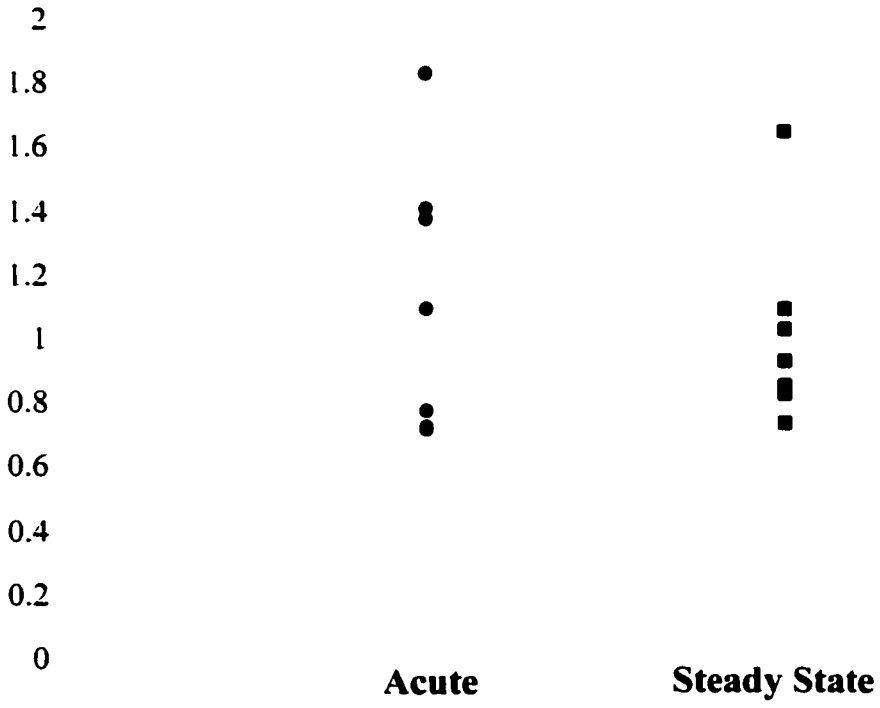

Figure 3.6: Variation in mean bell position with increase in viscosity. While there was no significant absolute shift in bell position as a response to increased seawater viscosity, there is variance around the mean in both the positive and negative direction. This is more pronounced in the acute than steady state treatment. Position shifts in either direction could force the jellyfish to operate at a different strain range and differentially exploit position-dependent bell stiffness.

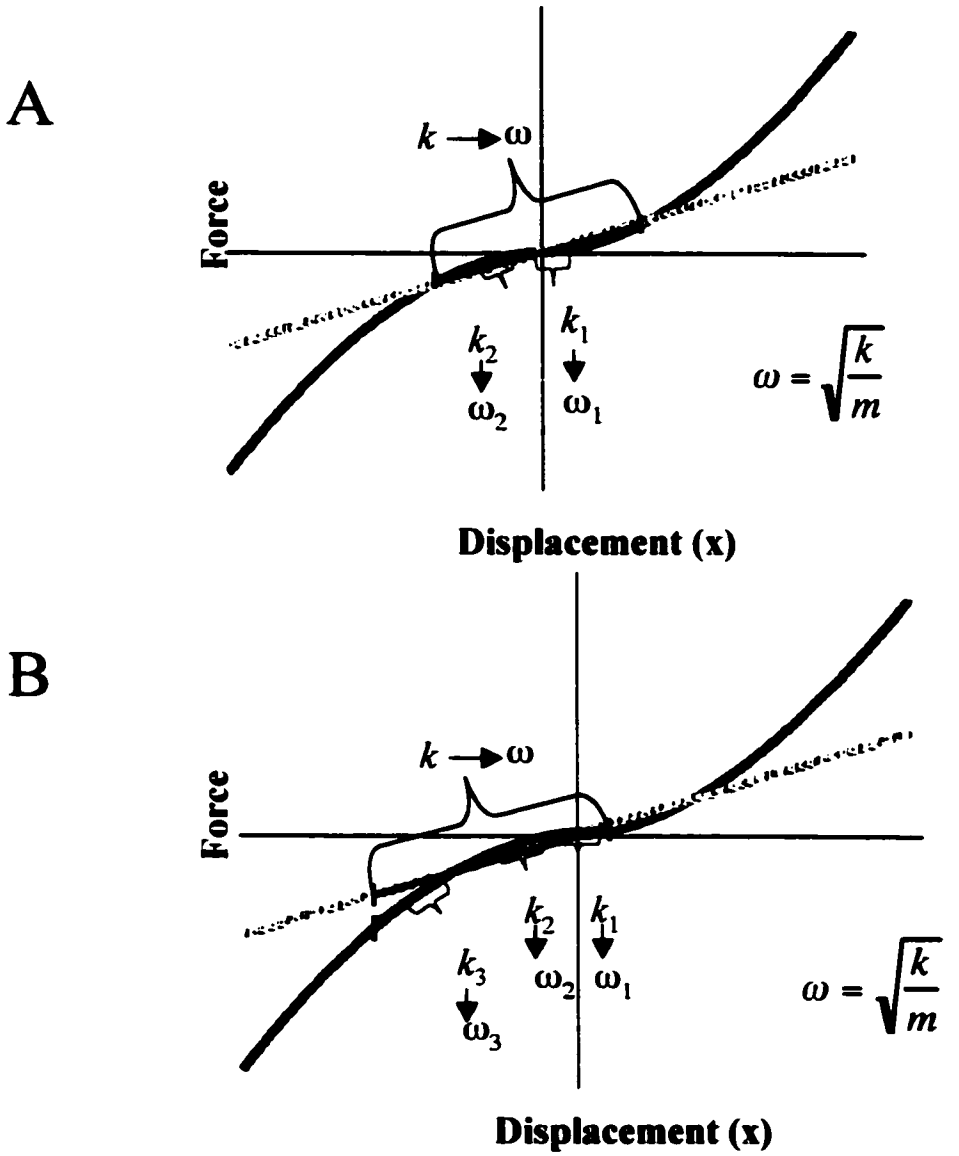

Figure 3.7 A,B: Position sensitivity of nonlinear force-displacement curve A) Comparison of a nonlinear and a linear force-displacement curve illustrates position-sensitivity of the resonant frequency in the nonlinear case. Over a given range, a linear spring will have only one spring constant and one resonant frequency for any given mass. In contrast, the spring constant of a nonlinear spring depends on position, and will thus vary continuously. B) A shift in mean bell position in either direction, as observed in the altered-viscosity perturbation experiment, would shift the operational range of the bell to a different part of the curve. In the linear case, this shift would not change the resonant frequency of the spring. In the nonlinear case, a position offset might provide an effectively stiffer spring constant that might store sufficient potential energy to resist the increased damping of the environment and restore bell amplitude to its pre-treatment value.

Chapter 4:

Tuning for swimming performance in hydrozoan jellyfish depends on nonlinear material properties and temporal patterns of force production

Summary

Composite swimming behavior of hydrozoan jellyfish incorporates neuronal control, muscle forces, passive mechanics, and fluid stresses. A coupled fluid-solid modeling approach enables integration of these elements to predict aspects of swimming performance, such as forward velocity. This theoretical framework allows an explicit test of the role of nonlinear material properties in the passive mechanics of the bell structure on forward swimming, along with an exploration of the interaction of nonlinear materials with bell size, shape, stiffness, and the temporal patterns of force production. Navigating a multi-dimensional parameter space that maps the role of nonlinear material properties against these structural and temporal variables reveals that nonlinearity enhances swimming velocity over a range of parameters, while creating a dynamic landscape of tuning optima in which specific combinations of parameters contribute differentially to swimming performance. Overall, smaller jellyfish have a larger set of "suitable" combinations of shape, stiffness, and muscle timing parameters available to them than large jellyfish. Increasing bell stiffness confers stability, eliminating performance peaks and troughs, but limits the maximum attainable speeds available. With respect to muscle forcing, nonlinearity enhances peaks and troughs in performance

and interacts with temporal patterns of force production to confer sensitivity over a fine scale, but robustness to perturbation on a large scale.

Introduction

The dynamic swimming behavior of a hydrozoan jellyfish derives from a complex interplay of neuronal control, muscle forces, passive mechanics, and fluid stresses. The jellyfish's relatively primitive morphology makes it an appealing subject for studies that synthesize the relative contributions of these different parts of the locomotor apparatus to swimming performance (Daniel, 1983; Daniel, 1985; Daniel, 1995; DeMont and Gosline, 1988b). In this study, I specifically examine the interaction between the nonlinear passive mechanics of the structure and temporal patterns of force production in shaping the swimming performance of the hydrozoan jellyfish *Polyorchis penicillatus*.

The mechanical properties of mesoglea, the extracellular matrix that comprises the bulk of the animal, and its functional role for elastic energy storage and return, have been studied in great detail since the 1950s (Alexander, 1962; Alexander, 1979; Chapman, 1953; DeMont and Gosline, 1988a; Koehl, 1977; Pabst, 1996). Fibers in the mesoglea deform during muscular contraction and the composite extracellular matrix stores elastic strain energy to power the refilling phase of the swimming contraction. Many studies observe that mesoglea, like most biological materials, shows a characteristic nonlinear response to an applied strain and suggest that this property might have important functional consequences for swimming performance (DeMont and

Gosline, 1988a; Gosline and Shadwick, 1983; Pabst, 1996; Wainwright et al., 1976) (Goldman, Chapter 2). For example, DeMont and Gosline (1988) suggest that the nonlinear stress/strain relationship may be advantageous for maximizing the force generation in a given swimming contraction. The initial low modulus region would allow easy deformation during the phase of the contraction which generates high hydrodynamic thrust, while the increasing stiffness at the end of the cycle would allow the storage of strain energy when the potential for hydrodynamic work is low. They extend their reasoning to argue that the extended plateau component of the swimming muscle action potential, noted by Spencer and Satterlie (1981), may be tuned to exploit mesoglea's nonlinear stress/strain curve, by allowing sufficient deformation of the fibers and mesoglea late in the contraction phase, where the modulus of stiffness is greatest. Pabst (1996) suggests that the parallel arrangement of elastic springs (collagenous fibers) and the circular subumbrellar muscle actually constrains the springs to be nonlinear, so that with similar deformations the muscles can effectively both generate thrust and load the spring to sufficiently power the refilling of the bell.

While mesoglea's nonlinear stress/strain relationship has been well-documented, both for a variety of species within the class *Hydrozoa* and for other classes within the phylum Cnidaria (Koehl, 1977), and that relationship has been shown to have important functional consequences for energy storage within a single swimming contraction, the role of nonlinear mechanical properties in dynamic movements is largely unexplored. In Chapter 2, I raised the general issue of the dynamic possibilities in nonlinear systems and examined the role of a nonlinear material in static deformation. In this study, I combine

experimental and theoretical approaches to ask the following questions: 1) how do measured nonlinear mechanics in jellyfish affect dynamic swimming behaviors? 2) How do structural factors such as size, shape, and stiffness of the bell interact with its nonlinear mechanical properties to affect tuning for swimming performance? 3) How does variation in the shape and timing of muscle forcing interact with nonlinear mechanical properties to confer either robustness or sensitivity to variation and perturbation?

Materials and Methods

Nonlinear mechanical properties

In a previous study, I determined the strain-dependent complex modulus, E*, a dynamic measurement of both elastic and viscous components of stiffness, for isolated strips of mesoglea from *Polyorchis penicillatus*. Since the elastic component of stiffness (E') dominates the mechanical behavior of mesoglea, it is possible to disregard the out-of-phase portion of the E* (Goldman, Chapter 2). From measured values for E*, an estimate for the magnitude of the nonlinear relationship between stress (σ) and strain (ε) derives from a fit to data using the power equation:

$$\sigma = a\varepsilon^{x}$$

where $\varepsilon = \Delta L/L_o$; $\sigma = F/A$; and a and x are the coefficients of the power relationship derived from a fit to existing data. An estimate for the average of x for *Polyorchis* is x = 1.8 +/- 0.10 (N = 6). For a complete description of methods and results of this study see Chapter 2.

Swimming kinematics

I collected representative individuals of the species *Polyorchis penicillatus* off the coast of Stuart Island, Washington. Medusae ranged in body size (bell radius) from 0.4 cm to 1.4 cm.

I placed medusae in a ten-gallon glass tank and filmed with orthogonal views at 30 frames/sec with 2 Sony Digital 8 handheld video cameras arranged at two sides of the tank, orthogonal to each other. Each camera had a field of view of 8cm X 14 cm and a 4.6 x 2.7 x 2.5-cm block, placed at a range of distances from each camera, functioned to calibrate linear scales. An LED flash, visible in both views, synchronized the two cameras. A tank cooling system circulated cold water through the bottom of the tank, maintaining an average temperature of 10-12°C.

With views from two cameras, it was possible to track the three-dimensional trajectory of the medusa as it swam. Video clips were hand-digitized (with Adobe Premiere 5.0 and Quick Time Pro) using a routine written by M.S. Tu in Matlab 5.0. This routine tracked the x-y position of three points on the medusa—the inner bell apex at the attachment point of the manubrium and two points on the bell margin—from each camera view. From x-y coordinates, a custom Matlab program applied the necessary linear scale calibrations to reconstruct a three-dimensional trajectory and to calculate the distance, velocity, and radius changes at each point (Figure 4.1).

Equipped with measured kinematics for medusae of a range of sizes, I use these data to both inform and ground-truth a theoretical framework for exploring the role of nonlinear mechanics in swimming performance.

Modeling jet propulsion in jellyfish: Coupling fluid to elastic forcing

Thrust

Jellyfish swim by periodic forcible expulsions of fluid from the subumbrellar cavity, through an aperture that is constrained by the velum, a thin ring of tissue that extends inward from the bell margin (DeMont, 1992). As swimming muscles contract they both deform the bell and eject fluid while developing thrust. Modeling this in the context of a nonlinear elastic structure requires an accounting of the stresses generated by each component of the locomotor apparatus.

Based on the model developed by Daniel (1983, 1985), the thrust (T) generated by the expelled fluid is equal to the rate at which momentum is ejected from the velar aperture.

$$T = \frac{\mathrm{d}(mu_e)}{\mathrm{d}t} \qquad [1]$$

where m is the mass of the animal and water within it, t is time and u_e is the velocity of the ejected water.

Using conservation of mass, this expression for thrust can be rewritten in terms of the area of the velar aperture (A_e) and the rate of volume change ($\mathrm{d}V/\mathrm{dt}$) of the animal during the contraction phase.

$$u_e = \left(\frac{1}{\rho A_e}\right)\left(\frac{\mathrm{d}m}{\mathrm{d}t}\right) \qquad [2]$$

$$\frac{\mathrm{d}m}{\mathrm{d}t} = \rho\left(\frac{\mathrm{d}V}{\mathrm{d}t}\right) \qquad [3]$$

$$T = \left(\frac{\rho}{A_e}\right)\left(\frac{dV}{dt}\right)\left|\frac{dV}{dt}\right| \qquad [4]$$

where ρ is the density of water.

Armed with an expression for thrust (T) that depends on the bell volume, I can derive an expression for the time-dependent volume of the bell (V), based on the geometry of the jellyfish and its radial symmetry. The medusan bell is a hemi-ellipsoid, whose volume is given by the expression:

$$V = \frac{2}{3} r(t)^2 h \qquad [5]$$

In [5] r is the bell radius and h is the bell height. By specifying the volume of the bell (V_b) as a constant, h, can be solved in terms of $r(t)$ (see Appendix C).

Thrust produces a rise in internal pressure

Thrust generated by the expulsion of fluid from the bell appears as a rise in the pressure (P) within the subumbrellar cavity. Therefore, an expression for the pressure within the cavity can be written as:

$$P = \frac{T}{A_e} \qquad [6]$$

$$P = \left(\frac{\rho}{A_e^2}\right)\left(\frac{dV}{dt}\right)\left|\frac{dV}{dt}\right| \qquad [7]$$

Assuming the subumbrellar cavity to be roughly cylindrical in shape, the circumferential force that results from the internal bell pressure can be written as:

$$F_{hydro} = 2\,\mathrm{Pr}\,h = 2\rho rh(dV/dt)|dV/dt|/A_e^2 \qquad [8]$$

Muscle forces generate circumferential forces and deform the structure

Contractions of the subumbrellar myoepithelial cells are responsible for generating the circumferential forces that produce the thrust of the jet as water is expelled from the bell (Spencer and Satterlie, 1981). Therefore, the force of the muscle must be balanced against these hydrodynamic forces. But, in addition to generating hydrodynamic thrust, the force of muscle contraction also deforms the passive structure of the bell, accelerating and decelerating the mass and storing energy in elastic fibers for the recoil phase of the swim cycle. Thus, a complete force balance describing the periodic production of thrust by the medusan bell must combine hydrodynamic and passive mechanical forces.

$$F_{muscle} = F_{hydro} + F_{passive}$$
$$F_{muscle} = 2\rho rh(dV/dt)|dV/dt|/A_e^2 + F_{passive} \qquad [9]$$

This description of the passive mechanical forces affords the opportunity to incorporate dynamic nonlinear responses to applied strains, since it accounts for inertial, elastic, and viscous components associated with changes in the bell caused by the action of the muscles. The inertial component is the force associated with periodic accelerations and deceleration of body parts during swimming, while the elastic component depends on the deformation of the structure, and the viscous component

depends on the rate of that deformation. Thus, the force to deform the bell can be written as:

$$F_{passive} = k|r(t) - r_o|^b (r(t) - r_o) + \eta dr/dt + m d^2r/dt^2 \qquad [10]$$

where r is the displacement of the radius from its rest position r_o, k is an effective spring constant for the structure, η is the damping coefficient, and m is the effective mass, which includes the mass of the animal plus any entrained fluid. The exponent b varies the strength of the nonlinear dependence of the spring on bell position. An exponent of b=0 defines a linear spring and any nonzero value for b makes the spring nonlinear.

Mechanical scaling

The spring constant k, the damping coefficient η, and the effective mass m all depend on the size or radius of the jellyfish (r) and on other structural bell parameters. The spring constant k derives from DeMont and Gosline's (1988c) approach. From Hooke's law in which:

$$k = F / \Delta r \qquad [11]$$

The circumferential force associated with the internal pressure of the bell defines F in [11] and follows from [8]:

$$F = 2Prh \qquad [12]$$

From this force and the known area over which the force acts,

$$A = 2th \qquad [13]$$

A circumferential stress can be calculated (Wainwright et al., 1976):

$$\sigma = Pr/t \qquad [14]$$

From the relationship for strain and Young's modulus of stiffness

$$\varepsilon = \Delta r / r_o \qquad [15]$$

I obtain an expression for the spring constant k,

$$k = \mathrm{E} * A_B / \mathrm{r_o} \qquad [16]$$

$$A_B = \pi / 2 r_o h_o - \pi / 2 (r_o - t)(h_o - t) \qquad [17]$$

As the magnitude of the nonlinear exponent b increases, the passive mechanical spring becomes increasingly nonlinear. Linear and nonlinear materials can be compared in a number of ways. I chose to conserve the effective mean slope of the stress/strain relationship. I scaled the value of the spring constant k so that the mean slope of the curve remains constant and equal to the slope of the linear stress/strain curve and prescribe its deformation on each contraction to be equal to half of the bell radius (see Chapter 2 for scaling method).

The damping coefficient, η, depends on both the size of the bell and the frequency of the bell contraction. An expression for η derives from its dependence on the rate of deformation and on E'', the viscous component of Young's modulus. Since force is proportional to both of the following expressions, the terms can be rearranged to solve for η. From Newton's law of viscosity: $F = \eta dr / dt \cong \Delta r / \Delta t$ and from dynamic mechanical experiments: $F = AE' \Delta r / r_o$. Since $\Delta t = 1 / f$:

$$\eta = \frac{AE'}{f r_o} \qquad [18]$$

In this expression for η, A = Bell Area, f = frequency, and E'' = viscous part of Young's modulus, where the complex modulus, E* is composed of both an elastic component, E', and a viscous component, E''. According to dynamic mechanical tests on mesoglea, E'' = 0.03*E* (Chapter 2).

Finally, an expression for the effective mass of the bell *m* derives from DeMont and Gosline's estimates for the amount of water entrained during swimming. They predict that an average effective mass is 4.35X the wet weight of the bell (DeMont and Gosline, 1988c). Mass can be calculated from bell volume and is scaled by the effective mass coefficient (C_m):

$$m = \rho V_b C_m$$
$$m = \rho(2/3\pi h_\omega r_\omega^2 - 2/3\pi(h_\omega - t)(r_\omega - t)^2)C_m \quad [19]$$

Force production by the muscles

Before creating a force balance that incorporates both hydrodynamic and passive mechanical forces, it is necessary to prescribe a function that describes the force of periodic muscle contraction, F_{muscle}. As there have been relatively few direct measurements of the force produced by the subumbrellar myoepithelium, I rely on published data to inform a best estimate of the magnitude of forces (See Table 4.1).

Although, Spencer and Satterlie (1981) provide clues to the shape of the muscle force output from their uncalibrated output from a strain gauge pressed against the muscle sheet, they do not calibrate for force magnitude. Furthermore, their measurements include both the force produced by muscle and the attached mesoglea and

therefore do not relate directly to the output of the muscles alone. Thus, while the shape of their strain gauge output serves as a guide, I explore the consequences of variation in the shape of the muscle forcing function, over a range of waveforms that vary from a sin wave to a near square wave, through a series of model simulations. The magnitude of the muscle force scales with the following relationship:

$$F_{muscle} = T_m \sigma_m A_m \lambda \qquad [20]$$

where T_m is the muscle thickness, σ_m is muscle stress, A_m is muscle area and λ is the specified waveform (Table 4.1).

A Matlab routine synthesizes a square wave forcing function (λ), with small fixed time steps of 0.001s, and scales it according to the muscle properties discussed above. I use a Butterworth filter of varying frequency cutoffs to filter the waveform. A frequency cutoff of 3 Hz corresponds with a nearly Sin wave forcing function, a frequency cutoff of 9 Hz corresponds with a rounded square forcing function, and a frequency cutoff of 20 Hz corresponds with a nearly square forcing function. Interpolation methods find the values for the forcing function, which correspond to the adaptive time steps of the ODE solution. In this chapter, these forcing functions are generally symmetric. I address the dynamic consequences of such common asymmetries as a rapid rise followed by a slower decline in a separate study that uses van der Pol equation to model the force output of the muscles (Goldman and Low, in prep).

Timing of muscle force production

Throughout the numerous studies on hydrozoan medusae, bigger jellyfish have been observed to swim with a slower frequency of contraction than small jellyfish (Gladfelter, 1972; Hyman, 1942; Passano, 1965; Spencer and Satterlie, 1981). Based on measured kinematics on *Polyorchis penicillatus* and Gladfelter's (1972) measurements of contraction duration as a function of size in *Polyorchis montereyensis*, I used a least-square minimization routine to fit a function that describes the relationship between contraction duration and bell radius (Figure 4.2).

$$T_m = -.0165 + 3.86 r_o^{1/2} \qquad [21]$$

A complete swim cycle, T_c includes the contraction phase, T_m, and the recovery phase, T_r. Gladfelter estimates that the recovery phase is 30% longer than the contraction phase. Thus, the complete cycle period is:

$$T_c = T_m + 1.3T_r \qquad [22]$$

$$f = 1/T_c \qquad [23]$$

With the appropriate frequency scaling in place, the effects of variation in muscle timing on resultant swimming velocity can be investigated. Varying the duty factor (T_m/T_c), the amount of time in a given cycle that the muscle is active, evaluates the sensitivity of the system to large-scale variations in timing. A variation in duty factor is analogous to how muscle force production in hydrozoan jellyfish might scale through ontogeny. For *Polyorchis penicillatus*, the duration of the action potential is directly proportional to time to peak tension of the muscles (Spencer and Satterlie, 1981).

Extending the duration of muscle contraction for a given cycle is equivalent to a higher duty factor.

In addition, I probe the system's sensitivity to error in the timing of muscle force production by injecting variation into the timing of muscle force production. This enables an evaluation of whether or not the sensitivity of the system to this error depends on the magnitude of the nonlinear stress/strain component. A set of ten random numbers of specified magnitudes corresponds with each swimming contraction. These numbers specify the number of time steps by which to offset each cycle. The magnitude of timing error injected into the system is set at one of three levels: 1x = ~7.5% per cycle, 2x = ~15% per cycle, and 3x = ~30% per cycle (Figure 4.3).

Solving for changes in bell shape

After specifying the temporal pattern of muscle force production and its various scaling arguments, the complete force balance can be solved for *r(t)*.

$$F_{muscle} = 2\rho r h(dV/dt)|dV/dt|/A_e^2 + k|r(t) - r_o|^b (r(t) - r_o) + \eta\, dr/dt + m\, d^2r/dt^2 \qquad [24]$$

A Matlab code solves this second order nonlinear ordinary differential equation numerically, using adaptive time stepping and solver ODE23S for solving stiff differential equations, which uses a low order method.

Calculating measures of performance

Predictions of how the bell radius changes as the jellyfish swims, *r(t)*, give informative measures of performance, such as swimming velocity and efficiency. Swimming velocity is the dominant performance measure considered in the remainder of this analysis. A fuller consideration of this choice of performance metric appears in the next section.

In order to calculate swimming velocity, I balance the force of thrust [1] against the forces of drag, added mass and inertia that resist the forward motion of the body.

$$\rho(\,dV/dt)|\,dV/dt|/A_e = 0.5\rho S C_D U^2 + \alpha\rho V\,dU/dt + \rho V\,dU/dt \qquad [25]$$

From r*(t)* specified by nonlinear differential equation and the specified hemi-ellipsoidal geometry of the bell, the time-dependent volume of the bell *(V)*and the thrust produced (*T*) can be determined.

$$T = \rho(\,dV/dt)|\,dV/dt|/A_e \qquad [26]$$

Substituting thrust into the balance of hydrodynamic forces [24], enables a solution for swimming velocity *U(t)*. Using a center-differenced iterative substitution into the balance of hydrodynamic forces ([15]), it is possible to determine $U_{(j+1)}$, the value for U at the j+1 time step, in which Uj_{-1} is the first time step of the solution and:

$$U_{j+1} = \frac{2U_i t_i - U_i(t_{i-1} + t_{i-1}) + U_{i-1}(t_{i-1} - t_i) + 2(t_{i-1} - t_i)(t_i - t_{i-1})\left[\dfrac{-T_{i-1} - 0.5\rho S_{i-1} C_d U_{i-1}|U_{i-1}|}{(1+\alpha)\rho V}\right]}{t_i - t_{i-1}} \qquad [27]$$

Evaluating medusan swimming performance

Swimming velocity is only one of many possible changes in performance that result from the addition of a nonlinear spring to a fluid-solid coupled model for medusan locomotion and maximizing swimming velocity is not necessarily an appropriate measure of performance for all medusae. Hydrozoan species with an oblate shape, such as *Mitrocoma cellularia* and *Aequorea victoria,* do not often swim with rapidly directed movements (Colin and Costello, 1996; Colin and Costello, 2002). Instead, they contract their bell without generating significant forward thrust, as a means of generating feeding currents—a finding that has been verified by flow visualization studies (Colin and Costello, 2002). Diversity in hydrodynamic profile between medusae of different shapes raises the question of whether or not maximizing swimming speed is, in fact, a reasonable measure of swimming performance across different morphologies.

Polyorchis penicillatus, along with other prolate species of hydrozoan medusae, swim with directed movements, in bouts of contractions that cause forward translation, both to feed and to escape from predators (Colin and Costello, 1996; Colin and Costello, 2002; Mills, 1981). While speed is only one of many possible measures of performance and may not be the optimal metric for comparing medusa of different shapes, I look closely at combinations of parameters that optimize the jellyfish's average swimming velocity at the end of a sustained bout of contractions.

Navigating a multi-dimensional parameter space

In order evaluate the role of nonlinear mechanical properties on dynamic swimming behavior, I explore the consequences of varying both the magnitude of the nonlinear stress/strain relationship and structural parameters such as shape, size, and bell stiffness. Shape, size, and bell stiffness vary throughout ontogeny, within a single species, and nonlinear mechanical properties may play a stronger or lesser role at different stages of development (Gladfelter, 1972). Although this has not yet been shown conclusively, the magnitude of the nonlinear exponent may also vary with growth and it is possible that a single animal may exploit a range of nonlinear stress/strain relationships during its life span.

Additional layers to this analysis emerge from evaluating the consequences of variation in both the timing and shape of muscle force production on swimming velocity, in conjunction with variation in size and bell stiffness. Nonlinear mechanical properties may interact with the structural and dynamic parameters in non-intuitive ways and may shed new light on traditional scaling arguments (Daniel, 1983; Daniel, 1995). Nonlinear mechanical properties may heighten the sensitivity of the system to subtle variations in the shape and timing of force production while simultaneously conferring a global ability to resist external perturbation.

Results

Validation of the model

Three dimensional distance trajectories from four individuals of the species *Polyorchis penicillatus* reveal that theoretical predictions match well with *in situ* swimming behavior (Figure 4.4). DeMont and Gosline (1988a) estimate that the dynamic structural stiffness of the passive structure falls between 500 – 1000 Pa. However, this is an invasive measurement and cannot be made on freely swimming animals, so precise dynamic structural stiffness of the animals that were filmed swimming remains unknowns. Consequently, I present model fits for both extremes of the predicted range of stiffness values. Similarly, from measured material properties and curve fits to these data, the average magnitude of the nonlinear exponent for *Polyorchis* is b= 0.8 +/-0.10, but the exact value of that exponent for the animals filmed is unknown. Therefore, measured distance trajectories are presented aligned with model results for the entire range of nonlinear exponents explored, b=0 to b=2 (Figure 4.4). The smallest jellyfish filmed was slightly faster than predicted by model simulations, while other sizes fall squarely within the range of predicted swimming velocities at reasonable values for the nonlinear exponent. If bell stiffness, like frequency, is also dependent on bell size, the discrepancy between theoretical and measured kinematics for small sizes might diminish. This possibility will be explored further in the *Discussion*.

Bell structural parameters

Variation in size

In the following simulations, traditional scaling arguments are revisited in a theoretical context that incorporates nonlinear mechanical properties. The radius of bell varies from 0.4-4 cm, encompassing a range generally observed, and the magnitude of the nonlinear exponent, b, from b =0, the linear case, to b = 2, a cubic nonlinearity, while keeping stiffness, bell shape, muscle forcing, and muscle timing constant. Bell shape, the ratio of bell height to bell radius is set to h/r = 2, which describes a prolate medusa much like *Polyorchis*. The y-axis, variation of the nonlinear exponent is constant throughout all of the simulations. The z-axis, swimming velocity (U) for the last complete cycle in a bout of ten contractions, is mapped on a fixed color scale, from –5 cm/s to 5 cm/s, and also remains constant through all of the simulation plots.

Low values for the nonlinear exponent, b, yield uniformly positive swimming motions across all bell sizes, but the resultant swimming velocity is lower that what can be achieved at higher values of b. High values for b yield high swimming velocities in medium-sized jellyfish, but negative velocities in large jellyfish. Finally, while achieving a uniformly positive swimming velocity, the smallest jellyfish do not achieve high swimming velocities, regardless of the magnitude of their nonlinear exponent (Figure 4.5).

Size sensitivity to bell stiffness

While swimming performance depends on both size and nonlinearity, that dependence differs depending on the on the stiffness of the bell. For three different measures of bell stiffness, 500 Pa, 1000 Pa, and 2000 Pa, there is a tradeoff between maximizing swimming speed and achieving slow, but stable forward velocities (Figure 4.6). Estimated dynamic structural stiffness for *Polyorchis* is approximately 750 Pa. At a low stiffness, 500 Pa, resultant swimming velocity is more sensitive to size and nonlinearity, while at a high stiffness, 2000 Pa, swimming velocity is largely insensitive to both. At 500 Pa tuning peaks are sharp and there is a large cost to missing the peak. At 1000 Pa tuning peaks are less pronounced and the cost to missing the peak diminishes. In all three cases, the smallest jellyfish remain least sensitive to variation in bell stiffness.

Variation in bell stiffness

Continuous variation of the stiffness of the bell over a range that encompasses measured stiffness values for *Polyorchis*, from 200-1000 Pa explores the effects of bell stiffness in greater detail, (DeMont and Gosline, 1988a). In this case, bell size, bell shape, and the shape and timing of muscle force production are all maintained as constants. Overall, higher values for the nonlinear exponent, b, yield higher swimming velocities (Figure 4.7). For stiffness values of 500 Pa and above, jellyfish achieve uniformly positive swimming velocities that increase in magnitude with increasing values for the nonlinear exponent. But, there is a region of extremely high swimming

velocities that corresponds with a stiffness range of 350-650 Pa for high values of the nonlinear exponent. At low bell stiffness values, only jellyfish with moderate-high values for nonlinear mechanical properties achieve a forward swimming velocity. Interestingly, there is an abrupt discontinuity at bell stiffness values between 450- 500 Pa. In this range, jellyfish do not achieve positive swimming velocities at all, except at very high values for the nonlinear exponent. This discontinuity appears real and does not appear to be the result of a numerical instability, implying a potentially important dynamic role for subtle variations in bell stiffness for different nonlinear exponents.

Stiffness sensitivity to bell size

The effects of bell stiffness on swimming performance also depend on the size of the bell. High swimming speeds are most pronounced at an intermediate value for bell size (Figure 4.8). All three size classes exhibit poor swimming performance at low bell stiffness, except at high values for the nonlinear exponent. Smaller jellyfish achieve their maximum swimming speed at a low stiffness and high values for the nonlinear exponent and uniformly positive but slow swimming speeds above a stiffness of 500 Pa, regardless of the magnitude of the nonlinear exponent. In contrast, medium and large jellyfish achieve higher swimming speeds for high values of the nonlinear exponent at bell stiffness values above 500 Pa. All three sizes show a similar discontinuity, a region of poor swimming performance between 450- 500 Pa, but this is least striking for medusa in the smallest size class.

Variation in bell shape

Within the class *Hydrozoa*, there is considerable variation in bell shape and different shapes tend to correlate with different swimming behaviors (Colin and Costello, 1996; Colin and Costello, 2002; Mills, 1981). Daniel (1985) defines a metric of bell shape called the fineness ratio or bell height / bell radius (h/r). By varying the fineness ratio continuously from 1-3, describing medusae that range from oblate to extremely prolate in shape, while keeping the bell stiffness fixed at 500 Pa, it is possible to explore the consequences of shape variation and the role of nonlinear mechanical properties on swimming velocity. Nonlinear mechanical properties enhance swimming velocity across a wide range of shapes (Figure 4.9). There is a pronounced peak in swimming velocity at a fineness ratio between 1.25-2, at high values for the nonlinear exponent, $b = 0.8$ and above. *Polyorchis* falls squarely within this range. But, within a similar range of fineness values, from 1.1 to 1.8, low values for b lead to negative swimming velocities. Therefore, for a range of shapes that describes many hydrozoan shapes; there is a clear benefit to having at least weakly nonlinear mechanical properties. Interestingly however, for high values of the fineness ratio, or extremely prolate medusae, nonlinear mechanical properties negatively affect swimming speed and positive velocities are only achieved or low values of b.

Shape sensitivity to bell stiffness

Increasing bell stiffness dampens the sensitivity of swimming speed to both shape and nonlinear mechanical properties (Figure 4.10). At a bell stiffness of 750 Pa peak

swimming velocities shift toward prolate medusae, occurring at values for the fineness ratio of 1.7 and above and values for *b* of 1.1 and above. Swimming speeds are uniformly lower, but positive for all shapes and all values of b, at bell stiffness values of 750 Pa and 1000 Pa. Medusae with a lower bell stiffness can achieve greater maximum swimming speeds for certain shapes and nonlinear mechanical properties, but are constrained within a smaller space of acceptable bell geometry (Thomas and Reif, 1993). Higher values for bell stiffness remove this geometric constraint but result in uniformly slower swimming speeds.

Structural determinants of swimming velocity are sensitive to the shape of muscle forcing

The temporal pattern of force production interacts with bell structural parameters such as size, stiffness, and shape and with nonlinear mechanical properties to shape tuning for swimming velocity. This interaction can be evaluated by examining the effect of three variants on the shape of the muscle forcing function on swimming velocity. Here, size of the bell and the nonlinear exponent *b* vary continuously, for bell stiffness values of 500 Pa, 1000 Pa, and 2000 Pa. The muscle forcing functions are explained above in *Materials and Methods.*

At low and intermediate values for bell stiffness, 500 Pa and1000 Pa, as the muscle forcing function becomes increasingly square, swimming velocity peaks and troughs become more pronounced (Figure 4.11). The stiffest bells are largely insensitive to variation in the shape of the muscle forcing function. At a bell stiffness of 500 Pa,

there are fewer bell sizes that correspond with positive swimming speeds as the forcing function becomes more square, regardless of the magnitude of the nonlinear exponent. At a bell stiffness of 1000 Pa, the range of bell sizes that correspond with positive swimming speeds shrinks slightly, but the highs become higher and the lows become lower. Over the bottom to middle of the size range, there is a clear benefit to nonlinear mechanical properties and that benefit becomes more pronounced as the muscle forcing function becomes increasingly square.

Continuous variation of muscle force frequency components

Continuous variation of the waveform cutoff frequency, from 1 to 20hz, from a sin wave to a square wave examines the role of the spectral components of muscle force production on swimming velocity in greater detail. The effect of varying cutoff is examined at four values for bell stiffness, 500 Pa, 750 Pa, 1000 Pa, and 2000 Pa, and three bell sizes, 1 cm, 2 cm, and 3 cm.

Spectral components of the waveform, nonlinear mechanical properties, size, and stiffness interacts in non-intuitive ways to influence swimming velocity (Figure 4.12). As observed previously, swimming velocity of medusae with the stiffest bells, E = 2000 Pa, is largely insensitive to parameter variation, in this case it is insensitive to the spectral components of the waveform or to the size of the bell. Except when the bell is very stiff, the largest medusae, r = 3 cm, perform poorly at high values for the nonlinear exponent and at high cutoff frequencies. For this size class, linear mechanical properties perform

better than nonlinear, for E = 500 Pa, 750 Pa, and 1000 Pa, except when the forcing function closely approaches a pure sin wave.

In contrast, for the smaller size classes, nonlinear mechanical properties amplify swimming speeds across a range of frequency components. At a bell radius of 2 cm, the benefit of nonlinear mechanical properties increases with increasing bell stiffness but the sensitivity to the shape of the forcing function decreases. This pattern is even more pronounced for the smallest size class of medusae, r = 1cm, but smaller jellyfish can exploit a larger range of bell stiffness values, achieving fast swimming speeds for high values of the nonlinear exponent at E= 500 Pa, where the larger medusae cannot.

Variation in the timing of muscle force production

Evaluating the contributions of temporal patterns of force production to resultant swimming velocity includes not only the shape of the muscle forcing, but the timing. While Gladfelter's (1972) measurements suggest that the swim cycles consist of a contraction phase plus a recovery phase that is 30% longer than the contraction phase, this ratio of contraction to relaxation is not hard-wired. In fact, an increase in the percent of the cycle that the muscle is active, or the duty factor, may be an important mechanism by which larger jellyfish can produce sufficient muscle force to expel a volume of water from their bell (Spencer and Satterlie, 1981). Since volume scales as the radius^3 and surface area scales as radius^2, the volume of water that a large jellyfish must expel from its bell is relatively larger than the volume that a small jellyfish must expel. Thus, size and duty factor should exhibit a high degree of interdependence.

Variation in duty factor

A swim cycle in which the relaxation phase is 30% longer than the contraction phase corresponds with a duty factor, or percentage of the cycle that the muscle is active of 43.5 (%). This value, 43.5 (%), is set as an intermediate and compared to swimming velocity sensitivity to a low duty factor, 25 (%), and a high duty factor, 75 (%). For a specified forcing function with a frequency cutoff of 3 Hz, bell stiffness of 1000 Pa, and continuously varying bell size, tuning peaks for swimming velocity are highly sensitive to the duty factor and interact with nonlinear mechanical properties (Figure 4.13). At low and intermediate duty factors, nonlinear mechanical properties amplify swimming velocity for medusae of small to medium bell size. At a low duty factor, large jellyfish show poor performance, regardless of the magnitude of the nonlinear exponent. At a high duty factor, medusae of medium to large bell size perform well over a wide range of values for the nonlinear exponent *b*. Thus, if duty factor does scale positively with increasing bell size, this mechanism would, in fact, provide larger medusae with a means to optimize the expulsion of fluid from the bell.

Sensitivity to variability in timing

Although a medusa of a given size generally operates at a fixed frequency of contraction, biological systems are inherently noisy and there is bound to be some error in the timing of muscle force production that may occur in response to certain environmental factors. Modifying the variability in the timing of muscle force

production tests the resilience of this system to perturbation and evaluates the role of nonlinear mechanical properties in the response. The method for injecting error in the timing of muscle contraction is described above in *Materials and Methods*.

Response to variability in timing is highly sensitive both to the duty factor and to the magnitude of the nonlinear exponent. At an intermediate duty factor, the insertion of error into the timing of muscle contraction eliminates the region of poor swimming performance found at high nonlinearities for large medusae (Figure 4.14). This zone of poor swimming performance completely disappears with an error magnitude of 2x or ~15%. Overall, adding a moderate amount of error to the system yields a region of positive/fast swimming speeds that spans a larger size range than adding no error at all. For a high level of error, 3x or 30%, the region of fast swimming velocity begins to diminish slightly, but there is still no evidence of negative swimming velocities for any size class of medusa. At all levels of error, the higher swimming velocities correspond with high values for the nonlinear exponent.

Cycle by cycle comparison

For variable timing simulations at low and high duty factors, tuning optima for swimming velocity develop on a cycle by cycle basis (Figures 4.15 and 4.16). In contrast to an intermediate duty factor, at a low duty factor, 25 (%), increasing the magnitude of error increases the size of the region of poor swimming performance for large medusae. Additionally, the region of peak swimming velocity shrinks with increasing error, narrowing the peak to a small area at high values for the nonlinear

exponent. Interestingly, for a high level of error, 3x, the region of peak swimming velocity shrinks initially, cycles 3 and 4, but increases again by cycle 6. Thus, at a low duty factor, swimming velocity is less sensitive to a large amount of error in cycle timing than a small amount of error.

At a high duty factor (Figure 4.16), increasing the amount of error shifts the location of the tuning peak and localizes it towards high values for the nonlinear exponent. With no error in timing, there is a broad, L-shaped peak, which spans a range of sizes and nonlinearities. At an error magnitude of 3x, the peak in swimming velocity is concentrated at high values of the nonlinear exponent. Injecting variability in timing does not introduce troughs to this tuning landscape, regions of poor performance, which suggests that this system is robust to perturbation. Since large nonlinearities enable high swimming velocities for large amounts of error, nonlinearity may heighten the ability of this system to resist perturbations such as variation in the timing of muscle force production.

Composite overview: Nonlinear mechanical properties interact with structural and dynamic parameters to shape swimming behavior

This multi-dimensional parameter space can be presented in a single consolidated plot (Figure 4.17) to summarize the major trends that relate the explored parameter space to tuning for swimming performance in a hydrozoan medusa such as *Polyorchis penicillatus*. Across all combinations of structural and dynamic parameters that affect

swimming performance, nonlinear mechanical properties play a crucial role in setting discrete tuning optima for swimming performance. All peaks in swimming performance, across the whole suite of parameters, occur at nonzero values for the nonlinear exponent.

A closer dissection of the layers of this plot reveals that swimming velocity is highly sensitive to size, stiffness, and duty factor and these parameters clearly interact with the magnitude of nonlinearity. Overall, there are a greater number of parameter combinations that yield positive swimming velocities for smaller jellyfish than for larger jellyfish, suggesting that it might be easier to meet the requirements for jet propulsion at the low end of the size scale. High values for bell stiffness induces uniformly forward, but slow, swimming speeds, suggesting a clear trade-off between speed and stability which may be tied to a higher energetic cost for swimming with a stiff structure. Subtle variation in the shape of muscle force production sharpens the peaks and troughs of swimming performance. Variation in the timing of muscle force production shows that the system as a whole is fairly insensitive to perturbation and nonlinear mechanical properties globally enhance this insensitivity.

Discussion

Nonlinearity yields emergent complexity

Nonlinear mechanical properties in a fluid-solid coupled model for medusan locomotion interact with scaling and forcing parameters to generate an interesting

landscape of local tuning optima. As introduced in Chapter 1, the dynamic consequence of nonlinearity in a complex system is often not easily represented as a simple sum of parts. In the case of medusan locomotion, interactions between nonlinear mechanical properties and a wide variety of physiological parameters provide several potential mechanisms for control. Small parameter variations in any of these can produce large changes in performance.

A composite view of a multidimensional parameter space reveals several overall trends. There are many potential ways to build a medusa that has adequate speed, indicating that that diversity in shape, material properties, and muscle forcing can be easily accommodated in the class *Hydrozoa*. But, smaller medusae seem to have more parameter combinations available to them than larger medusae, implying a possible constraint on the evolution of large body size. For large jellyfish, high bell stiffness, high duty factor, and a high value for the nonlinear exponent are required to generate fast forward swimming speeds (Figure 4.17). Small and intermediate-sized jellyfish achieve higher swimming velocities across a wider range of parameter values. At the smallest end of the size scale, increasing the magnitude of material nonlinearity does not increase swimming velocity (Figure 4.5). Small sizes might also encounter a lower limit, probably set by the fluid dynamic forces, below which it is not possible to achieve fast forward swimming speeds.

Across diverse taxa, animals do not fully occupy the spectrum of theoretically possible forms, but converge repeatedly on a limited number of architectural designs (Thomas and Reif, 1993). Shell coiling within the gastropods is a particularly well-

documented example of partial occupation of parameter space that corresponds with the functional purpose of a given shell shape (Raup, 1966). While these model predictions suggest that there are many ways to build a medusa capable of forward swimming, mapping the space of existing forms against the number of predicted forms would likely reveal the same trend towards incomplete occupation of a theoretical morphospace.

Scaling relationships in a nonlinear model for medusan locomotion

Recasting traditional scaling arguments in the context of the contribution of nonlinear mechanical properties to swimming performance reveals tuning peaks and troughs that are absent if one assumes the hydrozoan bell to be a linear mechanical structure. In addition to the energy storage benefits within a single contraction (Alexander, 1988; DeMont, 1992; DeMont and Gosline, 1988a; Farley et al., 1993; Gosline and Shadwick, 1983; Pabst, 1996), model simulations illustrate that nonlinear mechanical properties have significant dynamic consequences. Across the explored multi-dimensional parameter space, an increase of swimming speed occurs with the addition of a small nonlinearity to the passive mechanical spring [10].

How much do hydrozoan medusae actually differ in the nonlinearity of their passive mechanical structure? In Chapter 2, I show that the magnitude of mesoglea's nonlinearity does vary between species within the class *Hydrozoa*, while the value for the complex modulus (E*) is comparable at equivalent strains. The three species *Polyorchis penicillatus, Mitrocoma cellularia,* and *Aequorea victoria* have different measured value for the nonlinear exponent b in the expression for the passive mechanical force, $F_{passive}$

[10]. While overall material stiffness of mesoglea appears to be conserved, variation in the nonlinearity of the material may provide a source of variation in locomotor patterns in different species.

In addition to a potential source for locomotor variation between species, these theoretical results show that performance advantages would arise from modulation of the nonlinearity of mesoglea, as well as modulation of whole bell stiffness, through the ontogeny of a single individual. At low to intermediate values for bell stiffness, a high structural nonlinearity in small/medium jellyfish yields performance benefits, but performance costs in large jellyfish. But, these performance costs disappear at a high overall bell stiffness, where a high structural nonlinearity produces a region of maximum swimming velocities for large jellyfish.

Do jellyfish modify their dynamic structural stiffness and the magnitude of structural nonlinearity as they grow? While this has never been measured directly and is a clear avenue for future study, Gladfelter (1972) finds that the density of collagenous fibers in the bell decreases nonlinearly with increasing bell size. Since elastic energy storage in the fibers partially determines the magnitude of the nonlinear response to an applied strain, a decrease in fiber density in larger medusae suggests a corresponding decrease in the magnitude of the nonlinear stress/strain relationship. It is not clear, however, how the dynamic structural stiffness of the bell would necessarily scale with increasing size.

Perturbation sensitivity in a medusan nonlinear dynamical system

Variation in patterns of muscle force production, both in shape and timing, interact with nonlinear mechanical properties and bell structural parameters to enhance or temper existing tuning optima. The ability to withstand error in the timing of muscle force production, which is likely to be intrinsic to normal muscle function, suggests that medusae are equipped to resist environmental perturbations that might transiently offset synchronous control of swimming. Interestingly, however, with certain combinations of parameters, error in the timing of muscle forces actually enhances performance across a broader combination of parameters than no error at all.

These theoretical predictions hint at broad functional consequences for nonlinear mechanical properties in animal design, consistent with predictions from nonlinear dynamical system theory. Control and the maintenance of stability rests, in part, in the design of the material composition of the animal, rather than always in elaborate mechanisms for neural control (Full and Koditschek, 1999). In the case of the hydrozoan medusae, nonlinear mechanical properties not only amplify swimming speeds over a broad range of structural and dynamic parameters, but also confer robustness to perturbation on a broad scale.

Notes to Chapter 4

Alexander, R. M. (1962). Visco-elastic properties of the body-wall of sea anenomes. *Journal of Experimental Biology* 39, 373-386.

Alexander, R. M. (1979). *The Invertebrates*. Cambridge: Cambridge University Press.

Alexander, R. M. (1988). *Elastic Mechanisms in Animal Movement*. Cambridge: Cambridge University Press.

Chapman, G. (1953). Studies of the mesogloea of Coelenterates: I. Histology and chemical properties; II. Physical properties. *Quarterly Journal of Microscopical Science*, 155-176.

Colin, S. P. and Costello, J. H. (1996). Relationship between morphology and hydrodynamics during swimming by the hydromedusae *Aequorea victoria* and *Aglantha digitale*. *Scientia Marina* 60, 35-42.

Colin, S. P. and Costello, J. H. (2002). Morphology, swimming performance and propulsive mode of six co-occurring hydromedusae. *Journal of Experimental Biology* 205, 427-437.

Daniel, T. L. (1983). Mechanics and energetics of medusan jet propulsion. *Canadian Journal of Zoology* 61, 1406-1420.

Daniel, T. L. (1985). Cost of locomotion: Unsteady medusan swimming. *Journal of Experimental Biology* 119, 149-164.

Daniel, T. L. (1995). Invertebrate swimming: Integrating internal and external mechanics. In *Biological Fluid Dynamics*, eds C. P. Ellington and T. J. Pedley), pp. 61-89: Society for Experimental Biology.

DeMont, M. E. (1992). Locomotion of soft bodied animals. In *Advances in Comparative and Environmental Physiology*, vol. 11, pp. 167-190. Berlin: Springer-Verlag.

DeMont, M. E. and Gosline, J. M. (1988a). Mechanics of jet propulsion in the hydromedusan jellyfish *Polyorchis penicillatus*: I. Mechanical properties of the locomotor structure. *Journal of Experimental Biology* 134, 313-332.

DeMont, M. E. and Gosline, J. M. (1988b). Mechanics of jet propulsion in the hydromedusan jellyfish *Polyorchis penicillatus*: III. A natural resonating bell; The presence and importance of a resonant phenomenon in the locomotor structure. *Journal of Experimental Biology* 134, 347-361.

Farley, C. T., Glasheen, J. and McMahon, T. (1993). Running springs: Speed and animal size. *Journal of Experimental Biology* 185, 71-86.

Full, R. J. and Koditschek, D. E. (1999). Templates and anchors: Neuromechanical hypotheses of legged locomotion on land. *Journal of Experimental Biology* 202, 3325-3332.

Gladfelter, W. B. (1972). Structure and function of the locomotory system of *Polyorchis montereyensis* (Cnidaria, Hydrozoa). *Helgolander wiss. Meeresunters* 23, 38-79.

Gosline, J. M. and Shadwick, R. E. (1983). The role of elastic energy storage mechanisms in swimming: an analysis of mantle elasticity in escape jetting in the squid, *Loligo opalescens*. *Canadian Journal of Zoology* 61, 1421-1431.

Hyman, L. (1942). Observations and experiments on the physiology of medusae. In *Invertebrates*, vol. 1, pp. 282-296: McGraw Hill.

Koehl, M. A. R. (1977). Mechanical diversity of connective tissue of the body wall of sea anenomes. *Journal of Experimental Biology* 69, 107-125.

Mills, C. E. (1981). Diversity of swimming behaviors in hydromedusae as related to feeding and utilization of space. *Marine Biology* 64, 185-189.

Pabst, D. A. (1996). Springs in swimming animals. *American Zoologist* 36, 723-735.

Passano, L. M. (1965). Behavioral physiology of coelenterates: Introductory remarks. *American Zoologist* 5, 337-340.

Raup, D. M. (1966). Geometric analysis of shell coiling: General problems. *Journal of Paleontology* 40, 1178-1190.

Spencer, A. N. and Satterlie, R. A. (1981). The action potential and contraction in subumbrellar swimming muscle of *Polyorchis penicillatus* (Hydromedusae). *Journal of Comparative Physiology A.* 144, 401-407.

Thomas, R. D. K. and Reif, W.-E. (1993). The skeleton space: A finite set of organic designs. *Evolution* 47, 341-360.

Wainwright, S. A., Biggs, W. D., Currey, J. D. and Gosline, J. M. (1976). *Mechanical Design of Organisms*. Princeton: Princeton University Press.

Table 4.1: Parameter estimates for muscle properties used in equation 20 derived from a variety of literature sources.

Muscle Thickness (T_m)	20μm (Gladfelter, 1972)
Muscle Stress (σ_m)	1.25 x 10^5 Pa (DeMont and Gosline,1988b)
Bell Thickness (t)	0.4xr_o (r_o =radius at rest)
Muscle Area (A_m)	Half of inner bell circumference = $\pi(r_o-t)$ r_o = radius at rest, t = bell thickness
Muscle dependence on bell thickness	0.005 x t (Gladfelter, 1972)
Waveform (λ)	~Sin, Rounded Square, or ~Square

Table 4.2: Parameters used to calculate swimming velocity in equation 27.

ρ	Density of water = 1000 kg/m3
α	Added-mass coefficient = $(h_o/r_o)^{1.4}$ (Daniel, 1983) (h_o = height at rest, r_o = radius at rest)
A_e	Area of fluid efflux = $\pi(0.7r_o)^2$ r_{vel} = radius of the bell-radius of the velum ($0.7r_o$)
S	Projected area of the bell = πr^2 (Daniel, 1983) (r = radius)
C_d	Coefficient of Drag = $24/Re^{0.7}$ (Daniel, 1983) (Re = Reynolds number = 2Ur/v, where U=velocity and v = kinematic viscosity of water ($1.1x10^{-6}$ m^2/s)

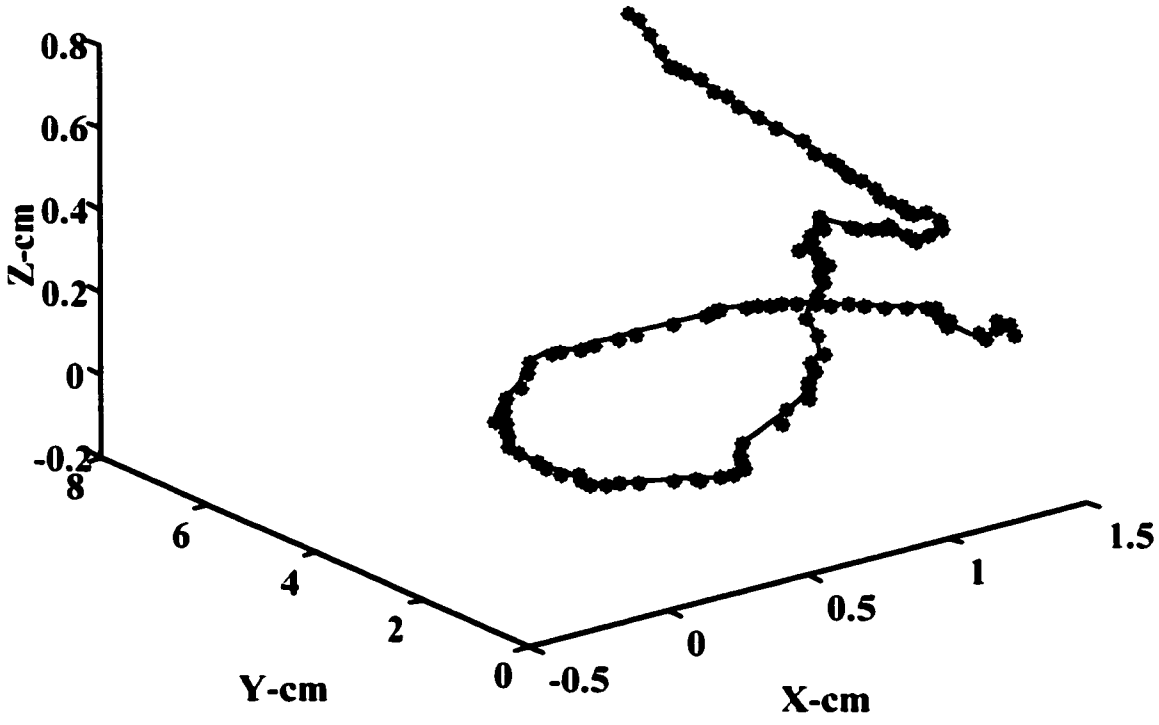

Figure 4.1-Sample kinematic trajectories for *Polyorchis penicillatus*: Example of a three-dimensional trajectory for *Polyorchis* showing its path through space. Axes are scaled in centimeters.

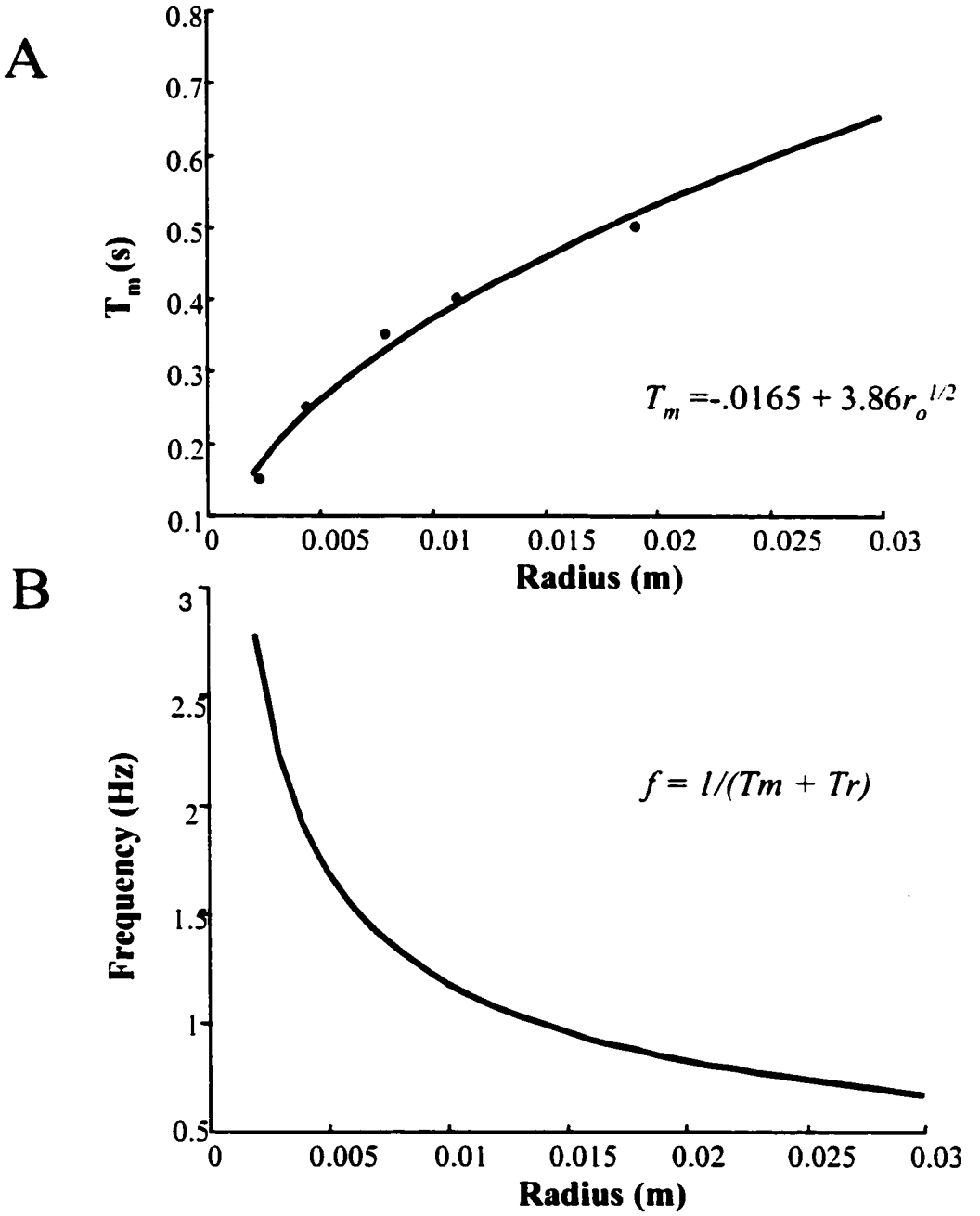

Figure 4.2A,B—Model size-frequency scaling relationship derived from Gladfelter (1972) data: A) Using published data on the duration of the muscle contraction as a function of bell radius, least square minimization routine predicts a square-root dependence. B) Frequency is calculated as the inverse of the sum of cycle duration and recovery time. Medusae exhibit frequency dependence consistent with resonant systems, in which size and frequency are inversely related.

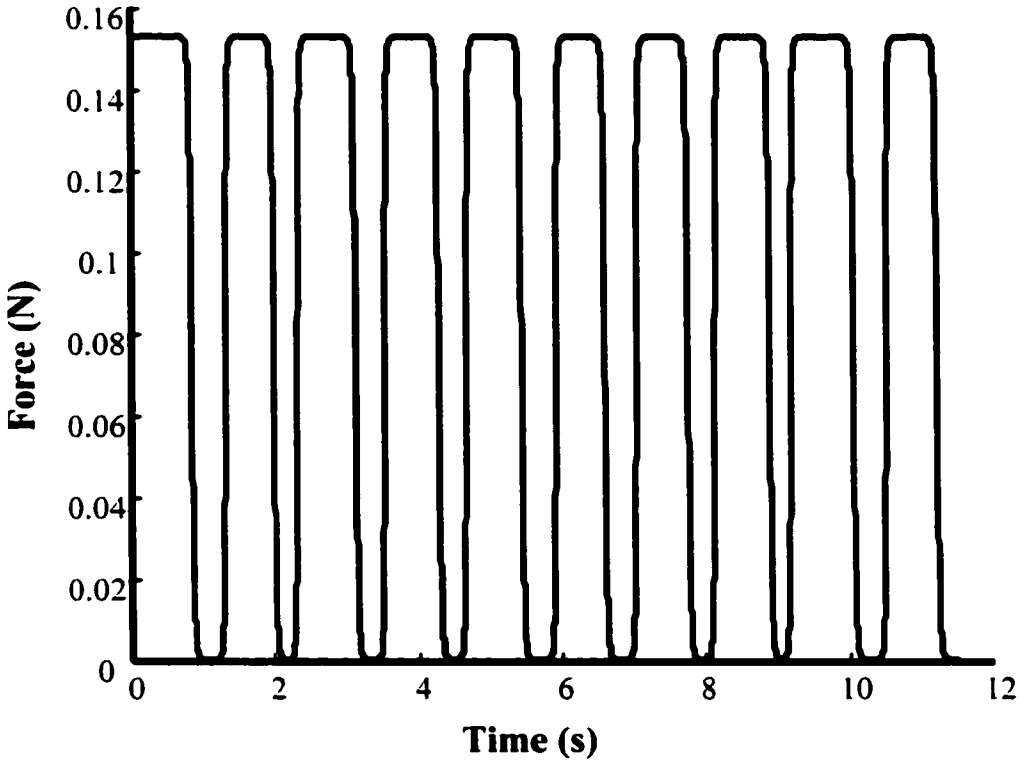

Figure 4.3 – Variability in timing of muscle force production: Error is injected into each cycle to generate a forcing function with cycles of unequal duration. This is a sample forcing function of an error magnitude of 2x, rounded square shape, and a duty factor of 43.5 (%)

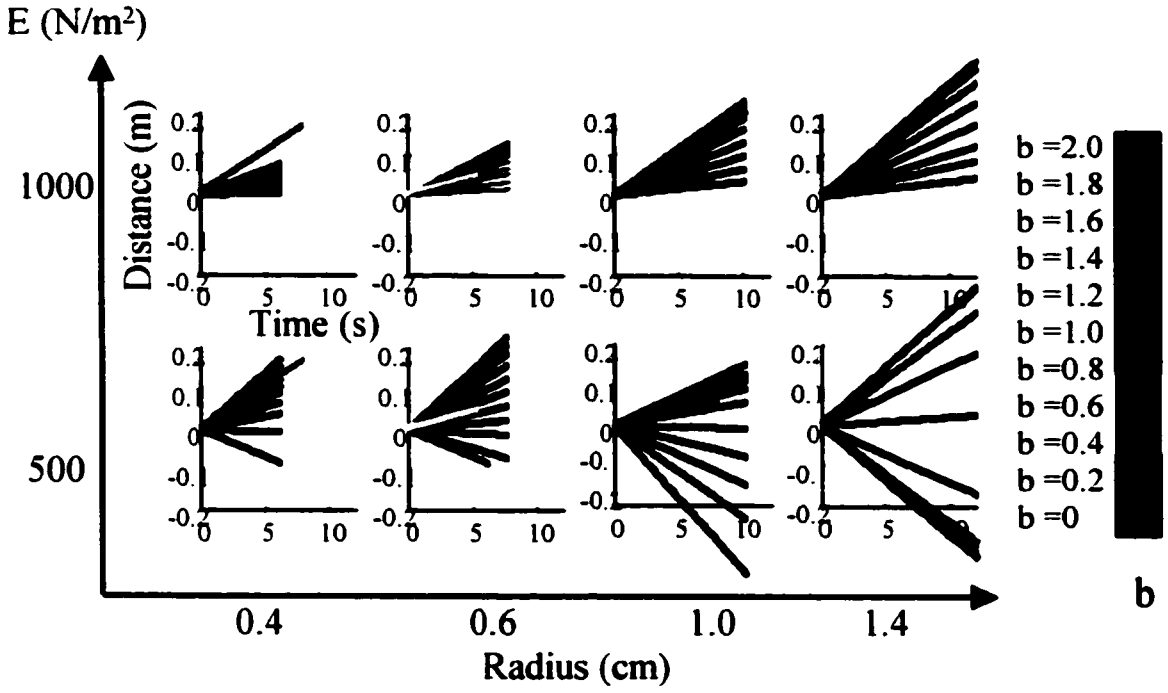

Figure 4.4-Alignment of kinematic and theoretical distance trajectories: Model predictions align well with measured kinematic data, but imply a strong sensitivity to both bell stiffness and the magnitude of the nonlinear exponent. The varying range of green to blue trajectories represents model distance output for different values for the nonlinear exponent *b*. The most green-hued line represents $b=0$ and the most blue-hued line represents $b=2$, a cubic nonlinearity. Pink, yellow, black, and red lines correspond with measured distance trajectories from four different *Polyorchis* of differing sizes. In all cases, measured and model data fall within the same range. Measured trajectories align with model predictions in a manner consistent with predictions for their nonlinear material properties.

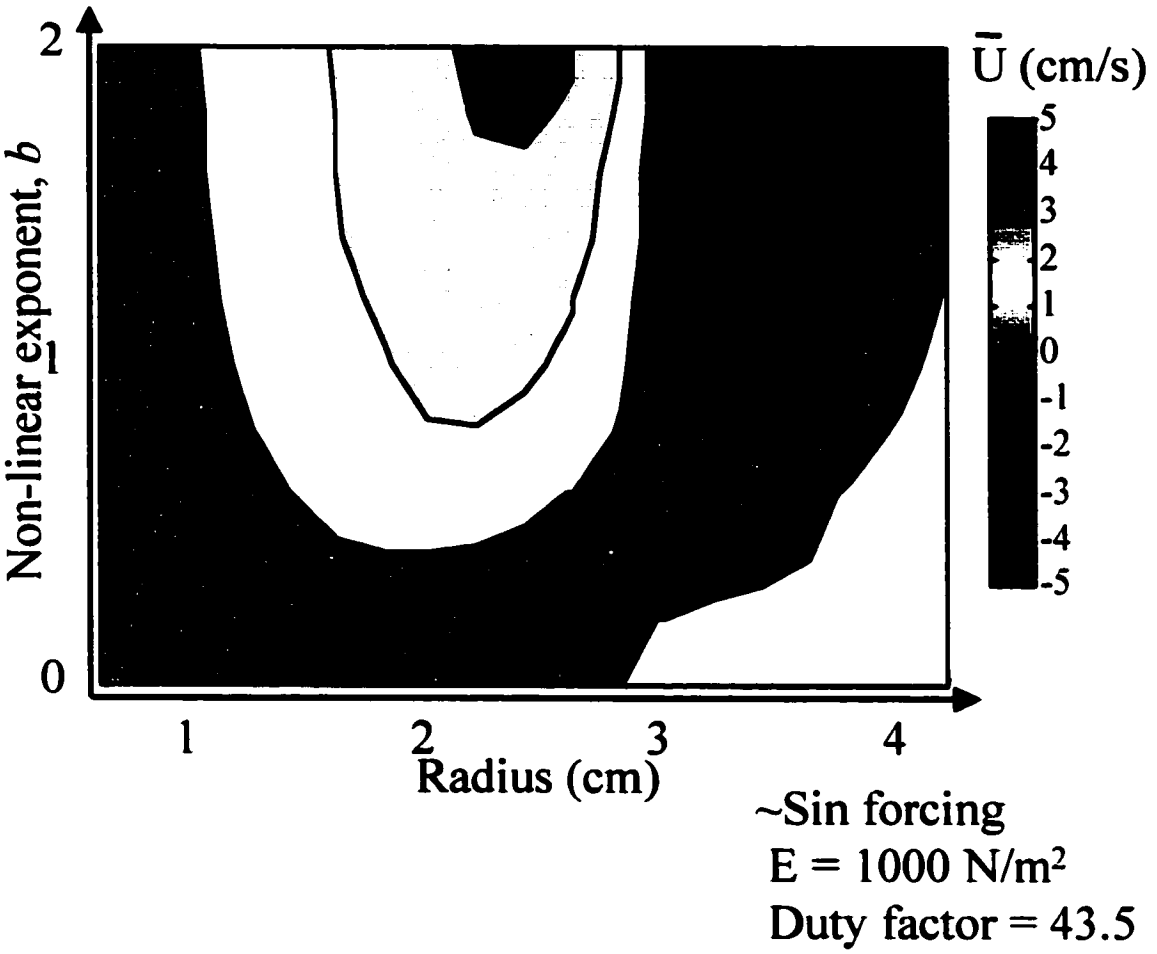

Figure 4.5-Size and spring nonlinearity: Swimming velocity depends on bell radius and on the magnitude of the nonlinear exponent, revealing discrete tuning optima at certain combinations of size and nonlinearity. The x-axis corresponds with bell radius and the y-axis corresponds with the nonlinear exponent *b*. Cool colors correspond with negative swimming velocities and warm colors correspond with positive swimming velocities. Green corresponds with weakly positive speeds. Peak swimming velocity occurs at an intermediate size and high value for the nonlinear exponent. An adjacent trough in swimming velocity corresponds with high nonlinearity at slightly larger sizes.

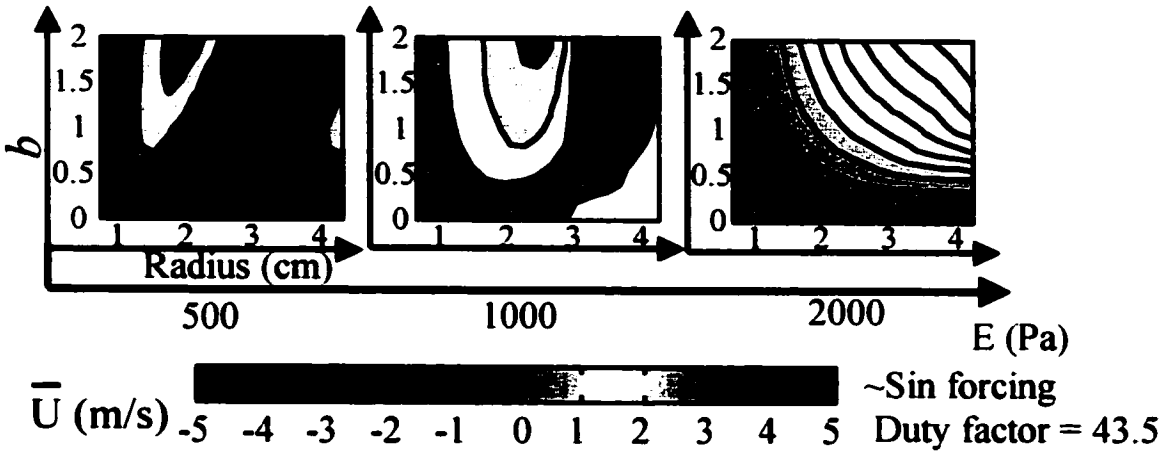

Figure 4.6-Size and spring nonlinearity for three stiffness values: The inner axes illustrate the effect of continuous variation in size and nonlinearity on swimming velocity. The outer axes show three different values for bell stiffness. Size-related tuning peaks and troughs are sensitive to bell stiffness. Peaks virtually disappear when E is high and become extremely pronounced E is low, with fewer combinations of size and nonlinearity that generate positive swimming velocities.

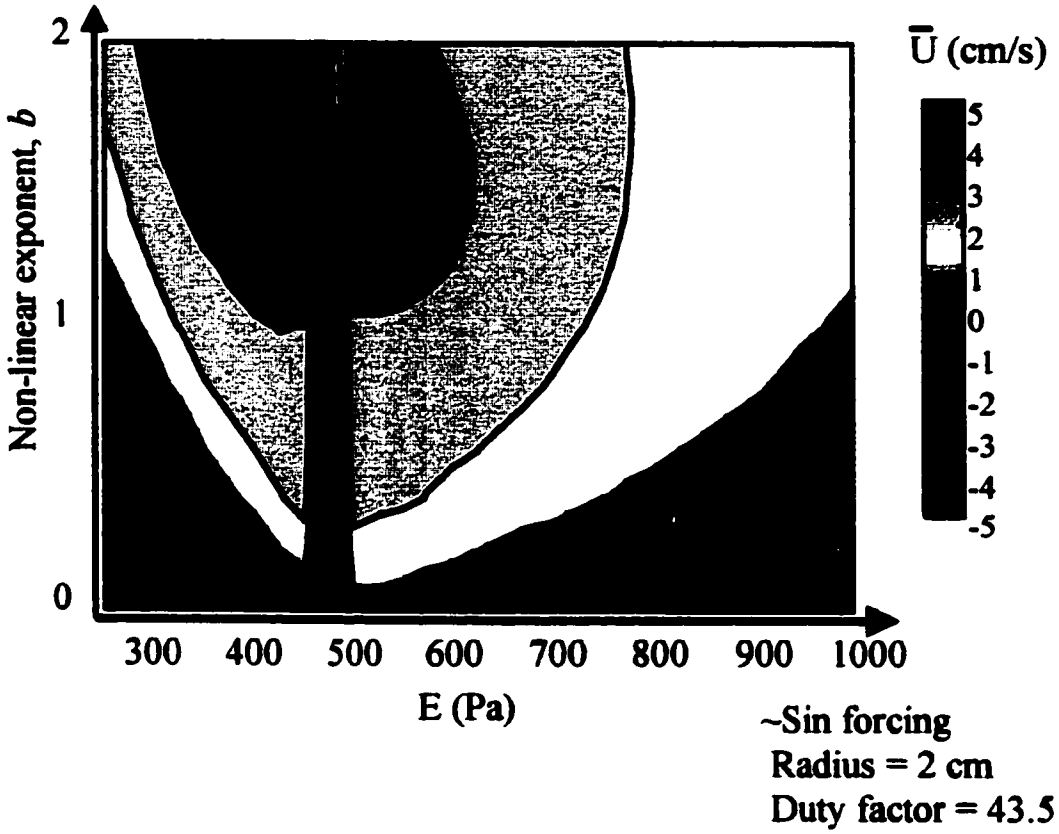

Figure 4.7-Stiffness and nonlinearity: Continuous variation in bell stiffness (E) along the x-axis reveals a distinct tuning optimum for high nonlinear exponents (y-axis) across low and intermediate values for E, but there is a sharp discontinuity between 450-500 Pa. This discontinuity is a tuning cusp, dividing the parameter space abruptly with a valley of negative swimming velocities just below E = 500 Pa. Interestingly, positive swimming velocities within this region of discontinuity exist only at the highest values for *b*.

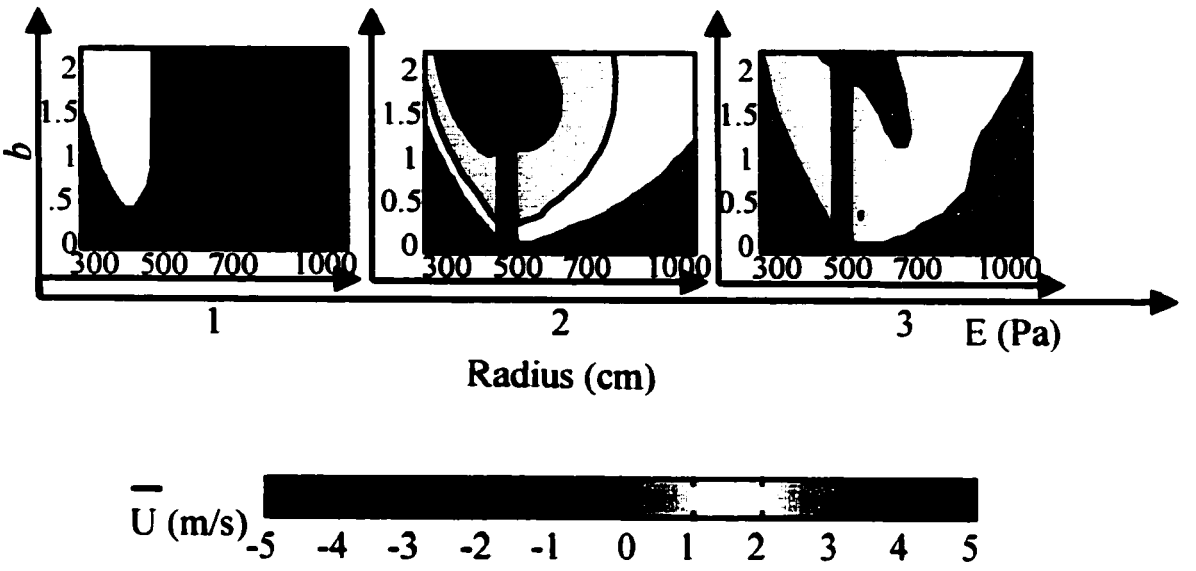

Figure 4.8-Stiffness and nonlinearity for three bell sizes: Stiffness dependent tuning optima also depend on bell size. Stiffness (E) varies continuously on the x-axis, with the nonlinear exponent *b* on the y-axis, across three different medusa size classes. The tuning cusp at E = 450-500 Pa is least obvious in the smallest size class and more pronounced for bigger jellyfish. In all cases, increasing nonlinear mechanical properties can offset regions of poor swimming performance at low values for bell stiffness.

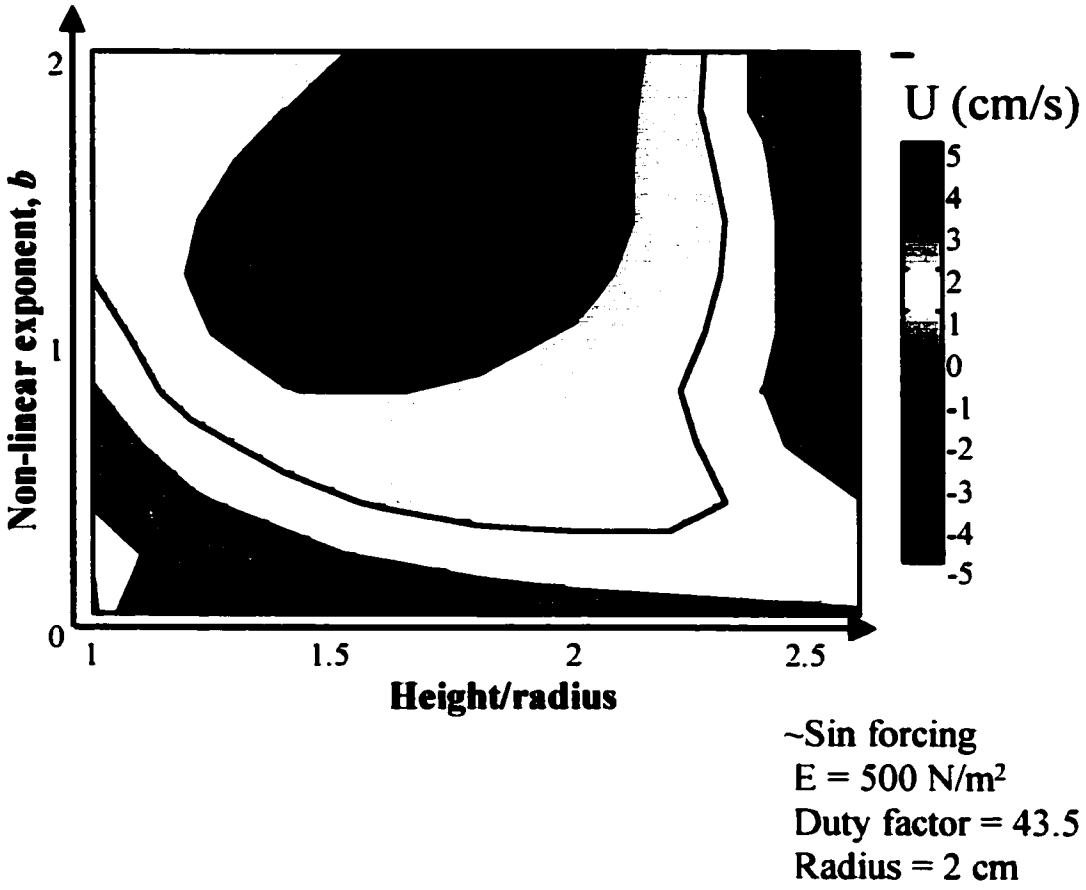

Figure 4.9-Shape and nonlinearity: Nonlinear mechanical properties enhance swimming speeds over a range of shapes that encompasses *Polyorchis penicillatus*. In this plot, the x-axis is fineness ratio, bell height/radius and the y-axis is the nonlinear exponent *b*, and the bell stiffness is 500 N/m^2. A large region of rapid swimming velocity corresponds with intermediate/high values for *b* and intermediate fineness ratios. A high fineness ratio causes negative swimming velocities except at low values for *b*. However, many fineness ratios and nonlinearities successfully produce positive, even rapid swimming velocities, suggesting there is a range of hydodynamically "acceptable" medusan shapes.

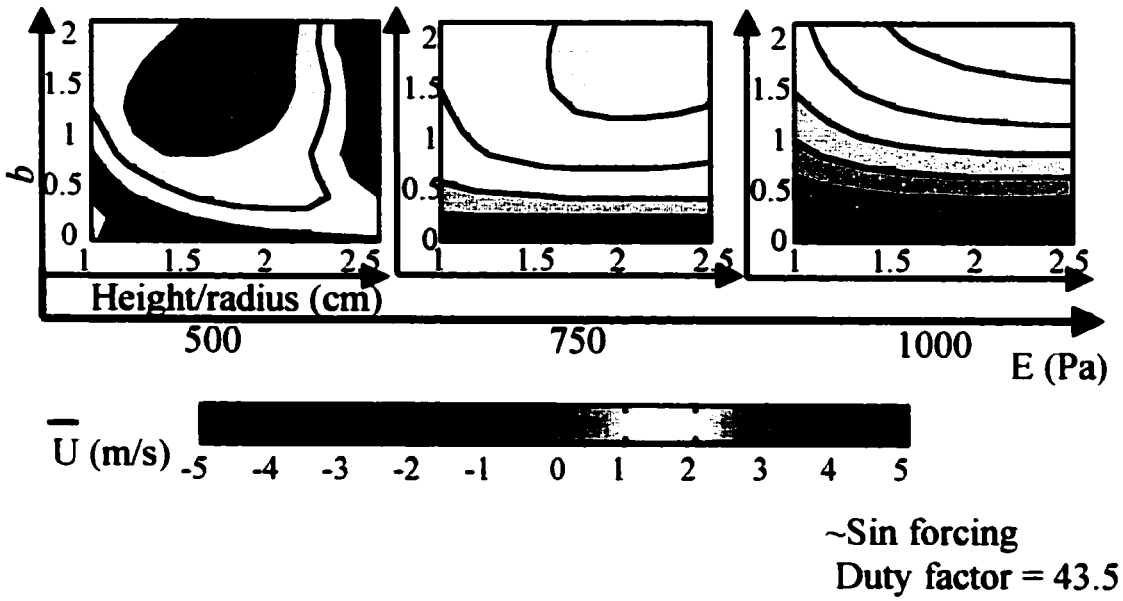

Figure 4.10-Shape and nonlinearity for three stiffness values: Increasing bell stiffness dampens the sensitivity of swimming speed to both shape and nonlinear mechanical properties. In these plots, the inner x-axis is the continuously varying bell fineness ratio (height/radius), the y-axis is the nonlinear exponent *b*. The outer x-axis is bell stiffness (E) for three different values.

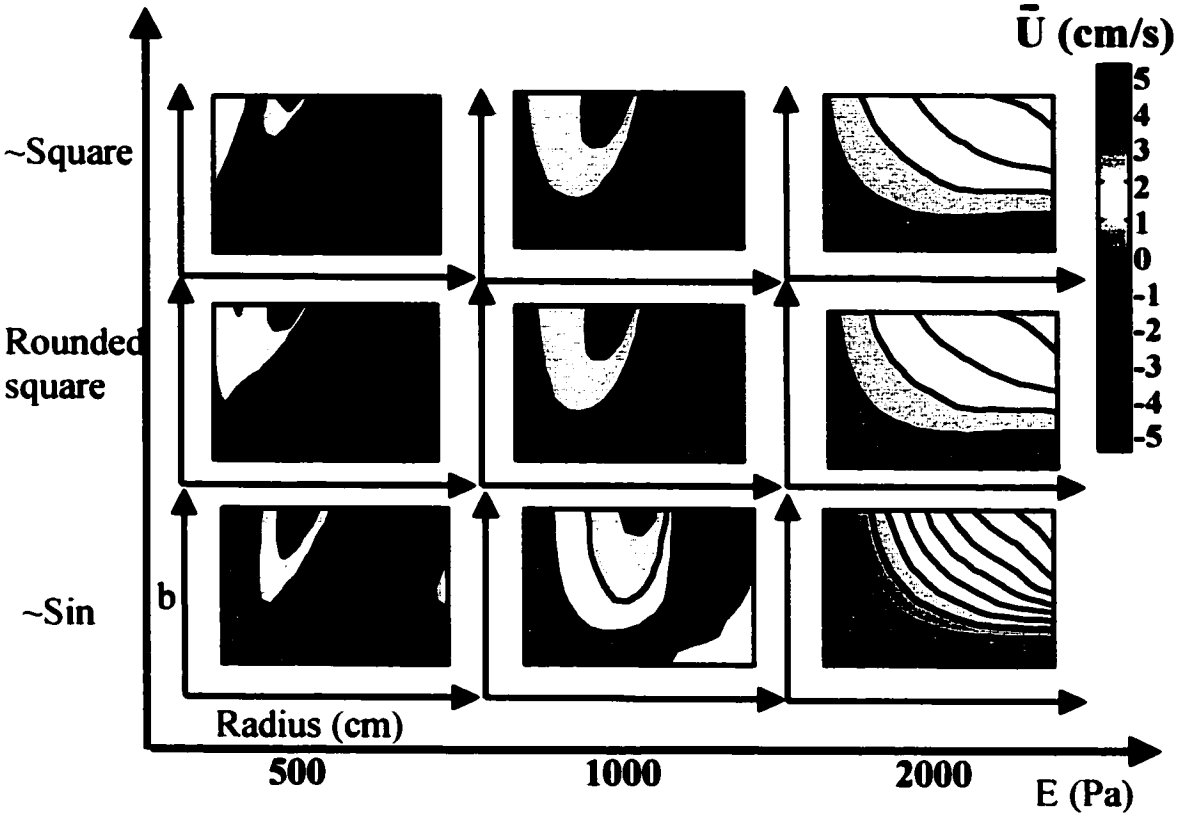

Figure 4.11-Size and nonlinearity for three shapes of muscle forcing and three stiffness values: The shape of the muscle forcing function heightens the sensitivity of swimming speed to nonlinear mechanical properties. Bell size varies continuously on the inner x-axis and the nonlinear exponent *b* varies on the inner y-axis. Stiffness (E) varies on the outer x-axis and the shape of the muscle forcing function varies on the outer y-axis. The colormap corresponds with swimming velocity. As the muscle forcing function becomes more square, for intermediate and low values for bell stiffness, the peaks and troughs in swimming velocity become more pronounced. Square waveform forcing is mostly unstable at low values for bell stiffness.

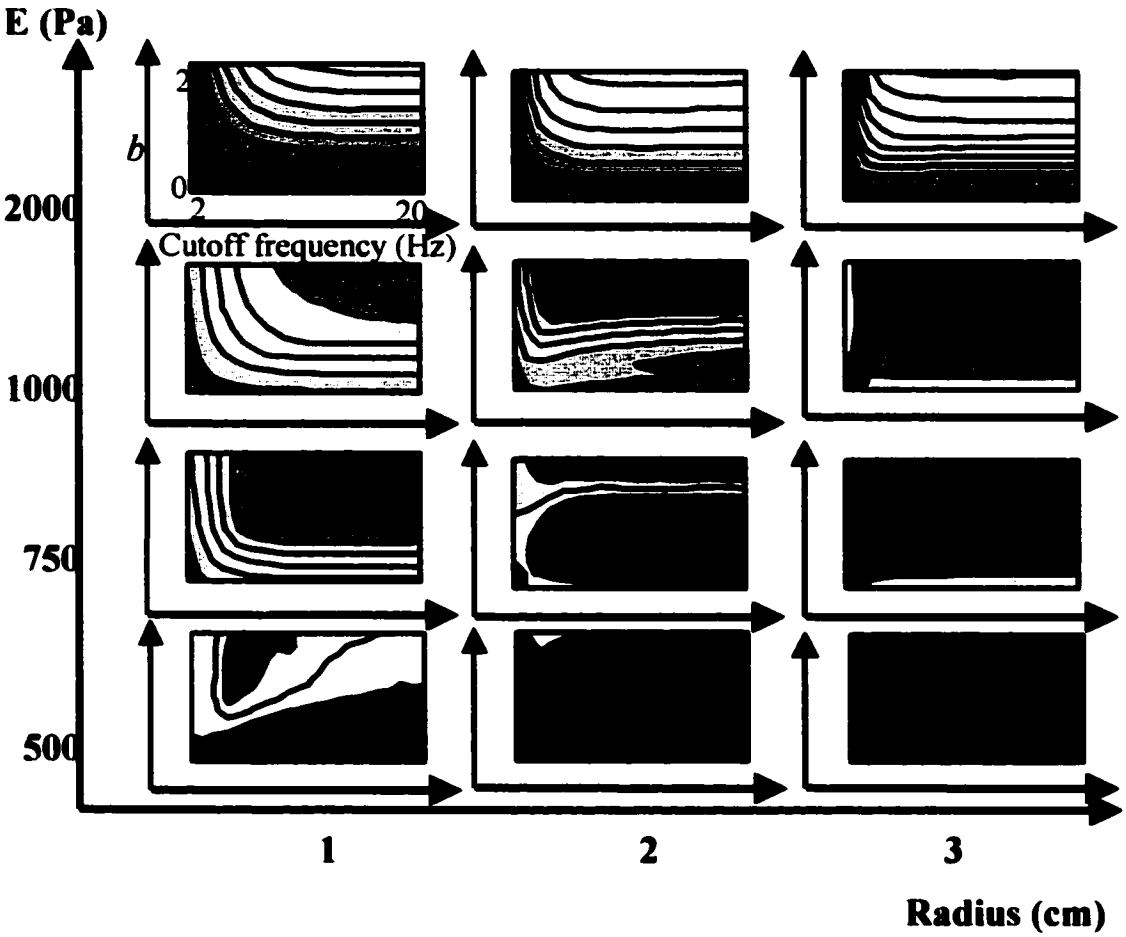

Figure 4.12-Continuous variation in the muscle forcing function for three bell sizes and four stiffness values: Continuous variation of the spectral components of muscle force production reveal size and stiffness specific tuning optima. The inner x-axis is the continuously varying waveform cutoff frequency and the y-axis is the nonlinear exponent *b*. The outer x-axis is bell size and the outer y-axis is bell stiffness. For low and intermediate stiffness and size, nonlinearity amplifies swimming speed and the rounded square range of cutoff frequencies optimize these velocities. But, nonlinear mechanical properties do not always amplify swimming speeds –especially for large bells at low and intermediate stiffness values. In these cases (right column) only a nearly Sin forcing function tolerates high nonlinear exponents.

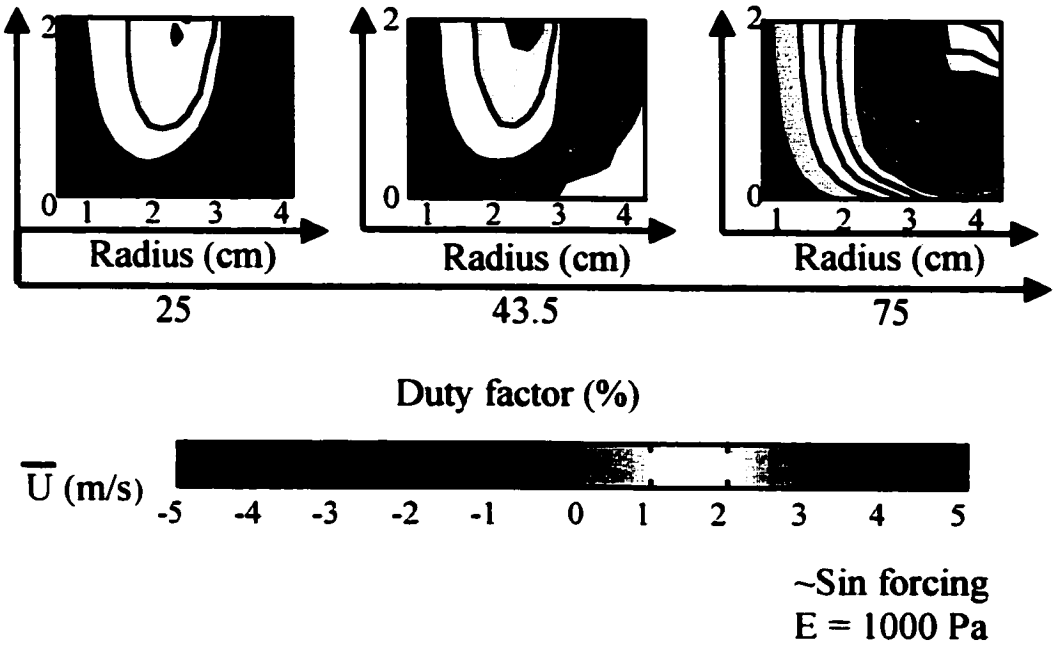

Figure 4.13-Size and nonlinearity for three duty factors: In this plot, the inner x-axis is bell radius and the inner y-axis is nonlinear exponent *b*. The outer x-axis is duty factor, or the fraction of the swim cycle comprised of muscle contraction. A high duty factor confers a particular advantage to swimming performance of large medusae, while a low duty factor is a clear detriment to large bell sizes. At all duty factors, there are peaks of swimming velocity that correspond with high values of the nonlinear exponent *b*.

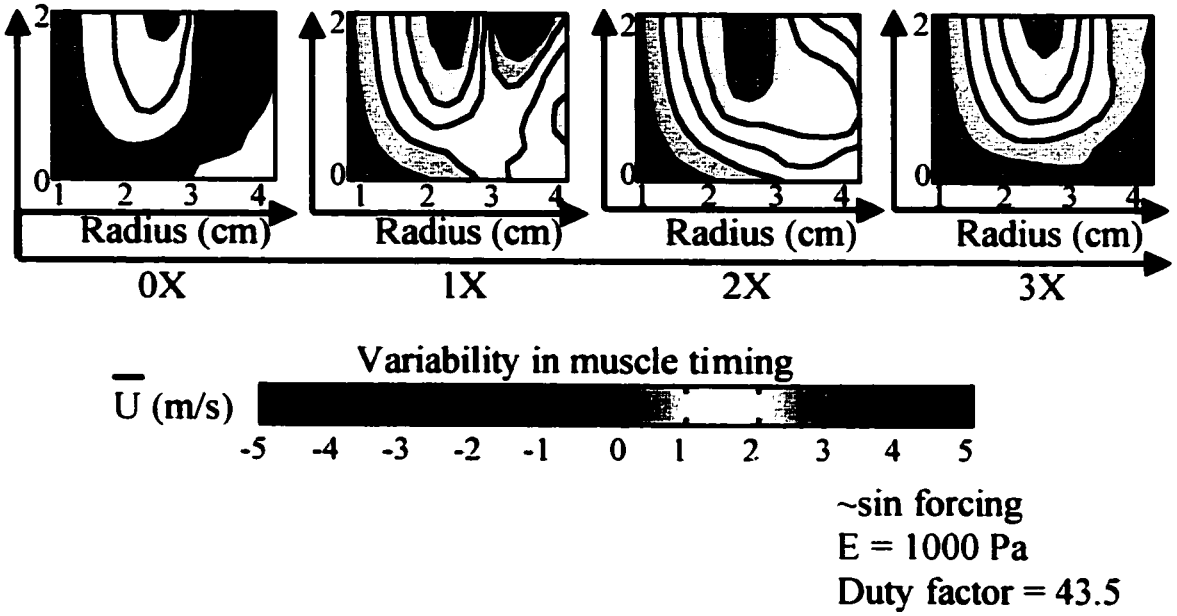

Figure 4.14-Variation in the timing of muscle force production at an intermediate duty factor: In this plot, the inner x-axis is bell radius and the inner y-axis is the nonlinear exponent *b*. The outer x-axis is the magnitude of variability in muscle timing. For this duty factor, 43.5 (%), the addition of variability in the timing of muscle contraction eliminates a region of poor swimming performance at large sizes and high values for the nonlinear exponent, *b*. A moderate amount of error in the timing of muscle contraction has an overall performance benefit across all sizes, although error eliminates maximal swimming velocity attained in the no-error case (far left).

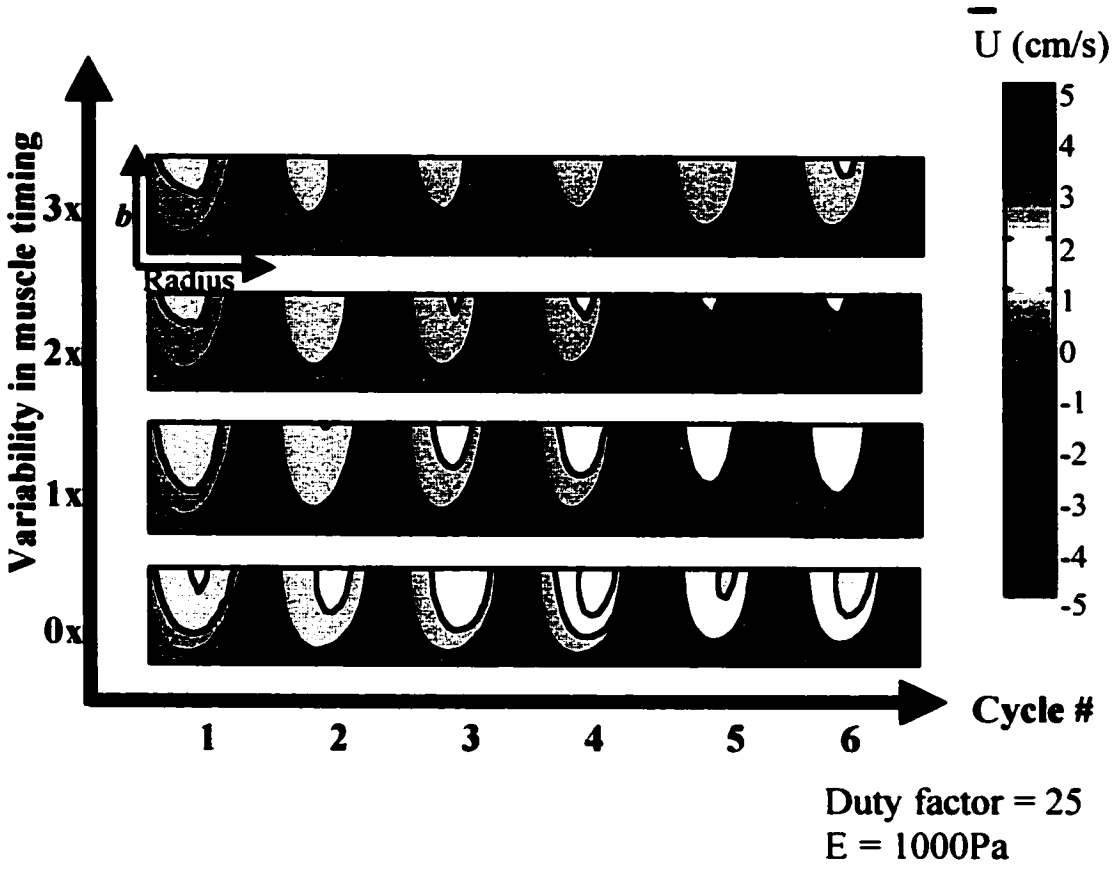

Figure 4.15 – Variability in muscle timing at a low duty factor: The effect of variability in the timing of muscle force production varies on a cycle by cycle basis. The inner axes of each of the small plots below are bell radius and nonlinear exponent *b*. The outer x-axis is the contraction cycle number and the outer y-axis is the magnitude of error the timing of muscle force production. At a low duty factor, increasing the amount of error enlarges the region of poor swimming performance for large medusae.

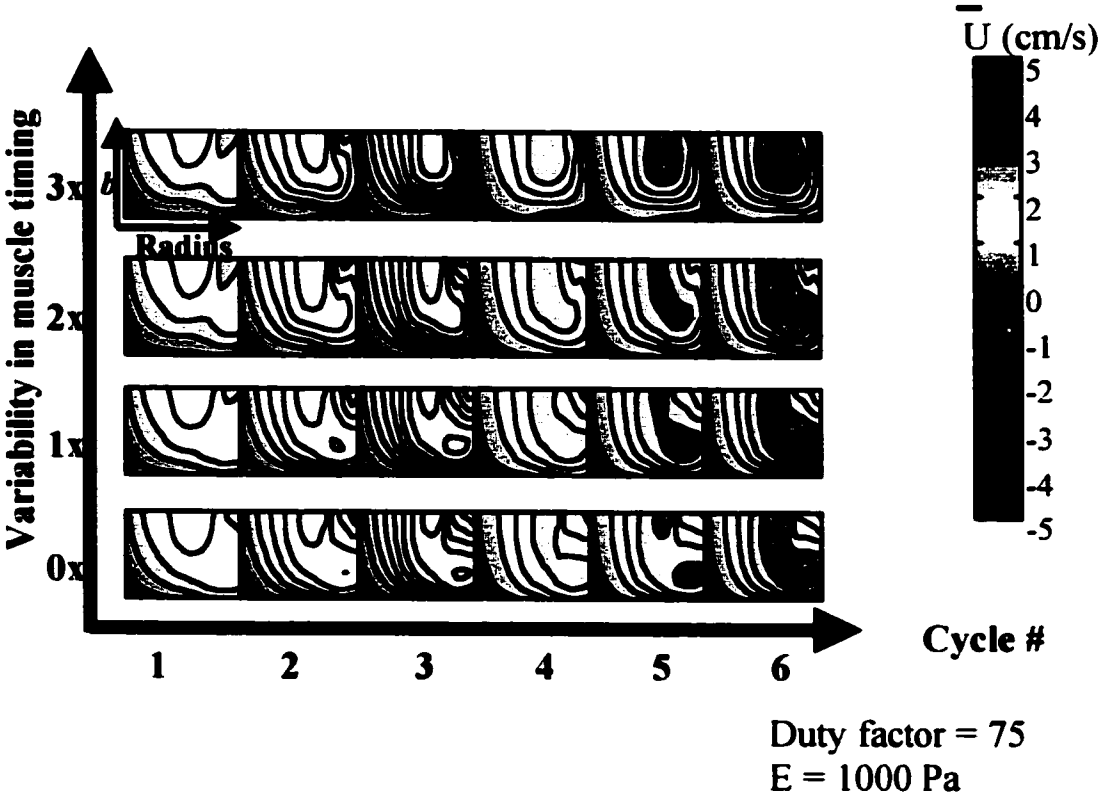

Figure 4.16- Variability in muscle timing at a high duty factor: The axes are the same as in Figure 15. Increasing nonlinearity reduces the sensitivity of this system to errors in the timing of muscle force production. For moderate levels of error in muscle timing, the region of high swimming velocities becomes more pronounced.

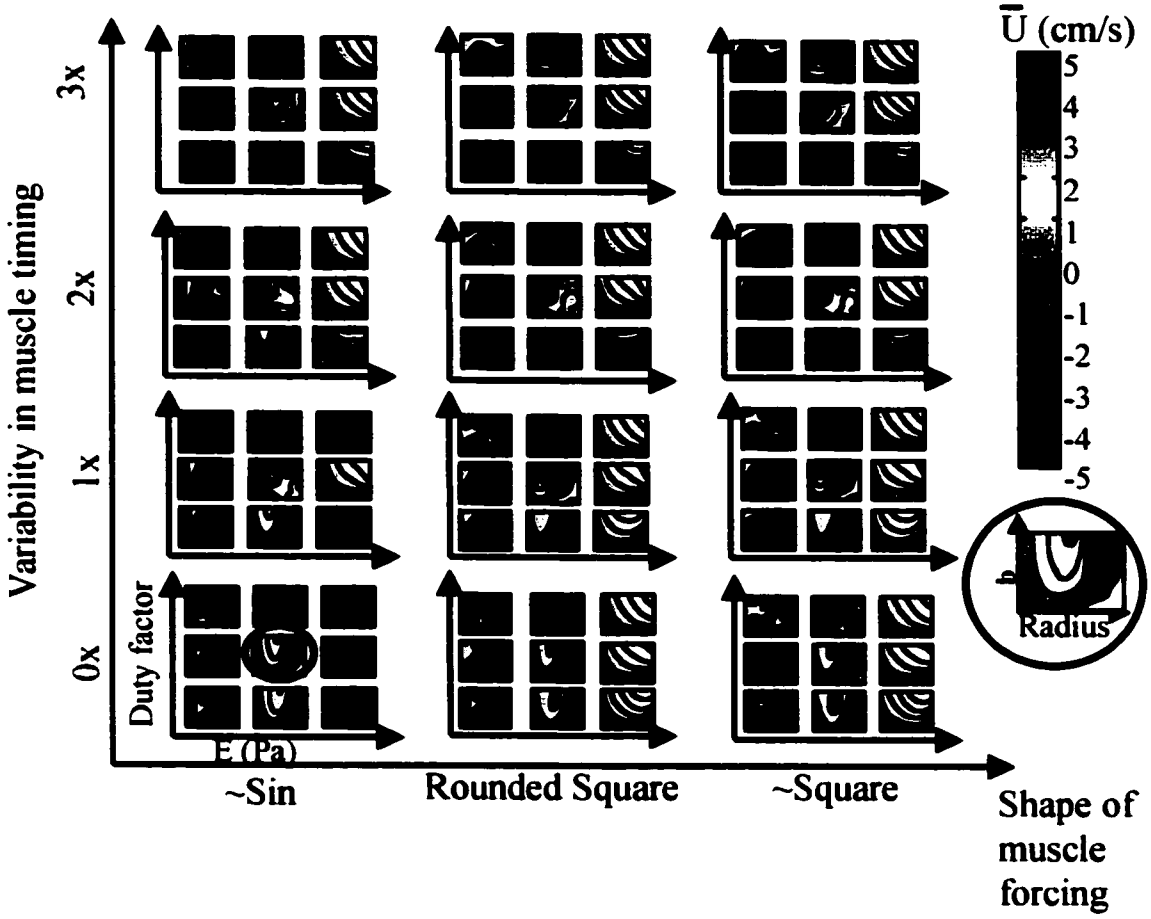

Figure 4.17-Composite overview of a multidimensional parameter space: Nonlinear mechanical properties set discrete tuning optima across a wide range of structural and dynamic parameters. The innermost x-axis on this plot (see circle below) is bell radius and the innermost y-axis is *b*. In the next layer of plots, the x-axis is stiffness (E = 500, 1000, 2000 Pa) and the y-axis is duty factor (25, 43.5, 75%). On the outermost axes, the x-axis is the shape of the muscle forcing function and the y-axis is the variability in the timing of muscle force production. Note that all peaks in swimming velocity (bright red) occur at nonzero values of the nonlinear exponent *b*.

BIBLIOGRAPHY

Alexander, R. M. (1962). Visco-elastic properties of the body-wall of sea anenomes. *Journal of Experimental Biology* 39, 373-386.

Alexander, R. M. (1979). *The Invertebrates*. Cambridge: Cambridge University Press.

Alexander, R. M. (1988). *Elastic Mechanisms in Animal Movement*. Cambridge: Cambridge University Press.

Alexander, R. M. e. and Goldspink, G. e. (1977). *Mechanics and energetics of animal locomotion*. London: Chapman and Hall.

Allen, J. C. and Logan, J. A. (1992). Nonlinear dynamics and chaos in insect populations. *Annual Review of Entomology* 37, 455-477.

Armentano, R. L., Barra, J. G., Levenson, J., Simon, A. and Pichel, R. H. (1995). Arterial wall mechanics in conscious dogs. *Circulation Research* 76.

Bar-Yam, Y. (1997). *Dynamics of Complex Systems*. Reading: Addison-Wesley.

Berger, C. S. and Malpas, S. C. (1998). Modeling of the dynamic relationship between arterial pressure, renal sympathetic nerve activity and renal blood flow in conscious rabbits. *Journal of Experimental Biology* 201, 3425-3430.

Bi, Q. and Yu, P. (1999). Double Hopf bifurcations and chaos of a nonlinear vibration system. *Nonlinear Dynamics* 19, 313-332.

Bjornstad, O. N. and Grenfell, B. T. (2001). Noisy clockwork: Time series analysis of population fluctuations in animals. *Science* 293, 638-643.

Bohoeffer, S., May, R. M., Shaw, G. M. and Nowak, M. A. (1997). Virus dynamics and drug therapy. *Proceedings of the National Academy of Sciences* 94, 6791-6976.

Boriek, A. M. and Rodarte, J. R. (1997). Effects of transverse fiber stiffness and central tendon on displacement and shape of a simple diaphragm model. *Journal of Applied Physiology* 82, 1626-1636.

Boriek, A. M., Kelly, N. G., Rodarte, J. R. and Wilson, T. A. (2000). Biaxial constitutive relations for the passive canine diaphragm. *Journal of Applied Physiology* 89, 2187-2190.

Bouillon, J. and Coppois, G. (1977). Etude comparative de la mesoglee des cnidaires. *Cahiers de Biologie Marine* 18, 339-368.

Bronski, J. C., Segev, M. and Weinstein, M. I. (2001). Mathematical frontiers in optical solitons. *Proceedings of the National Academy of Sciences* 98, 12872-12873.

Buchanan, C. I. and Marsh, R. L. (2001). Effects of long-term exercise on the biomechanical properties of the Achilles tendon of guinea fowl. *Journal of Applied Physiology* 90, 164-171.

Campbell, K. B., Razumova, M. V., Kirkpatrick, R. D. and Slinker, B. K. (2001). Nonlinear myofilaments regulatory processes affect frequency-dependent muscle fiber stiffness. *Biophysical Journal* 81, 2278-2296.

Cartwright, J. H. E., Gonzalez, D. L. and Piro, O. (2001). Pitch perception: A dynamical-systems perspective. *Proceedings of the National Academy of Sciences* 98, 4855-4859.

Chang, H.-S., Staras, K. and Gilbey, M. P. (2000). Multiple oscillators provide metastability in rhythm generation. *Journal of Neuroscience* 20, 5135-5143.

Chapman, G. (1953). Studies of the mesogloea of Coelenterates: I. Histology and chemical properties; II. Physical properties. *Quarterly Journal of Microscopical Science*, 155-176.

Christini, D. J., Stein, K. M., Markowitz, S. M., Mittal, S., Slotwiner, D. J., Scheiner, M. A., Iwai, S. and Lerman, B. B. (2001). Nonlinear-dynamical arrhythmia control in humans. *Proceedings of the National Academy of Sciences* 98, 5827-5832.

Colin, S. P. and Costello, J. H. (1996). Relationship between morphology and hydrodynamics during swimming by the hydromedusae *Aequorea victoria* and *Aglantha digitale*. *Scientia Marina* 60, 35-42.

Colin, S. P. and Costello, J. H. (2002). Morphology, swimming performance and propulsive mode of six co-occurring hydromedusae. *Journal of Experimental Biology* 205, 427-437.

Cooper, N. P. and Rhode, W. S. (1995). Nonlinear mechanics at the apex of the guinea-pig cochlea. *Hearing Research* 82, 225-243.

Czirok, A., Janosi, I. M. and Kessler, J. O. (2000). Bioconvective dynamics: Dependence on organism behaviour. *Journal of Experimental Biology* 203, 3345-3354.

Damiano, E. R. and Stace, T. M. (2002). A mechano-electrochemical model of radial deformation of the capillary glycocalyx. *Biophysical Journal* 82, 1153-1175.

Daniel, T. L. (1983). Mechanics and energetics of medusan jet propulsion. *Canadian Journal of Zoology* 61, 1406-1420.

Daniel, T. L. (1985). Cost of locomotion: Unsteady medusan swimming. *Journal of Experimental Biology* 119, 149-164.

Daniel, T. L. (1995). Invertebrate swimming: Integrating internal and external mechanics. In *Biological Fluid Dynamics*, eds. C. P. Ellington and T. J. Pedley), pp. 61-89: Society for Experimental Biology.

Daniel, T. L., Helmuth, B. S., Saunders, W. B. and Ward, P. D. (1997). Septal complexity in ammonoid cephalopods increased mechanical risk and limited depth. *Paleobiology* 23, 470-481.

Daniel, T. L., Trimble, A. C. and Chase, P. B. (1998). Compliant realignment of binding sites in muscle: Transient behavior and mechanical tuning. *Biophysical Journal* 74, 1611-1621.

De Zee, M., Bojsen-Moller, F. and Voigt, M. (2000). Dynamic viscoelastic behavior of lower extremity tendons during simulated running. *Journal of Applied Physiology* 89, 1352-1359.

DeMont, M. E. (1990). Tuned oscillations in the swimming scallop *Pecten maximus*. *Canadian Journal of Zoology* 68, 786-791.

DeMont, M. E. (1992). Locomotion of soft bodied animals. In *Advances in Comparative and Environmental Physiology*, vol. 11, pp. 167-190. Berlin: Springer-Verlag.

DeMont, M. E. and Gosline, J. M. (1988). Mechanics of jet propulsion in the hydromedusan jellyfish *Polyorchis penicillatus*: I. Mechanical properties of the locomotor structure. *Journal of Experimental Biology* 134, 313-332.

DeMont, M. E. and Gosline, J. M. (1988b). Mechanics of jet propulsion in the hydromedusan jellyfish *Polyorchis penicillatus*: II. Energetics of the jet cycle. *Journal of Experimental Biology* 134, 333-345.

DeMont, M. E. and Gosline, J. M. (1988b). Mechanics of jet propulsion in the hydromedusan jellyfish *Polyorchis penicillatus*: III. A natural resonating bell; The presence and importance of a resonant phenomenon in the locomotor structure. *Journal of Experimental Biology* 134, 347-361.

Dickinson, M. H. (1990). Linear and nonlinear encoding properties of an identified mechanoreceptor on the fly wing measured with mechanical noise stimuli. *Journal of Experimental Biology* 151, 219-244

Dorsey, N. E. (1940). *Properites of Ordinary Water Substance*: Litton Educational Publishing, Inc.

Farley, C. T., Glasheen, J. and McMahon, T. (1993). Running springs: Speed and animal size. *Journal of Experimental Biology* 185, 71-86.

French, A. S. and Korenberg, M. J. (1989). A nonlinear cascade model for action potential encoding in an insect sensory neuron. *Biophysical Journal* 55, 655-661.

French, A. S., Korenberg, M. J., Jarvilehto, M., Kouvalainen, E., Juusola, M. and Weckstrom, M. (1993). The dynamic nonlinear behavior of fly photoreceptors evoked by a wide range of light intensities. *Biophysical Journal* 65, 832-839.

Fu, Y. B. and Ogden, R. W. (2001). *Nonlinear Elasticity: Theory and Applications*. Cambridge: Cambridge University Press.

Full, R. J. and Koditschek, D. E. (1999). Templates and anchors: Neuromechanical hypotheses of legged locomotion on land. *Journal of Experimental Biology* 202, 3325-3332.

Fussmann, G. F., Ellner, S. P., Shertzer, K. W. and Hairston, N. G. J. (2000). Crossing the Hopf bifurcation in a live predator-prey system. *Science* 290, 1358-1360.

Garcia, A. E., Soumpasis, D. M. and Jovin, T. M. (1994). Dynamics and relative stabilities of parallel and antiparallel stranded DNA duplexes. *Biophysical Journal* 66, 1742-1755.

Gilchrist, M. A. and Nijhout, H. F. (2001). Nonlinear developmental process as sources of dominance. *Genetics* 159, 423-432.

Gladfelter, W. B. (1972). Structure and function of the locomotory system of *Polyorchis montereyensis* (Cnidaria, Hydrozoa). *Helgolander wiss. Meeresunters* 23, 38-79.

Goldberger, A. L. (1991). Is the normal heartbeat chaotic or homeostatic? *News in Physiological Sciences* 6, 87-91.

Goldberger, A. L., Bhargava, V., West, B. J. and Mandell, A. J. (1985). On a mechanism of cardiac electrical stability. The fractal hypothesis. *Biophysical Journal* 48, 525-528.

Gosline, J. M. and Shadwick, R. E. (1983). The role of elastic energy storage mechanisms in swimming: an analysis of mantle elasticity in escape jetting in the squid, *Loligo opalescens*. *Canadian Journal of Zoology* 61, 1421-1431.

Gosline, J. M. and Shadwick, R. E. (1983). The role of elastic energy storage mechanisms in swimming: an analysis of mantle elasticity in escape jetting in the squid, *Loligo opalescens*. *Canadian Journal of Zoology* 61, 1421-1431.

Gosline, J. M. and Shadwick, R. E. (1996). The mechanical properties of fin whale arteries are explained by novel connective tissue designs. *Journal of Experimental Biology* 199, 985-997.

Guckenheimer, J., Gueron, S. and Harris-Warrick, R. M. (1993). Mapping the dynamics of a bursting neuron. *Philosophical Transactions: Biological Sciences* 341, 345-359.

Hastings, H. M., Evans, S. J., Quan, W., Chong, M. L. and Nwasokwa, O. (1996). Nonlinear dynamics in ventricular fibrillation. *Proceedings of the National Academy of Sciences* 93, 10495-10499.

Higgins, K., Hastings, A., Sarvela, J. N. and Botsford, L. W. (1997). Stochastic dynamics and deterministic skeletons: Population behavior of Dungeness Crab. *Science* 276, 1431-1435.

Hyman, L. (1942). Observations and experiments on the physiology of medusae. In *Invertebrates*, vol. 1, pp. 282-296: McGraw Hill.

Imura, T., Yamamoto, K., Satoh, T., Kanamori, K., Mikami, T. and Yasuda, H. (1990). In vivo viscoelastic behavior in the human aorta. *Circulation Research* 66, 1413-1419.

Ivanov, P. C., Amaral, L. A. N., Goldberger, A. L., Havlin, S., Rosenblum, M. G., Struzik, Z. R. and Stanley, H. E. (1999). Multifractality in human heartbeat dynamics. *Nature* 399, 461-465.

Johnson, A. S. and Koehl, M. A. R. (1994). Maintenance of dynamic strain similarity and environmental stress factor in different flow habitats: Thallus allometry and material properties of a giant kelp. *Journal of Experimental Biology* 195, 381-410.

Kasapi, M. A. and Gosline, J. M. (1996). Strain-rate dependent mechanical properties of the Equine hoof wall. *Journal of Experimental Biology* 199, 1133-1146.

Kasapi, M. A. and Gosline, J. M. (1999). Micromechanics of the Equine hoof wall: Optimizing crack control and material stiffness through modulation of the properties of keratin. *Journal of Experimental Biology* 202, 377-391.

Kharakoz, D. P. (2000). Protein compressibility, dynamics, and pressure. *Biophysical Journal* 79, 511-525.

Klapper, I. and Qian, H. (1998). Remarks on discrete and continuous large-scale models of DNA dynamics. *Biophysical Journal* 74, 2504-2514.

Klapper, I. and Qian, H. (1998). Remarks on discrete and continuous large-scale models of DNA dynamics. *Biophysical Journal* 74, 2504-2514.

Koehl, M. A. R. (1977). Mechanical diversity of connective tissue of the body wall of sea anenomes. *Journal of Experimental Biology* 69, 107-125.

Lawrence, A. F., McDaniel, J. C., Chang, D. B. and Birge, R. R. (1987). The nature of phonons and solitary waves in alpha-helical proteins. *Biophysical Journal* 51, 785-793.

Lin, E. C. and Cantiello, H. F. (1993). A novel method to study the electrodynamic behavior of actin filaments. Evidence for cable-like properties of actin. *Biophysical Journal* 65, 1371-1378.

Long, J. H. J., Pabst, D. A., Sheperd, W. R. and McLellan, W. A. (1997). Locomotor design of dolphin vertebral columns: Bending mechanics and morphology of *Delphinus delphis*. *Journal of Experimental Biology* 200, 65-81.

Maksym, G. N. and Bates, J. H. T. (1997). A distributed nonlinear model of lung tissue elasticity. *Journal of Applied Physiology* 82, 32-41.

McMahon, T. A. and Greene, P. R. (1979). The influence of track compliance on running. *Journal of Biomechanics* 12, 893-904.

Millor, J., Pham-Delegue, M., Deneubourg, J. L. and Camazine, S. (1999). Self-organized defensive behavior in honeybees. *Proceedings of the National Academy of Sciences* 96, 12611-12615.

Mills, C. E. (1981). Diversity of swimming behaviors in hydromedusae as related to feeding and utilization of space. *Marine Biology* 64, 185-189.

Mosekilde, E. and Mouritsen, O. G. e. (1995). *Modelling the Dynamics of Biological Systems: Nonlinear Phenomena and Pattern Formation*. Berlin: Springer-Verlag.

Murray, J. D. (1977). *Nonlinear-differential equation models in biology*. Oxford: Clarendon Press.

Nassar, P. N., Jackson, A. C. and Carrier, D. R. (2001). Entraining the natural frequencies of running and breathing in guinea fowl (*Numida meleagris*). *Journal of Experimental Biology* 204, 1641-1651.

Ngo, L. G. and Roussel, M. R. (1997). A new class of biochemical oscillator models based on competitive binding. *European Journal of Biochemistry* 245, 182-190.

Ospeck, M., Eguiluz, V. M. and Magnasco, M. O. (2001). Evidence of a Hopf bifurcation in frog hair cells. *Biophysical Journal* 80, 2597-2607.

Pabst, D. A. (1996). Springs in swimming animals. *American Zoologist* 36, 723-735.

Passano, L. M. (1965). Behavioral physiology of coelenterates: Introductory remarks. *American Zoologist* 5, 337-340.

Pece, A. E., French, A. S., Korenberg, M. J. and Kuster, J. E. (1990). Nonlinear mechanisms for gain adaptation in locust photoreceptors. *Biophysical Journal* 57, 733-743.

Pikkujamsa, S., Makikallio, T. H., Sourander, L. B., Raiha, I. J., Puuka, P., Skytta, J., Peng, C.-K., Goldberger, A. L. and Huikuri, H. V. (1999). Cardiac interbeat interval dynamics from childhood to senescence. *Circulation* 100, 393-399.

Podolsky, R. D. and Emlet, R. B. (1993). Separating the effects of temperature and viscosity on swimming and water movement by sand dollar larvae (*Dendraster excentricus*). *Journal of Experimental Biology* 176, 207-221.

Romashko, D. N., Marban, E. and O'Rourke, B. (1998). Subcellular metabolic transients and mitochondrial redox waves in heart cells. *Proceedings of the National Academy of Sciences* 95, 1618-1623.

Ruesink, J. L. (1998). Variation in per capita interaction strength: Thresholds due to nonlinear dynamics and nonequilibrium conditions. *Proceedings of the National Academy of Sciences* 95, 6843-6847.

Scheinerman, E. R. (1996). *Invitation to Dynamical Systems*. Upper Saddle River: Prentice Hall.

Schimz, A. and Hildebrand, E. (1992). Nonrandom structures in the locomotor behavior of *Halobacterium*: A bifurcation route to chaos? *Proceedings of the National Academy of Sciences* 89, 457-460.

Schmidt, G. and Tondl, A. (1986). *Non-Linear Vibrations*. Cambridge: Cambridge University Press.

Shadwick, R. E. (1999). Mechanical design in arteries. *Journal of Experimental Biology* 202, 3305-3313.

Small, M., Judd, K., Lowe, M. and Stick, S. (1999). Is breathing in infants chaotic? Dimension estimates for respiratory patterns during quiet sleep. *Journal of Applied Physiology* 86, 359-376.

Spencer, A. N. and Satterlie, R. A. (1981). The action potential and contraction in subumbrellar swimming muscle of *Polyorchis penicillatus* (Hydromedusae). *Journal of Comparative Physiology A.* 144, 401-407.

Spencer, A. N. and Satterlie, R. A. (1981). The action potential and contraction in subumbrellar swimming muscle of *Polyorchis penicillatus* (Hydromedusae). *Journal of Comparative Physiology A.* 144, 401-407.

Suki, B., Yuan, H., Zhang, Q. and Lutchen, K. R. (1997). Partitioning of lung tissue response and inhoogeneous airway constriction at the airway opening. *Journal of Applied Physiology* 82, 1349-1359.

Sun, C., Vaccaro, E. and Waite, J. H. (2001). Oxidative stress and the mechanical properties of naturally occurring chimeric collagen-containing fibers. *Biophysical Journal* 81, 3590-3595.

Szulgit, G. K. and Shadwick, R. E. (2000). Dynamic mechanical characterization of a mutable collagenous tissue: Response of sea cucumber dermis to cell lysis and dermal extracts. *Journal of Experimental Biology* 203, 1539-1550.

Thomas, N. and Thornhill, R. A. (1996). Stretch activation and nonlinear elasticity of muscle cross-bridges. *Biophysical Journal* 70, 2807-2818.

Thomas, R. D. K. and Reif, W.-E. (1993). The skeleton space: A finite set of organic designs. *Evolution* 47, 341-360.

Timoshenko, S., Young, D. H. and Weaver, W. J. (1974). *Vibration Problems in Engineering.* New York: John Wiley & Sons.

Tozeren, A., Skalak, R., Sung, K. L. and Chien, S. (1982). Viscoelastic behavior of erythrocyte membrane. *Biophysical Journal* 39, 23-32.

Tsai, M. A., Frank, R. S. and Waugh, R. E. (1993). Passive mechanical behavior of human neutrophils: power-law fluid. *Biophysical Journal* 65, 2078-2088.

Tulppo, M. P., Hughson, R. L., Makikallio, T. H., Airaksinen, K. E. J., Seppanen, T. and Huikuri, H. V. (2001). Effects of exercise and passive head-up tilt on fractal and complexity properties of heart rate. *American Journal of Physiology: Heart Circulatory Physiology* 280, 1081-1087.

Vikman, S., Makikallio, T. H., Yi-Mayry, S., Pikkujamsa, S., Koivisto, A.-M., Reinikainen, P., Airaksinen, K. E. J. and Huikuri, H. V. (1999). Altered complexity and correlation properties of R-R interval dynamics before the spontaneous onset of paroxysmal atrial fibrillation. *Circulation* 100, 2079-2084.

Vongehr, S. Solitons: The Net Advance of Physics.
http://physics1.usc.edu/~vongehr/solitons_html/solitons.html

Wainwright, S. A., Biggs, W. D., Currey, J. D. and Gosline, J. M. (1976). *Mechanical Design of Organisms*. Princeton: Princeton University Press.

Wang, X. T. and Ker, R. F. (1995). Creep rupture of wallaby tail tendons. *Journal of Experimental Biology* 198, 831-845.

Weiss, J. N., Garfinkel, A., Karagueuzian, H. S., Qu, Z. and Chen, P.-S. (1999). Chaos and the transition to ventricular fibrillation. *Circulation* 99, 2819-2826.

Wilson, H. R. (1993). Nonlinear processes in visual pattern discrimination. *Proceedings of the National Academy of Sciences* 90, 9785-9790.

Zhou, J. and Fung, Y. C. (1997). The degree of nonlinearity and anisotropy of blood vessel elasticity. *Proceedings of the National Academy of Sciences* 94, 14255-14260

APPENDIX A:

Matlab Code for Chapter 2

HappyLoadRealData.m – Data processing file that calculates complex moduli of mesoglea

```
clear all;
%cd(DataPath);
close all
%Enter dimensions of strip of tissues
L = 0.00782; %(m)
W = .00246; %(m)
H = 0.0016; %(m)
Area = W * H; %(m^2 - cross-sectional area)
SampleFreq = 1; %(Hz)

%Parameters that correspond to the force and length calibrations
al = .0056;
bl = -0.0046;
cl = .119;
dl = 0.0038;

af = .0627;
bf = 0.00003;

alf = .9787;
blf = .0152;


%Constant specifying what percent of peak to search around
c = 0.1;

%Specify auto or manual mode
mode = 'auto';
  mode = 'manual';

%Enter sample rate of data acquisition
SampleRate = 1000; %'points/s'
SamplePeriod = 1/SampleRate; %(s)
FreqCutOff = 1.5;
FilterOrder = 3;
```

```
%Specify input and output path
%[DefaultDataPath, OutputPath] = IOPaths;
HomePath = cd;
FileFilter = '*';

%Two different procedures for getting files, depending on whether
%mode is set to manual or auto

  if strcmp(mode, 'auto');
        Data = AutoReadTextFile(DefaultDataPath, FileName);
        DataPath = DefaultDataPath;
        else
        DialogString = 'Select File to Import';
%get the file name and the path to the desired file
        [FileName FilePath]=uigetfile(FileFilter,DialogString);
        cd(FilePath)
fopen(FileName, 'r+')

%Reads data in from a text file
Data = ReadTextFile;
Data =fscanf(3, '%f', [2,inf]);
% fscanf(fid, 'format', size)
Data = Data';
fclose(3);
end
 % Data = Data(10:end, :);
%Creates data matrix
%cd(DataPath)
[rows, columns] = size(Data)
%Creates a time vector that corresponds to the number of rows of data
t = (1:rows)';
time = t * SamplePeriod; %(s)
clear t;

%Applies calibration to convert voltages to length and force
VLength = Data(:,2);
VForce = Data(:,3);
clear Data

VForce = VForce/1000;
Lcalib = (al * VLength.^3 + bl * VLength.^2 + cl * VLength + dl)/1000; %(m)
LFcalib = ( alf * VForce + blf)/1000; %m
Fcalib =  af * VForce + bf; %(N)
```

```
clear VLength VForce

size(time);
size(Fcalib);
size(Lcalib);
Lcalib2 = Lcalib - LFcalib;
MeanLength = Mean(Lcalib2); %(m)
MeanForce = Mean(Fcalib); %(N)
%Subtract mean from the length signal
LengthNormal = Lcalib2 - MeanLength; %(m)
%Calculate strain from length
RawStrain = LengthNormal/L; %(strain is deltaL/L)
clear Lcalib LFcalib Lcalib2 LengthNormal

%Filter strain signal
Strain = RawStrain;
Strain = bwfilter(RawStrain, FilterOrder, FreqCutOff, SampleRate);

%Subtract the mean from the force signal
ForceNormal = Fcalib - MeanForce;
clear Fcalib

%Calculate stress from force
RawStress = ForceNormal./Area;
clear ForceNormal

%Filter stress signal
Stress = RawStress;
Stress = bwfilter(RawStress, FilterOrder, FreqCutOff, SampleRate);


%Apply function to generate index numbers for max and min on length record
[StrainMax, StrainMin] = findpeakindex(Strain);
%Apply function to generate index numbers for max and min on stress record
[StressMax, StressMin] = findpeakindex(Stress);
%Find important values and times corresponding to stress and strain records
StrainMinVal = Strain(StrainMin);
StrainMintime = time(StrainMin);
StrainMaxVal = Strain(StrainMax);
StrainMaxtime = time(StrainMax);
StressMinVal =Stress(StressMin);
StressMintime = time(StressMin);
StressMaxVal = Stress(StressMax);
```

```
StressMaxtime = time(StressMax);
 %PLOTS
%*******************************
newfig('initialize', 'StrainPlot');
%sets the current axis to add points as you go
set(gca,'nextplot','add');
%Plot strain data
RawStrainplot = plot(time, RawStrain, 'c-');
Strainplot = plot(time, Strain, 'b-');
clear RawStrain

%plot original wave with max and min points superimposed
Strainplot2 = plot(time, Strain, 'md');
StrainMaxplot = plot(StrainMaxtime, StrainMaxVal, 'r*');
StrainMinplot = plot(StrainMintime, StrainMinVal, 'g+');
%Generate a stress and strain plot
StrMaxVal = Stress(StressMax);
StrMinVal = Stress(StressMin);
StrMaxTime = time(StressMax);
StrMinTime = time(StressMin);
StrMax = mean(StrMaxVal);
StrMin = mean(StrMinVal);
StrAmp = StrMax - StrMin;

NStr = ((Stress-StrMin)/StrMax)+1.5;
NStrMaxVals = ((StrMaxVal - StrMin)/StrMax)+1.5;
NStrMinVals = ((StrMinVal - StrMin)/StrMax)+1.5;


StrnMax = mean(StrainMaxVal);
StrnMin = mean(StrainMinVal);
StrnAmp = StrnMax - StrnMin;

NStrn = (Strain - StrnMin)/StrnMax;
NStrnMaxVals = (StrainMaxVal - StrnMin)/StrnMax;
NStrnMinVals = (StrainMinVal - StrnMin)/StrnMax;

%NewFig('initialize', 'Stress and Strain');
%set(gca,'nextplot','add')

plot(time, NStr,'c');
plot(StrMaxTime, NStrMaxVals,'*g');
plot(StrMinTime, NStrMinVals,'*g');
```

```
plot(time, NStrn, 'm');
plot(StrainMaxtime, NStrnMaxVals,'b*');
plot(StrainMintime, NStrnMinVals,'b*');
%*****************************
%number of iterations
n = length(StrainMintime);

%Use find to match stress and strain and calculate phase
for i = 1: n-1
        StrainMintime(i+1);
        StrainMintime(i);
        Period = StrainMintime(i+1) - StrainMintime(i);
        a = StrainMintime(i) - c*Period;
        b = StrainMintime(i) + c*Period;
        StressPoint = find((StressMintime<b) & (StressMintime>a));
        TimeStressPoint = StressMintime(StressPoint);
        CyclePhase(i) = (StrainMintime(i) - TimeStressPoint)/Period;
end % for i = 1:n

%Make sure that stress signal is referenced to the strain signal and that there are equal
numbers of peaks
        while StrainMin(1) <= StressMin(1);
                StrainMin = StrainMin(2:end);
         end
         while  StressMin(end) >= StrainMin(end);
                disp('running 2nd while loop');
                strainindex = StrainMin(end);
                stressindex = StressMin(end);
                  StressMin = StressMin(1:end - 1);
                  NewStrainIndex = StrainMin(end);
          end

StressMinVal =Stress(StressMin);
StressMintime = time(StressMin);
StressMaxVal = Stress(StressMax);
StressMaxtime = time(StressMax);
%newfig('initialize', 'StressPlot')

%Plot stress data
set(gca,'nextplot','add')
RawStressplot = plot(time,RawStress, 'c-');
Stressplot = plot(time,Stress, 'b-');
```

```
Stressplot2 = plot(time, Stress, 'md');
StressMaxplot = plot(StressMaxtime, StressMaxVal, 'r*');
StressMinplot = plot(StressMintime,StressMinVal, 'g+');
figure;
set(gca,'nextplot', 'add');
PhasePlot = plot(Strain, Stress, 'm-', 'LineWidth', 1);
xlabel('Strain');
ylabel('Stress');

clear RawStress

%Calculate stress and strain amplitude
StrainAmp = Mean(StrainMaxVal) - Mean(StrainMinVal); %(m)
StressAmp = Mean(StressMaxVal) - Mean(StressMinVal); %(N)
%Calculate stress and strain time
StrainMinTime = time(StrainMin);
StressMinTime = time(StressMin);

%Calculate phase angles
PhaseAng = mean(CyclePhase) * 360;
PhaseAngRad = PhaseAng * (pi/180);

%Calculate moduli of materials
Estar = StressAmp/StrainAmp; %(N/m^2)
Ei = Estar * cos(PhaseAngRad);
Eii = Estar * sin(PhaseAngRad);
k = (Estar .* Area)/L; %(N/m)

%Write stress/strain data to text output files
OutputStringDat ='time        stress   strain';
OutStressStrain = [time, Stress, Strain];
OutFileName1 = [FileName(1:end)  '.stresstrain'];
cd(OutputPath)
WriteTextFile(OutFileName1, OutStressStrain, OutputStringDat, 'w');
cd(HomePath)
```

FindPeakIndex.m – Peak finder routine

```
function [max, min]=findpeakindex(input)

% [max, min]=findpeakindex(input)
%function will generate index number of peaks and separate max and min
```

```
deriv = diff(input);
%Generates 1s for positive numbers and 0s for negative numbers
posneg = deriv';
posneg(find (posneg>0)) = 1; posneg(find(posneg<0)) = 0;
derivdiff = diff(posneg);
%returns index number of inflection points
I = find((derivdiff>0) | (derivdiff< 0));
min = find((derivdiff>0));
min = min + 1;
max = find((derivdiff<0));
max = max +1;
```

ToStartOdeGood.m – Calculates solution to a simple dynamical system with a nonlinear spring

```
clear all;
%close all;
GreatestMat = [];

 HomePath = 'Guinea Beast:Applications:MATLAB 5:Erica m-files:Toy Model:';
 cd(HomePath);
global mass
global eta
global Eo
global freq
global a
global b

SaveDir = mkdir('WideMassRangeEta.2Fine');
SavePath = 'Guinea Beast:Applications:MATLAB 5:Erica m-files:Toy
Model:WideMassRangeEta.2Fine:';
strainA = [0:.01:3.5];
a1 = 89; %from Polyorchis data curve fits
stress = a1*strainA.^1.8;
LinA = (stress(end)-stress(1))/(strainA(end)-strainA(1));

Eo = 0;
bo = [0:.2:2];
bo = repmat(bo,1,20)';
mo = [.005:.05:1];
mo = mo; %scale for area - based on a bell = .01R
```

```
mo = repmat(mo,11,1);
m = [mo(:,1); mo(:,2); mo(:,3); mo(:,4); mo(:,5); mo(:,6); mo(:,7); mo(:,8); mo(:,9);
mo(:,10);...
 mo(:,11); mo(:,12); mo(:,13);  mo(:,14); mo(:,15); mo(:,16); mo(:,17); mo(:,18);
mo(:,19);...
 mo(:,20)];
 %mo(:,21); mo(:,22); mo(:,23)];
Param =[bo                                    m];
freq = 1;
eta = .2;
%mass = .5; %kg estimated from Demont and Gosline-includes mass and effective mass
%scaled for area of the jellyfish


initconds = [0 0];  %  two initial conditions for a second order ode in strain
          %  ic1   strain is 0 at t = 0
          %  ic2   strain rate is 0 at t = 0
%for i =1:length(Param);
for i = 1:length(Param);
b = Param(i, 1);
mass = Param(i,2);
exp = b+1;
 a = LinA./(mean(exp.*strainA.^(exp-1)));
 AOut(i,1) = a;
stress2 = a.*strainA.^exp;
%plot(strainA,stress, strainA,stress2);
%set(gca, 'nextplot', 'add');

tmax = 50; %s
options = odeset('RelTol',1e-4,'AbsTol',[1e-6 1e-6]);

%ODE solution
[t2,PVL] = ode23s('Ode',tmax,initconds,options);
 strain = PVL(:,1);
 MeanStrain = mean(strain);
 StrainOut(i,1) = MeanStrain;
 GlobalMaxOut(i,1) = max(strain);
 Bout(i,1) = b;
 Mout(i,1) = mass;
 Transient = 10; %s
 Tcut = find(t2>Transient);
 t2 = t2(Tcut);
 strain = strain(Tcut);
```

```
%Interpolate data for even spacing
time = [10.01:.001:tmax];
EvenStrain = interp1(t2,strain,time,'spline');
SampleRate = 1000;% /sec
%FilteredStrain = bpfilter(EvenStrain,1,.5, .9, SampleRate);

%plot fft

%plot(t2,strain,time, EvenStrain);
[FDomain, AmpCoef, PwCoef] = FFTransform((EvenStrain-mean(EvenStrain)),
SampleRate);
FDomain = FDomain(1:250);
AmpCoef = AmpCoef(1:250);
[FFTMax, FFTMin] = findpeakindex(AmpCoef);
AmpPeaks = AmpCoef(FFTMax);
FreqLoc = FDomain(FFTMax);
ImpMax = find(AmpPeaks>.1*max(AmpPeaks));
FreqMax = FreqLoc(ImpMax);
AmpMax =  AmpPeaks(ImpMax);

plot(FDomain, AmpCoef,'b', FreqMax , AmpMax, 'y*', 'LineWidth', 2);
hold on;
FreqOut(i,1:length(FreqMax)) = FreqMax;
AmpOut(i,1:length(AmpMax)) = AmpMax;

% %Output peaks and amplitudes
space = zeros(1, 12);
size = length(FreqMax);
IndF = [1:2:2*size];
IndA = [2:2:2*size];
space(IndF) = FreqMax;
space(IndA) = AmpMax;
GreatestMat = [GreatestMat;space];
%

FreqNum(i,1) = length(FreqMax);


 [Max, Min] =findpeakindex(strain);
 LengthMax(i,1) = length(Max);
 LengthMin(i,1) = length(Min);
```

```
%Save strain data
cd(SavePath);
Outmat = [t2                                strain];
BaseFileName = 'Strain.';
OutputString = 'time                        strain';
FileName = sprintf('StrainOut.B%02dM%02d',mod((i-1),21)+1,floor((i-1)/21)+1);
FormatString = '%2.4f                       %2.4f\n';
WriteTextFile(FileName, Outmat, OutputString, 'w', FormatString);
%
 %strTitle2 = ['StrainPlot ' num2str(i)];
  %plot(t2,strain, 'k', 'b',t2(Max), strain(Max), 'm*', t2(Min), strain(Min), 'g*',
'LineWidth', 2);

 %hold on;
%   xlabel('time (s)');
%   ylabel('position');
   clear PVL
  clear strain
  clear t2;
 disp(i);
 cd(HomePath);
end
%Save FFT data
 cd(SavePath);
 FFTName = 'FFTOutput';
  %FFTString = 'FreqMax                  AmpMax';
 % FormatString = '%2.4f                  %2.4f\n';
 WriteTextFile(FFTName, GreatestMat);

%Derived outputs to save to a file
cd(SavePath);
DerivedOut = [Bout   Mout   StrainOutGlobalMaxOut   LengthMax        LengthMin        F
DString = 'NonLin   Mass   MeanPos   MaxAmp   PeakNum   TroughNum   FreqNum';
DFileName = 'DerivedOutput';
WriteTextFile(DFileName, DerivedOut, DString, 'w');
cd(HomePath);
% figure(2);
% plot(bo,LengthMin./(tmax-Transient), 'b*');
% xlabel('b')
% ylabel('number of troughs/sec');
% %axis([min(bo) max(bo) 0 max(LengthMax)]);
% figure(3);
% plot(bo,GlobalMaxOut, 'm');
```

```
% xlabel('b');
% ylabel('Signal Amplitude');
% newfig;
% plot(bo,StrainOut, 'g*');
% xlabel('bo');
% ylabel('Mean Position');
```

Ode.m-- Basic ODE file for a simple mass-spring system

```
 function dPVdt = odefile(t,PV)

global mass
global eta
global Eo
global freq
global a
global b
 stress = cos(freq*2*pi*t);

 %stress = 1;

dPVdt = [(PV(2))
      ((stress - eta*PV(2) - a*(PV(1).*abs((PV(1).^b))))/mass)
```

PlotToyModel.m – File to make 3D plots of the output data from the simple dynamical system

```
clear all;
close all;

%Plot output from Toy Model simulations

HomePath = 'Guinea Beast:Applications:MATLAB 5:Erica m-files:Toy Model:';
SavePath = 'Guinea Beast:Applications:MATLAB 5:Erica m-files:Toy Model:';
cd(SavePath);

tmax = 50; %s
Transient= 10; %s
Data = ReadTextFile;
%Data = load('BigRangeFFT.1');
B = Data(:,1);
```

```
Mass = Data(:,2);
MeanPos = Data(:,3);
MaxAmp = Data(:,4);
Peaks = Data(:,5)./(tmax-Transient);
Troughs = Data(:,6)./(tmax-Transient);
NumFreq = Data(:,7);

%Find evenly spaced z values for output
Mass1 = (min(Mass):.05:max(Mass));
B1 = (min(B):.2:max(B))';
MaxAmp1 = griddata(B,Mass, MaxAmp, B1, Mass1, 'v4');
SubHarm = griddata( B,Mass,Troughs, B1, Mass1, 'v4');
MeanPos1 = griddata(B,Mass,  MeanPos, B1, Mass1, 'v4');
NumFreq1 = griddata(B,Mass, NumFreq, B1, Mass1, 'nearest');

%Plots
Amp = figure(1);
AmpPlot = contourf(B1, Mass1,MaxAmp1);
xlabel('Non-lin parameter','FontSize', 10);
ylabel('Mass', 'FontSize', 10);
caxis([0, .6]);
%h = colorbar('vert');
h = colorbar('horiz');

Sub = figure(2);
SubHarmPlot = contourf(B1, Mass1, SubHarm);
xlabel('Non-lin parameter','FontSize', 10);
ylabel('Mass', 'FontSize', 10);
caxis([1, 12]);
%h2 = colorbar('vert');
h = colorbar('horiz');

Pos = figure(3);
PosPlot = contourf(B1, Mass1, MeanPos1);
xlabel('Non-lin parameter','FontSize', 10);
ylabel('Mass', 'FontSize', 10);
caxis([-.05, .05]);
%h3 = colorbar('vert');
h = colorbar('horiz');

Freq = figure(4);
PosPlot = contourf(B1, Mass1, NumFreq1);
xlabel('Non-lin parameter','FontSize', 10);
```

```
ylabel('Mass', 'FontSize', 10);
caxis([1, 4]);
h = colorbar('horiz');
```

APPENDIX B:

Matlab Code for Chapter 3

BellDiam.m – Analyze digitized video in viscosity experiment

```
% analyze the jellyfish data!
% input:  pointnclick2 output files from the jellyfish videotapes
% output: what we need

 close all
clear all

% Set up the preliminaries

InputPath = 'Mongo:Erica:jellyvideo:Bell Diameter (adequate...):data files:Bell Diameter
Corrected Distances:'; % base path

% FilePath = 'Mongo:Erica:jellyvideo:etc:Effect of holes in data';


adjustments = autoreadtextfile(InputPath, 'Guide'); % file containing start times, enlarge
factor, frame length

% the big loop

for x = 1:1;

% load the data file in question

input = autoreadtextfile2(InputPath, num2str(x)); % load up the file

latitude = (size(input,1)); % figure out how long she is

% put times and bell diameters in the output vector

StartMins = adjustments(:,2);
StartSecs = adjustments(:,3);
StartFrac = adjustments(:,4);
enlarge   = adjustments(:,5);
SecsFrame = adjustments(:,6);
```

```
StartTime = (StartMins .* 60) + StartSecs + (StartFrac ./ 100);

FrameNum = (1:latitude)';
Times = StartTime(x) + (SecsFrame(x) .* FrameNum);

a = (input(:,4) - input(:,2));
b = (input(:,5) - input(:,3));
csqrd = a.^2 + b.^2;
Distances = sqrt(csqrd) .*enlarge(x);

% Remove data points with zeros as distances

BadInd = find(Distances < 5 | Distances > 400);
BadTimes = [BadInd                    Times(BadInd)];
%GoodInd = setdiff(    (1:length(Distances)), BadInd);
%Distances = Distances(GoodInd);

% calculate the mean distance roughly

% Plot things

%strTitle2 = ['FFTplot for file # ', num2str(x)];
%                                  newfig('initialize', strTitle2);
%                                    set(gca, 'nextplot', 'add');
%                                        axis([0,5,0,50]);

%FFTPlot = plot(FDomain, AmpCoef);

strTitle = ['Distances for file # ', num2str(x)];
                                   newfig('initialize', strTitle);
                                     set(gca, 'nextplot', 'add');
                        axis([StartTime(x), (StartTime(x) +50),0,350])
                                         title = strTitle;
FilteredDistances = bwfilter(Distances, 3, 3, 30);

DistPlot = plot(Times, Distances, 'b*', Times,FilteredDistances, 'm');
Index = find(Times);
TimesDistances = [Index                Times                              Distances];


OutputHeader = 'Index                  Times                              Distances';
```

```
Outputpath = 'Mongo:Erica:jellyvideo:Bell Diameter (adequate...):data files:Bell
Diameter Distance Files:';
cd(Outputpath);
WriteTextFile(num2str(x), TimesDistances, 'w', OutputHeader);

%This chunk makes a 2 column matrix for the files where we didn't need to add points
% FileNameCopy = [num2str(x), '.copy'];
% cd('Mongo:Erica:jellyvideo:Bell Diameter (adequate...):data
files:BellDiamCorrectedDistances:')
% TimesDistShort = [Times                Distances];
% WriteTextFile(FileNameCopy, TimesDistShort, 'w', 'Times                    Distances');

end
```

ChopClips.m

Purpose: Split up each sinusoidal a clip into sections of length f, where f is the period of the sinusoid, which can then be overlaid on each other to find a "composite waveform." Various statistics (e.g average maximum height, etc.) can then be performed on that average waveform to gain information on the entire signal.

```
% How it works:

% It finds the length of each individual frequency in the clip by
% running a filter on the original data and taking the maxima
% of that filter. Intervals between maxima are the individual
% cycles.

% It finds the shortest (narrowest / smallest time length) cycle.
%
%
% It then splines the other cycles to the size of the smallest
% cycle.
%
% It then creates a "composite cycle" by taking the mean of the different
% diameters at the same "relative time point"
%
% It finally finds the max, min, amplitude, and mean position
% for that composite cycle.
```

```
%   preliminaries

close all;
clear all;
format long;

% Cubazoa paths

DistanceDataPath = 'Cubozoa:erica:Bell Diam Corrected Distances:';

% Paths for when working at home

% DistanceDataPath = 'Guinea Beast:Matlab Input:data files:Bell Diam Corrected
Distances:';

%   Main Loop

for filenum = 1:17;

%   NB:  The routine relies on moving from maxima to maxima once it
%   runs the filter.  Therefore, for clips that only have one maxima
%   (and hence only one cycle), this routine does not work.
%   For our data, this was true only for filenum = 18.

% clear things out

clear TimesVsDiameter;
clear Filtered;
clear MajorCycleLength;
clear ClipLength;
clear MaxCycles;
clear ChoppedLengthInPoints;
clear TheoreticalSizeInPoints;
clear Overshoot;
clear cyclenum

%   Load the file

TimesVsDiameter = autoreadtextfile(DistanceDataPath, [num2str(filenum), '.adjusted']);

%   How many cycles are we dealing with?
```

```
%   To figure this out, first run a butterworth filter to the data and have a look

Filtered(:,1) = TimesVsDiameter(:,1);
Filtered(:,2) = bwfilter(TimesVsDiameter(:,2), 3, 1.5, 30);

%   Now, on the filtered data, what are the indexes of the minimums?

[FilteredMaxIndexes, FilteredMinIndexes] = findpeakindex(Filtered(:,2));
FilteredMaxIndexes = FilteredMaxIndexes';
FilteredMinIndexes = FilteredMinIndexes';

%   Compute cycle start times and the length of each cycle.
%   Skip the last one -- we can't go any further.
%   Try both the maxes and the mins.  Use whichever gives
%   the most cycles.

SecsPerFrame = TimesVsDiameter(2,1) - TimesVsDiameter(1,1);

%                                       using mins

CycleStartTimesN = TimesVsDiameter(FilteredMinIndexes,1);
CycleLengthsInTimeN = diff(CycleStartTimesN);
CycleStartTimesN = CycleStartTimesN(1:end-1);
CycleEndTimesN = CycleStartTimesN + CycleLengthsInTimeN - SecsPerFrame;
CyclesWeAreSamplingN = length(CycleStartTimesN);

%                                       using maxes

CycleStartTimesX = TimesVsDiameter(FilteredMaxIndexes,1);
CycleLengthsInTimeX = diff(CycleStartTimesX);
CycleStartTimesX = CycleStartTimesX(1:end-1);
CycleEndTimesX = CycleStartTimesX + CycleLengthsInTimeX - SecsPerFrame;
CyclesWeAreSamplingX = length(CycleStartTimesX);

%which one is bigger? make that the reality.
%if it doesn't matter, use the max.

if CyclesWeAreSamplingX >= CyclesWeAreSamplingN

CycleStartTimes = CycleStartTimesN;
CycleLengthsInTime = CycleLengthsInTimeN;
CycleStartTimes = CycleStartTimesN;
CycleEndTimes = CycleEndTimesN;
```

```
CyclesWeAreSampling = CyclesWeAreSamplingN;
else
CycleStartTimes = CycleStartTimesX;
CycleLengthsInTime = CycleLengthsInTimeX;
CycleStartTimes = CycleStartTimesX;
CycleEndTimes = CycleEndTimesX;
                    CyclesWeAreSampling = CyclesWeAreSamplingX;
end

%   Now that this has been resolved...
%   And, in points, what is the SMALLEST cycle we'll be whacking?
%   (We need this for splining the larger cycles later...)
%   Be sure to find it in seconds too for splining purposes...

SmallestCycle = min(CycleLengthsInTime);

%   Find the indexes in the original data which correspond to the projected
%   cycle start / end times
%  (Yes I know this is a mess and slow and a big loop etc etc etc
%   BUT it is vestigal from some earlier mess we devised and it WORKS)

for i = 1 : CyclesWeAreSampling;
  if length(findindex(TimesVsDiameter(:,1), CycleStartTimes(i))) == 2;
    Tempindex = findindex(TimesVsDiameter(:,1),...
    CycleStartTimes(i));
    CycleStartIndexes(i) = Tempindex(1,1);
    clear Tempindex;
  else
    CycleStartIndexes(i) = findindex(TimesVsDiameter(:,1),...
    CycleStartTimes(i));
end

if length(findindex(TimesVsDiameter(:,1), CycleEndTimes(i))) == 2;
  Tempindex = findindex(TimesVsDiameter(:,1),...
  CycleEndTimes(i));
  CycleEndIndexes(i) = Tempindex(1,1);
  clear Tempindex;
else
  CycleEndIndexes(i) = findindex(TimesVsDiameter(:,1), ...
  CycleEndTimes(i));
end
end
```

```
%   We would also like to know how big each cycle is in index units:

CycleSizeIndexes = (CycleEndIndexes - CycleStartIndexes + 1)';
CycleStartIndexes = CycleStartIndexes';
CycleEndIndexes = CycleEndIndexes';

%   What is the smallest cycle in index-units?

SmallestCycleIndex = min(CycleEndIndexes - CycleStartIndexes);


%   Plot what we have so far:

newfig;
set(gca,'nextplot','add');
plot(TimesVsDiameter(:,1), TimesVsDiameter(:,2), 'b*');      % This is the original data
plot(Filtered(:,1), Filtered(:,2), 'g');                     % This is the filter.
plot(CycleStartTimes, max(Filtered(:,2)) , 'mv');
% These pink triangles are the cycle start points.
% Subsequent chopping up is done between these triangles.

%   Now then.  We will now begin the whacking process.
%   (Aieee...) (Music)
%   We will loop through the cycles.
%   The output of this loop is a composite matrix, "Composite."
%   The size should be CyclesWeAreSampling columns by SmallestCycleIndex rows.

for CycleNum = 1 : CyclesWeAreSampling;

%    We shall spline everything in sight -- even the smallest cycle, because
%   the new sampling interval is the same as the smallest cycle's, so it
%   ends up outputting the same thing.

OriginalXs = TimesVsDiameter(  (CycleStartIndexes(CycleNum)  :
CycleEndIndexes(CycleNum))  ,1);
OriginalYs = TimesVsDiameter(  (CycleStartIndexes(CycleNum)  :
CycleEndIndexes(CycleNum))  ,2);
XofInterestInterval = CycleLengthsInTime(CycleNum) / SmallestCycleIndex;
XofInterest = (CycleStartTimes(CycleNum) : XofInterestInterval :
CycleEndTimes(CycleNum))';
Composite(:,CycleNum) = spline(OriginalXs, OriginalYs, XofInterest);

clear OriginalXs;
```

```
clear OriginalYs;
clear XofInterestInterval;
clear XofInterest;

end

%   Now, what is the mean cycle or "composite cycle?"

for PointNum = 1 : SmallestCycleIndex;
   MeanCycle(PointNum) = mean(Composite(PointNum,:));
end

%   Plot the new composite cycle in a overlay fashion.

newfig;
set(gca,'nextplot','add');

for CycleNum = 1 : CyclesWeAreSampling;
   plot(1:SmallestCycleIndex, Composite(:,CycleNum), 'b+');
% These are all the original
% cycles, splined so that
% they can be laid on top of
% each other.
end

plot(1:SmallestCycleIndex, MeanCycle(1:SmallestCycleIndex), 'g*');  % This is the
"composite index!"

%   The statistics we're interested in

LaData(filenum,1)  = filenum;                                          % filenum
LaData(filenum,2)  = (max(MeanCycle))';                                  % max
LaData(filenum,3)  = (min(MeanCycle))';                                  % min
LaData(filenum,4)  = (max(MeanCycle) - min(MeanCycle));                % amplitude
LaData(filenum,5)  = (mean([LaData(filenum,2), LaData(filenum,3)]));% mean of max and min
LaData(filenum,6)  = mean(MeanCycle);                                  % mean of y's
LaData(filenum,7)  = mean(CycleLengthsInTime);       % realtime swimming frequency

%   Please note the exciting Latin accent to the data matrix.

%                                  Clear out the matrices

clear Composite
```

```
clear MeanCycle

end

%    Save LaData (music please)

FileName = 'ChopClipsOutput';
OutputPath = 'Cubozoa:erica:';
Header = 'filenum max    min    amplitude    meanmaxmin    mean Ys        realtimef';
cd(OutputPath);
WriteTextFile(FileName, LaData, 'w', Header);

%   Have a tall cool one.
```

interpolation.m-- Interpolation routine

This routine computes missing points from the distance data record. Run it one record at a time to replace one segment at a time. This ensures you make sure you are doing something reasonable and allows separate and tailored spline input for each point set.

```
close all;

% temporary fix for file 1
% cd('Mongo:Erica:jellyvideo:Bell Diameter (adequate...):data files:Bell Diam Corrected
Distances:');
%
% One = ReadTextFile;
%
% BadPt = find(One(:,2) == 0)
% Times = One(:,1);
% Distances = One(:,2);

StartNum =276:286;                    %    this is the front end input for the spline
EndNum = 288:298;                     %    this is the back end input for the spline

%   compute the sampling interval

SecsFrame = Times(2) - Times(1);

%    put the original data in a vector based on the above input
```

```
XVal = [Times(StartNum)            Times(EndNum)];
XVal = [XVal(:,1); XVal(:,2)];

YVal = [Distances(StartNum)     Distances(EndNum)];
YVal = [YVal(:, 1); YVal(:, 2)];

%     Identify the points missing between StartNum and EndNum that we'll replace

Xi = Times(StartNum(end)):SecsFrame:Times(EndNum(1))

%     Compute the missing points using a cubic spline function

Yi = interp1(XVal, YVal, Xi, 'spline');

%   Put the new points back into the start function.

Distances(StartNum(end):EndNum(1)) = Yi;
%     Save the file with a new name.

NewDistances = Distances;
NewTimes = Times;
CorrDist = [NewTimes                NewDistances];
FileName = [num2str(x), '.adjusted'];
%FileName = [num2str(1), '.adjusted']
 newfig;
 plot(NewTimes, NewDistances, 'b*', Xi, Yi, 'm*');
cd('Mongo:Erica:jellyvideo:Bell Diameter (adequate...):data files:Bell Diam Corrected
Distances:');
WriteTextFile(FileName, CorrDist, 'w', 'Time                                    Distance');

% %This is a section of temporary code to deal with file 2 adjusted
% %It breaks up the file into chunks of (a) transient, (b) two steady state chunks
% %on either side of a big gap.  It can be modified to split up any data file.
% % Transient
%
% NewTimesTrans = (NewTimes(1:475));
% NewDistTrans = (NewDistances(1:475));
% CorrDistTransient = [NewTimesTransNewDistTrans];
% plot(NewTimesTrans, NewDistTrans, 'c*');
% FileNameTrans = '2.adjusted';
% cd('Mongo:Erica:jellyvideo:Bell Diameter (adequate...):data
files:BellDiamCorrectedDistances:');
% WriteTextFile(FileNameTrans, CorrDistTransient, 'w', 'Time                    Distance');
```

```
%
% %Block 1
% NewTimesBlock1 = (NewTimes(476:1263));
% NewDistBlock1 = (NewDistances(476:1263));
% CorrDistBlock1 = [NewTimesBlock1NewDistBlock1];
% plot(NewTimesBlock1, NewDistBlock1, 'c*');
% FileNameBlock1 = '31.adjusted';
% cd('Mongo:Erica:jellyvideo:Bell Diameter (adequate...):data
files:BellDiamCorrectedDistances:');
% WriteTextFile(FileNameBlock1, CorrDistBlock1, 'w', 'Time                Distance');
%
% %Block2
% NewTimesBlock2 = (NewTimes(1325:1852));
% NewDistBlock2 = (NewDistances(1325:1852));
% CorrDistBlock2 = [NewTimesBlock2NewDistBlock2];
% plot(NewTimesBlock2, NewDistBlock2, 'c*');
% FileNameBlock2 = '32.adjusted';
% cd('Mongo:Erica:jellyvideo:Bell Diameter (adequate...):data
files:BellDiamCorrectedDistances:');
% WriteTextFile(FileNameBlock2, CorrDistBlock2, 'w', 'Time                Distance');
```

APPENDIX C:

Matlab Code for Chapter 4

RunMe.m – File executes batches of model simulations storing each in its own directory

```
clear all;
global E
global Cutoff
global Jitter
global duty
global JitterIndex
global CutoffIndex
global p1
global p2

BasePath = cd;
addpath(BasePath);

JitterIndex = 1;
CutoffIndex = 1;

JitterValues = [0 1 2 3];
CutoffValues = [3 9 20];
DutyValues = [25 43.5 75];
StiffnessValues = [500 1000 2000];

for p1 = 1:length(DutyValues)
        for p2 = 1:length(StiffnessValues)
                disp('I am about to make one plot.  Wish me luck.');
                Jitter = JitterValues(JitterIndex);
                Cutoff = CutoffValues(CutoffIndex);
                duty = DutyValues(p1);
                E = StiffnessValues(p2);
                %CurrentDataDir =
sprintf('J%01dC%01dD%01dE%01d',JitterIndex,CutoffIndex,p2,p1);%PROBLEM
                CurrentDataDir =
sprintf('J%01dC%01dD%01dE%01d',JitterIndex,CutoffIndex,p1,p2);%fixed
                mkdir(CurrentDataDir);
                cd(CurrentDataDir);
                ToStartJellyNonLinJitter;
                cd ..;
        end
end
rmpath(BasePath);
```

ToStartJellyNonLinJitter.m – This is the code that executes and parameterizes the model

```
% clear all;
close all;
tic;

global mass
global eta
global k
global Ro
global T
global rho
global Avel
global drive
global Vb
global cP
global cM
global h
global Fm
global freq
global duty
global b
global LinMeanSlope
global Xm
global Fch
global U
global t2
global Drag
global VolOut
global R
global alpha
global Cd2
global EffMass
global Cutoff
global inc
global tmax
global to
global ncycles
global Locations
global E
global Jitter
global JitterIndex
global CutoffIndex
global p1
global p2

%cd(HomePath);
r = [.004:.002:.04];
r = repmat(r, 11,1);
```

```
Ro = [r(:,1); r(:,2); r(:,3); r(:,4); r(:,5); r(:,6); r(:,7); r(:,8); r(:,9); r(:,10); r(:,11); r(:,12);...
                r(:,13); r(:,14); r(:,15); r(:,16); r(:,17); r(:,18); r(:,19)];
bo = [0:.2:2];
b = repmat(bo,1,19)';
Param = [Ro   b];
[rownum, columnum] = size(Param);

options = odeset('RelTol',1e-5,'AbsTol',[1e-7 1e-7]);
%options = odeset('RelTol',1e-4,'AbsTol',[1e-6 1e-6]);

%cd(HomePath);
Rvel = .7;
EiiFact = .03;
EffMass = 4.35;



% Value to modify fluid forces
cP = 1;

for i =1:rownum
        Ro = Param(i,1); %Bell radius at rest
        b = Param(i, 2);%Non-linearity parameter
        ho = 2*Ro; %Bell height at rest
        T = .4*Ro; %Thickness
        Avel = pi*(Rvel*Ro)^2;%Area of velum
        Eii = EiiFact*E; %Viscous portion of complex modulus
        EffMass = 4.35;%Multiplicative factor to determine the added mass of the bell



%How long does this take?
tic;
%Fluid stuff

%Cd = 1;  % coefficient of drag - single value for Cd
alpha = (ho/Ro)^1.4; % added mass coefficient - relationship derived by TLD (ref Can J.
Zool - 1983)
nu = 1.1*10^-6; % Kinematic viscosity of sea water m^2/s;
mu = 1.1*10^-3; %Dynamic viscosity of sea water Ns/m^2;
rho = 1000; %kg/m^3

%SCALING STUFF!!!

%Calculate coefficient for muscle forcing - scaling it as a function of muscle thickness

MuscleStress = 1.25*10^5; %Pa 2*10^5 as cited by DeMont and Gosline - Jet propulsion
2
%MuscleThickness = 2*10^-5; %Pa - 20 micrometers from Gladfelter 1972-switch to
this to keep this a constant
```

```
MuscleThickness  = .005*T; %represent muscle thickness as a fraction of T such that for
a jellyfish with a radius of
%0.01m the muscle thickness = 2*10^-5; %Pa - 20 micrometers from Gladfelter 1972
cM = MuscleThickness*MuscleStress*(1/2*2*pi*(Ro-T)); %Coeff to modify muscle
force. Estimate height of muscle as half of
%the inner circumference of the bell


%Frequency scaling

ncycles = 10;

Tm = -.0165 + 3.86*Ro^0.5; %From fmins fit to Gladfelter's data for cycle duration as
related to circumference
Trecov = 1.3*Tm;%s - Gladfelter estimates that the recovery part of the cycle is on
average 30% longer than the contraction phase
CyclePeriod = Tm +Trecov;%s
freq = 1/CyclePeriod;%hz
to = 0;
tmax = ncycles*CyclePeriod;
inc = .001;
%duty = 43.5;
%duty = 25;

FmJitter;
%Isometric scaling of k for size changes


Area = (pi/2*Ro*ho) - (pi/2*(Ro-T)*(ho-T));
LinMeanSlope = (E*Area)/(Ro);% N/m - k calculated from DeMont and Gosline's
structural stiffness estimate of 500Pa

%Isometric scaling for mass based on the volume of the bell at rest.

Vbo = (2/3*pi*ho*Ro^2) - ((2/3*pi*(ho-T))*((Ro-T)^2));
mass = rho*Vbo;

%Scaling argument for the damping term.  Eta = AE"/fRo;

 %Based on actual dynamic stiffness measurements, E" is less than 5% of E*
%Note that this is based on estimates from individual pieces rather than whole bell
estimates
EtaScaled = (Area*Eii)/(freq*Ro);
eta = EtaScaled;

%This m-file scales the mean slope of the deformation so that the linear case and non-
linear
%case has the same mean slope

%set Xm for KscaleJelly
```

```
Xm = 0.5*Ro; %Xm = Rmax -Ro
KscaleJelly;

%Determine some of the constants used in subsequent formulas

        Vb = mass/rho;
        NonLinParam = b+1;
        KMatIndex = find(KMat(:,2)==NonLinParam);
        ScaledSlope = KMat(KMatIndex,1);
        k = ScaledSlope;

%Set initial conditions for ode solution

initconds = [Ro 0];  %  two initial conditions for a second order ode in radius

%ODE solution
disp('running');
[t2,PV] = ode23s('NonLinOdeJitter',tmax,initconds,options);


%Now use the computed values of R(t) and R'(t) to solve for fluid forces

 R = PV(:,1);
 RP = PV(:,2);



%Compute change in volume in time

dVdtOut = (((8*pi^2*T.*R.^2.*(-T+R).*RP)./(9*(2/3*pi*T^2-4/3*pi*T.*R)))...
                - ((8*pi^2*T.*R.^2.*(Vb-2/3*pi*T*(-T+R).^2).*RP))./((9*(2/3*pi*T^2-
4/3*pi*T.*R).^2))...
                -((4*pi.*R.*(Vb-2/3*pi*T.*(-T+R).^2).*RP)./(3*(2/3*pi*T^2-
4/3*pi*T.*R))));


%Compute thrust

 Thrustout = (rho*(dVdtOut).*abs(dVdtOut))/Avel;

%Split up inertial and fluid forces
 P = Thrustout/Avel;
 FluidForce = 2*P*Ro*h;
 %SpringTerm = k.*(R-Ro);
 SpringTerm = 2*(R-Ro);
 EtaTerm = eta.*RP;
 InertialTerm = (cM*Fm + FluidForce - EtaTerm - SpringTerm);
 BellTerm = (cM*Fm  - EtaTerm - SpringTerm);
```

```
%check relative ratios
%  figure;
%  plot(t2,FluidForce,t2,SpringTerm, t2, EtaTerm)
%Projected area of the body as a function of radius-Tom 1983 from hemi-ellipsoid

S = pi *R.^2;


%Calculate body velocity from R(t) and Thrust -using center differencing
time = length(t2);
U = zeros(time,1);

        for j = 2:time-1
        Hout = (2/3*pi*T*(R(j-1)-T)^2 - Vb)/(2/3*pi*T^2-4/3*pi*T*R(j-1));
        VolOut = 2/3*pi*Hout*R(j-1)^2;


%This is the old way of calculating Ui+1 without center differencing.  We think that this
might be leading to error build-up

%       U(j+1) = U(j) + (t2(j+1) - t2(j))*((-Thrustout(j) +
0.5*rho*S(j)*Cd*U(j)*abs(U(j)))...
%       /((1+alpha)*rho*VolOut));

% Here I am going to try to insert my calculation for the center differenced formulation
for U(j+1)

        U(j+1) = ((2*U(j)*t2(j)) - (U(j)*(t2(j-1)+t2(j+1))) + (U(j-1)*(t2(j+1)-t2(j))) +
(2*(t2(j+1)-t2(j))*(t2(j)-t2(j-1)))...
                        *((-Thrustout(j-1)-0.5*rho*S(j-1)*(24/(.000001+(U(j-
1)*2*Ro)/nu)^0.7)*U(j-1)*abs(U(j-1)))...
                        /((1+alpha)*rho*VolOut)))/(t2(j)-t2(j-1));

        end


%Cd = 0.1+ 24/Re^.7 - put a cap on it so it doesn't blow up
%Cd = 0.1

%Split off acceleration portion of the velocity record

 accel2;


% Plots!!


%Plot Force
```

```
strTitle1 = ['Fm' ];
 FmSq2 = -(0.5*(1+ square(2*pi*freq*t2,duty)));
        if Jitter > 0
                        for c = 1:length(Locations)
                                FmSq(Locations(c):Locations(c)+JitterVector(c)) = 1-
ones(1, JitterVector(c)+1);
                        end
        end
FmSq2 = FmSq2 *cM;
tspan = tmax/length(t2);
 FmFilt2=bwfilter(FmSq2,1,9,1/tspan);
subplot(5,1,1), plot(t2, FmFilt2, 'k');
title(strTitle1);
set(gca, 'nextplot', 'add');

%Plot radius
strTitle2 = ['Radius(t)'];
subplot(5,1,2), plot(t2, PV(:,1), 'b');
title(strTitle2);
set(gca, 'nextplot', 'add');

%Plot dr/dt
strTitle3 = ['R`(t)' ];
subplot(5,1,3), plot(t2, PV(:,2), 'm');
title(strTitle3);
set(gca, 'nextplot', 'add');


%plot thrust
 strTitle4 = ['Thrust' ];
 subplot(5,1,4), plot(t2, Thrustout, 'g');
 title(strTitle4);
 set(gca, 'nextplot', 'add');


 %plot body velocity
strTitle5 = ['BodyVelocity' ];
 subplot(5,1,5), plot(t2, U, 'r');
 title(strTitle5);
 set(gca, 'nextplot', 'add');


% %Now save output info for each run
BaseFileName= sprintf('J%01dC%01dD%01dE%01dR%02dB%02d',...
                JitterIndex,CutoffIndex,p2,p1,mod((i-1),19)+1,floor((i-1)/19)+1);
 FileName = [BaseFileName, 'tRRPU'];
 OutputMatrix = [t2    R       RP      U];
 OutputString = 'time  R       RP      U';
 FormatString = '%2.4f         %2.17f%2.17f%2.17f\n';
 WriteTextFile(FileName, OutputMatrix, 'w', OutputString,  FormatString);
```

```
%cd(HomePath);

%Calculate and output efficiencies and mean velocities
EfficiencyJitter;
disp(i)
toc
end

OutputAccel = [AccelOut];
 OutputString = 'AccelJitter';
 FileName = [BaseFileName,'Accel'];
 FormatString = '%2.15f\n';
 WriteTextFile(FileName, OutputAccel, 'w', OutputString,  FormatString);
 %cd(HomePath);
toc
clear R RP t2 U FmFilt2 FmSq2 FakeT1 FmSq FmFilt
```

NonLinOdeJitter.m – This is the ode file at the crux of the model

```
 function dRnUdt = odefile(t,PV)

global mass
global eta
global k
global Ro
global T
global rho
global Vb
global Avel
global cP
global h
global cM
global freq
global duty
global alpha
global Fch
global b
global EffMass
global Cutoff
global to
global tmax
global inc
global ncycles
global Fm
global FakeT1
global FmFilt

%Create new muscle force that will generate muscle forces and allow them to be rounded
instead of square
```

```
        %interpolate to find Fm value at the real t value
        Fm = interp1q(FakeT1,FmFilt,t);

%Solved in Mathematica based on the equations for thrust that are based on
%change in bell volume in time. Forced is derived from pressure where
%F = 2Prh = 2rhorh(dV/dt)^2/Ae^2

%Geometry is based on a hemi-ellipsoid whose volume = 2/3R^2h

h = (2/3*pi*T*(PV(1)-T)^2 - Vb)/(2/3*pi*T^2-4/3*pi*T*PV(1));


Vol = ((2/3*pi*T*(T-PV(1))^2-Vb)*PV(1)^2)/(T*(T-2*PV(1)));

dVdt = (((8*pi^2*T*PV(1)^2*(-T+PV(1))*PV(2))/(9*(2/3*pi*T^2- 4/3*pi*T*PV(1))))...
        - ((8*pi^2*T*PV(1)^2*(Vb-2/3*pi*T*(-
T+PV(1))^2)*PV(2)))/(9*(2/3*pi*T^2-4/3*pi*T*PV(1))^2)...
        -((4*pi*PV(1)*(Vb-2/3*pi*T*(-T+PV(1))^2)*PV(2))/(3*(2/3*pi*T^2-
4/3*pi*T*PV(1)))));


%Solve for fluid forces
Fch = 2*rho*Ro*h*(dVdt*abs(dVdt))/Avel^2;


dRnUdt  = [(PV(2))

        ((Fm + cP*Fch - eta*PV(2) - k*abs(PV(1)-Ro)^b*(PV(1) -
Ro))/(mass*EffMass))

        ];


%Justify effective mass 4.35x bell mass based on an the average value calculated by
DeMont and
%Gosline-max of there observed range
```

FmJitter.m – This is the code that generates the forcing function with which to drive the model jellyfish

```
global to
global inc
global tmax
global FakeT1
```

```
global FmFilt
global JitterVector
global Cutoff
global duty
global E
global Jitter

                FakeT1 = (to:inc:tmax)';
                FmSq = -(0.5*(1+ square(2*pi*freq*FakeT1,duty)));
                FmSq = cM*FmSq;
                DiffFm = diff(FmSq);
                Locations = find(DiffFm<0);
        if Jitter == 0

        else
                switch Jitter
                case 1
                JitterVector = [71   42   70   78   7   2   75   36   20   83];
                case 2
                JitterVector = [ 190   46   121   97   178   152   91   4   164   89];
                case 3
                JitterVector = [185   238   277   221   53   122   281   275   123   268];
                end
                        for c = 1:length(Locations)
                                FmSq(Locations(c):Locations(c)+JitterVector(c)) = 1-
ones(1,JitterVector(c)+1);
                        end
        end
FmFilt=bwfilter(FmSq,1,Cutoff,1/inc);
```

1

EfficiencyJitter.m – This code calculates swimming velocity and efficiency for each cycle through the model and stores the output in a separate file

```
% This m-file takes the values from the velocity vector that correspond to
%the mean velocity of the response (with acceleration chopped off) and uses
%these values to compute efficiency (effic = power out/power in)

global Fm
global U
global Drag
global VolOut
global R
global alpha

%to generate cycle periods
% for cyc = 1:ncycles
%       a= (to:CyclePeriod:tmax);
% [index, value] = MatchVal(t2, a(cyc));
```

```
% FmInd(cyc,1) = index;
% end
FmInd = findpeakindex(FmFilt2);
diff(FmInd);
%plot(t2(FmInd), FmFilt(FmInd), 'b*', t2, FmFilt, 'm');
        %To shift index back to original t2 -- before I took the diff
        %FmInd = FmInd+1;

        for k = 2:length(FmInd)
        IndCycle = [FmInd(k-1)        FmInd(k)];

        %Mean velocity is equal to the asymptotic mean velocity of the last cycle
        Ubar = mean(U(IndCycle(1):IndCycle(2)));

        Cd2 = (24/(.000001+(Ubar*2*Ro)/nu)^0.7);

        %Velocities for the last cycle-pull in one extra point here so that diffU/difft is
referenced to the
        %first point of the cycle
        Ucycle = U(IndCycle(1):IndCycle(2));
        Tcycle = t2(IndCycle(1):IndCycle(2));
        Rcycle = R(IndCycle(1):IndCycle(2));
        RPcycle = RP(IndCycle(1):IndCycle(2));

        %Calculate dUdt bast on deltaU/deltaT

        dUdt = diff(Ucycle)./diff(Tcycle);

        %Calculate volume out per cycle
        VolCycle = (((2/3*pi*T*(T-Rcycle).^2)-Vb).*Rcycle.^2)./(T*(T-2*Rcycle));

        VolCycle = VolCycle(2:end); %cut off first point of VolCycle so that it
references to the first
        %point of dUdt

        %Calculate drag for a cycle
        Hcycle = (2/3*pi*T.*(Rcycle-T).^2 - Vb)./(2/3*pi*T^2-4/3*pi*T.*Rcycle);

        dVdtcycle = (((8*pi^2*T.*Rcycle.^2.*(-T+Rcycle).*RPcycle)./(9*(2/3*pi*T^2-
4/3*pi*T.*Rcycle)))...
                - ((8*pi^2*T.*Rcycle.^2.*(Vb-2/3*pi*T*(-
T+Rcycle).^2).*RPcycle))./((9*(2/3*pi*T^2-4/3*pi*T.*Rcycle).^2))...
                -((4*pi.*Rcycle.*(Vb-2/3*pi*T.*(-
T+Rcycle).^2).*RPcycle)./(3*(2/3*pi*T^2-4/3*pi*T.*Rcycle))));


        Scycle = pi*Rcycle.^2;
        DragCycle = 0.5*Cd2*rho*Scycle.*Ucycle.*abs(Ucycle);
        DragCycle = DragCycle(2:end);  %cut off first point of VolCycle so that it
references to the first
```

```
        %point of dUdt
        ThrustCycle = (rho*(dVdtcycle).*abs(dVdtcycle))/Avel;
        ThrustCycle = ThrustCycle(2:end);

        InertiaAddedMass = (1+alpha)*rho.*VolCycle.*dUdt;

        ForceTot = DragCycle +InertiaAddedMass;
        %PowerOut = mean(abs(ForceTot).*(Ucycle(2:end))); %This is the numerator of
the efficiency term
        %PowerOut = mean((abs(ThrustCycle).*(Ucycle(2:end)));
        PowerOut =mean(abs(ThrustCycle).*(Ucycle(2:end)));

        %Now for the denominator of the efficiency term

        ForceCycle = FmFilt2(IndCycle(1):IndCycle(2));
        ForceCycle = ForceCycle(2:end);
        dRCycle = diff(Rcycle);
        WorkCycle = sum(ForceCycle.*(2*pi*dRCycle));
        PowerIn = WorkCycle/(Tcycle(end)-Tcycle(2)); %Start time at 2 so that it is
referenced correctly
        %with dr/dt
        Cost = PowerIn/(mass*9.8*.1*Ubar); %Assume a muscle efficiency-
        %chemical to mechanical energy of 10%

        effic = PowerOut/PowerIn;
        EfficCycle(k-1,1) = effic;
        UPerCycle(k-1,1) = Ubar;
        EfficCycleUCycle = [UPerCycle      EfficCycle];
        UFileName = [BaseFileName, 'UEff'];;
        String = 'Ubar Effic';
        FormatString = '%2.6f%2.6f\n';

        %cd('Hexapod:Goldman:JellyModelOutput:');
        %cd('HomeStretch:Erica:ModelOutput:Forcing:JitterForcing:JitterSizeVariesE50
0Mag2DHigh')
        %cd('Cubozoa:erica:Erica.m-files:JellyModel:Model
Output:E750hr2Size01RoundVaries:')

        WriteTextFile(UFileName, EfficCycleUCycle, 'w', String, FormatString);
        %cd(HomePath);

end
clear EfficCycleUCycle
clear UPerCycle
clear EfficCycle
```

KscaleJelly.m – This code scales the mean slope of the nonlinear oscillations so that they match the mean slope of the linear case

```
global LinMeanSlope;
```

```
global Xm

%This m-file generates a list of parameters to test in the nonlinear spring
%equation based on maintaining the same mean slope throughout the parameter
%space
%MeanSlope = 1/xmax * integral (0, xmax) (a*b*x^(b-1))dx
% Evaluate integral in Mathematica
%MeanSlope = k = a*xm^(b-1)

%mean slope of stress/strain curve for Polyorchis based on DeMont and
%Gosline's estimates for whole bell stiffness of 500 Pa



Exponent = (1:0.1:4)'; %exponent of non-linearity
K = LinMeanSlope.*ones(length(Exponent),1);


a = K./(Xm.^(Exponent-1));


%Matrices to use in model simulations
KMat = [a       Exponent        K];
```

Calibration2D.m – Code used for calibration of video sequences in kinematic measurements

```
%This file generates scale factors to be applied in the digitized 2D
%sequences

InputPath = 'HomeStretch:Matlab Input:2D Video Analysis:Calibration Poly3:';
cd(InputPath);

data = ReadTextFile;

c = (data(:,4) - data(:,2));
d = (data(:,3) - data(:,1));
CubeWidth = sqrt(c.^2 + d.^2);

%CalibRatio = mean(CubeWidth/4.57) %pixels/mm -use for cube length

CalibRatio = mean(CubeWidth/2.53) %pixels/mm -use for cube width- camera b
```

JellyMove2.m – This code converts digitized x,y coordinates to appropriately scaled distances.

```
%This converts digitized points to distances
clear all;
close all;
global CalibFactorA
global CalibFactorB

InputPath = 'HomeStretch:Matlab Output:VideoOutput:';
cd(InputPath);

CoordData = ReadTextFile;

%Replace frame numbers with time values in 1/30 second increments

Frames = length(CoordData);
Seconds = Frames/30;
%Time = (0:1/30:Frames/30)';
Time = (0:1/15:Frames/15)';%use for every other frame
Time = Time(2:end);
CoordData(:,1) = Time;

%Separate apex point from data set and track in space

 CalibFactorA = 27.6;%pix/cm 1A,2A (Poly1,4) - smallest, largest
%CalibFactorA = 38.2;%3A,4A       (Poly2,3)
CalibFactorB = 32.1;%pix/cm 1B,2B
%CalibFactorB = 39.6;%3B,4A

ApexXa = CoordData(:,4)/CalibFactorA;%pix/cm - calib factor for 1A
ApexXaNorm = ApexXa/min(ApexXa)-1;
ApexYa = CoordData(:,5)/CalibFactorA;
ApexYaNorm = ApexYa/min(ApexYa)-1;
ApexZb = CoordData(:,10)/CalibFactorB;
ApexZbNorm = ApexZb/min(ApexZb)-1;
ApexYb = CoordData(:,11)/CalibFactorB;
ApexYbNorm = ApexYb/min(ApexYb)-1;


MeanY = (ApexYa + ApexYb)/2;
```

```
MeanYNorm = (MeanY/min(MeanY))-1;

% figure;
% plot(Time, ApexYa, Time, ApexYb, Time, MeanY);

%Now, plot path in 3D

figure;
plot3(ApexXaNorm, MeanYNorm, ApexZbNorm, 'b*');
%plot(Time,ApexXaNorm, Time,MeanYNorm, Time,ApexZbNorm);
hold on;

%Filter position data to get rid of pointnclick jitters
% FilteredApexXa = bwfilter(ApexXa, 2, 5, 30);
% FilteredMeanY = bwfilter(MeanY, 2, 5, 30);
% FilteredApexZb = bwfilter(ApexZb, 2, 5, 30);

%Use for every other frame
FilteredApexXa = bwfilter(ApexXaNorm, 2, 5, 15);
FilteredMeanY = bwfilter(MeanYNorm, 2, 5, 15);
FilteredApexZb = bwfilter(ApexZbNorm, 2, 5, 15);


xlabel('x');
ylabel('y');
zlabel('z');

h =  plot3(FilteredApexXa, FilteredMeanY, FilteredApexZb, 'm');
set(h, 'LineWidth', 2);
set(gca, 'FontSize', 14);
xlabel('X-cm', 'FontSize', 14);
ylabel('Y-cm', 'FontSize', 14);
zlabel('Z-cm', 'FontSize', 14);

% %Calculate radius change in time
Rx = (CoordData(:,6) - CoordData(:,2))/CalibFactorA;
RyA = (CoordData(:,7) - CoordData(:,3))/CalibFactorA;
RyB = (CoordData(:,13) - CoordData(:,9))/CalibFactorB;
Rz = (CoordData(:,12) - CoordData(:,8))/CalibFactorB;

MeanRy = (RyA +RyB)/2;

%Check that using MeanY is vaguely kosher
```

```
% figure;
% plot(Time,RyA, Time, RyB, Time, MeanRy);
%
% %Filter radius data
% RxFilt = bwfilter(Rx, 3, 1, 30);
% MeanRyFilt = bwfilter(MeanRy, 3, 1, 30);
% RzFilt = bwfilter(Rz, 3, 1, 30);

%Use for every other frame
RxFilt = bwfilter(Rx, 2, 1.0, 15);
MeanRyFilt = bwfilter(MeanRy, 2, 1.0, 15);
RzFilt = bwfilter(Rz, 2, 1.0, 15);


%Calculate radius in time
RadDist = .5 *sqrt(Rx.^2 + MeanRy.^2 + Rz.^2);
RadDistFilt = .5*sqrt(RxFilt.^2 + MeanRyFilt.^2 + RzFilt.^2);

%Find cycle peaks and troughs
[RadMax, RadMin] = findpeakindex(RadDistFilt);



%Calculate swimming frequency
FrequencyMax = 1/(mean(diff(Time(RadMax(1:end))))); %hz
FrequencyMin = 1/(mean(diff(Time(RadMin(2:end))))); %hz
MeanFreq = (FrequencyMax+FrequencyMin)/2;

%Radius excursion during swimming
DeltaRadius = (RadDist(RadMax(2)) - RadDist(RadMin(2)));

%Mean bell position
MeanRadius = mean(RadDist);


%Calculate distance traveled vector for apex
ApexDistance = sqrt(ApexXa.^2 + MeanY.^2 + ApexZb.^2);
MinDist = repmat(ApexDistance(1), length(ApexDistance), 1);
ScaledDist = ApexDistance - MinDist;
SumScaledDist = sum(abs(diff(ScaledDist)));%convert to arc length
DistLine = (SumScaledDist/Time(end)) *Time;
FiltDistance = sqrt(FilteredApexXa.^2 + FilteredMeanY.^2 +FilteredApexZb.^2);
```

```
MinFiltDist = repmat(FiltDistance(1), length(FiltDistance), 1);
ScaledFiltDist = FiltDistance - MinFiltDist;

%Calculate height of the bell

RtSideRadx = CoordData(:,6)/CalibFactorA;
RtSideRady = (CoordData(:,7)/CalibFactorA + CoordData(:,13)/CalibFactorB)/2;
RtSideRadz = CoordData(:,12)/CalibFactorA;
ApexRHypot = sqrt((ApexXa - RtSideRadx).^2 + (MeanY - RtSideRady).^2 + (ApexZb-
RtSideRadz).^2);


H = mean(sqrt(RadDist.^2 + ApexRHypot.^2));
HRratio = H/mean(RadDist);

%Calculate velocity from filtered distance data

DeltaT = diff(Time);
Velocity = abs(diff(ScaledDist))./DeltaT;

AvgVel20 = mean(Velocity(end-20:end)); % Gives average velocity over end of record
AvgVel40 = mean(Velocity(end-40:end));
MaxVel = find(Velocity == max(Velocity));
TmaxVmax = [Time(MaxVel)        Velocity(MaxVel)];
ClipLength = Time(end);

%PLOTS

%Plot Radius in time
figure;
plot(Time(15:end), RadDist(15:end), 'b*', Time(15:end), RadDistFilt(15:end), 'g',
Time(RadMax), RadDistFilt(RadMax), 'm*',...
Time(RadMin), RadDistFilt(RadMin), 'yx');

%plot  distance traveled
figure;
plot(Time, ScaledDist, 'b*', Time, ScaledFiltDist, 'g');
xlabel('Time (s)');
ylabel('Distance (cm)');
title('Distance traveled');
%
%Velocity plot for apex position
```

```
figure;
plot(Time(1:end-1), Velocity, 'm');
xlabel('Time (s)');
ylabel('Velocity (cm/s)');

cd('HomeStretch:Erica:Erica.m-files:JellyModelM-Files:');
%VideoToModel;
%Poly1Smallest;
%Poly2R2ndSmallest;
% Poly3R2ndLargest;
% Poly4Largest;
```

VideoToModel.m – This code aligns model data with measured kinematics to evaluate how well the model is doing

```
% This m-file will extract relevant pieces of model data and see how
% well they match video kinematics for polyorchis

for q = 1:209

DataPath = 'HomeStretch:Erica:ModelOutput:Scaling:E1000hr2SizeVariesFnew:';
FileNameModelOut = ['E1000hr2SizeVariesFnew.' num2str(q)];
FileNameVelocity = ['UEfficE1000.' num2str(q)];
UEffData = AutoReadTextFile(DataPath, FileNameVelocity);
MeanU(q,1) = UEffData(end-1,1);
Eff(q,1) = UEffData(end-1,2);
UendEfficend = [MeanU      Eff];

end

%Make one giant matrix of results

cd('HomeStretch:Erica:Erica.m-files:JellyModelM-files:Parameters');

InData = load('ParamsSizeVariesE1000fixed.m');
InData = InData(1:q,:);
data = [InData UendEfficend];
Ro = data(:,1);
hr = data(:,2);
b = data(:,5);
E = data(:,6);
Vel = data(:,9);
```

```
Effik = data(:,10);

%Look at relevant sizes to video data
%Radius = .014, .004, .006 - h/r ~2
%Ro            Ustead Umax
%.004 2.34     7.12
%.006 0.72     2.87
%.014 1.58     5.70



Poly1 = find(Ro == .004);
Poly2 = find(Ro == .006);
Poly3 = find(Ro == .010);
Poly4 = find(Ro == .014);

R1 = repmat(.004, 11,1);
R2 = repmat(.006, 11,1);
R3 = repmat(.010, 11,1);
R4 = repmat(.014, 11,1);
RX4 = [R1     R2     R3     R4];

bval = b(Poly1);


U1 = Vel(Poly1);
U2 =  Vel(Poly2);
U3 = Vel(Poly3);
U4 = Vel(Poly4);
UX4 = [U1     U2     U3     U4];

PolyX4 = [bval        RX4    UX4];


%Ro            Ustead Umax cm/s
%.004 2.34     7.12
%.006 0.72     2.87
%.014 1.58     5.70
%.010 0.67     3.00

%Poly1 real

BInd1= find(U2>.023); %U (m/s) measured
```

```
U1Real = .023; %avg steady state velocity (m/s)
ClosestModelU1 = U1(BInd1(1));
ClosestModelB1 = bval(BInd1(1));
ApproxB1 = (ClosestModelB1 + (ClosestModelB1-.2))/2;

%Poly2 real
BInd2= find(U2>.0072); %U (m/s) measured
U2Real = .0072; %avg steady state velocity (m/s)
ClosestModelU2 = U2(BInd2(1));
ClosestModelB2 = bval(BInd2(1));
ApproxB2 = (ClosestModelB2 + (ClosestModelB2-.2))/2;

%Poly3 real
BInd3= find(U2>.0067); %U (m/s) measured
U3Real = .0067; %avg steady state velocity (m/s)
ClosestModelU3 = U3(BInd3(1));
ClosestModelB3 = bval(BInd3(1));
ApproxB3 = (ClosestModelB3 + (ClosestModelB3-.2))/2;

%Poly4 real
BInd4 = find(U4>.016); %U (m/s) measured-mean from two clips
U4Real = .016; %avg steady state velocity (m/s)
ClosestModelU4 = U4(BInd4(1));
ClosestModelB4 = bval(BInd4(1));
ApproxB4 = (ClosestModelB4 + (ClosestModelB4-.2))/2;

figure;
h = plot3(RX4, bval, UX4, R1(1), ApproxB1, U1Real, 'r*', R2(1),...
ApproxB2, U2Real,'k*', R3(1), ApproxB3, U3Real, 'b*', R4(1), ApproxB4,...
U4Real,'m*');
set(gca, 'FontSize', 14);
set(h, 'LineWidth', 3);
xlabel('Radius (m)', 'FontSize', 16);
ylabel('non-linear exponent', 'FontSize', 16);
zlabel('U (m/s)', 'FontSize', 16);
```

TRRPU.m – This code looks at time/velocity data from the model output, aligns it with measure kinematics, and plots measured and theoretical data on the same plot

```
%This m-file will look at the continuous time/velocity record from the
%model output in order to generate longer term distance plots
%close all;
```

```
clear all;
cd('HomeStretch:Erica:Erica.m-files:JellyModelM-files:Parameters');
data = load('ParamsSizeVariesE1000fixed.m');
Ro = data(:,1);
hr = data(:,2);
b = data(:,5);
E = data(:,6);

for q =57:61;

%       Params = load('DistanceModelInput.m');
%       for i = 1:length(Params)
%       DataPath = Params(i,1);
%       FileNameModel = Params(i,2);
%       CalibFactorA = Params(i,3);
%       CalibFactorB = Params(i,4);

DataPath = 'HomeStretch:Erica:ModelOutput:Scaling:E1000hr2SizeVariesFnew:';
%DataPath = 'HomeStretch:Erica:ModelOutput:Scaling:E750hr2SizeVariesFnew:';
%DataPath = 'HomeStretch:Erica:ModelOutput:Scaling:E500hr2SizeVariesFnew:';

%FileNameModel = [FileNameModel, num2str(q)];
FileNameModel = ['E1000hr2SizeVariesFnew.tRRPU' num2str(q)];
%FileNameModel = ['E750hr2SizeVariesFnew.tRRPU' num2str(q)];
%FileNameModel = ['E500hr2SizeVariesFnew.tRRPU' num2str(q)];

TimeVelData = AutoReadTextFile(DataPath, FileNameModel);
TimeMod = TimeVelData(:,1);
Radius =TimeVelData(:,2);
Velocity = TimeVelData(:,4);
Distance = TimeMod.*Velocity;
MeanDistance= TimeMod* mean(Velocity);
NonLin = b(q);
NonLinVect = repmat(NonLin, length(TimeMod), 1);
NonLinTimeDist = [NonLinVect      TimeMod      Distance];
cd(DataPath);
FileName = 'DistTime';
OutputString = 'NonLin        Time   Distance';
FormatString = '%2.4f%2.17f%2.17f%2.17f\n';
WriteTextFile(FileName, NonLinTimeDist,'w', OutputString, FormatString)
figure(1);
subplot(2,2,2); %plot(Time, MeanDistance, 'b');
text(TimeMod(end), MeanDistance(end), ['b =',num2str(NonLinVect(1))], 'FontSize',
```

```
12);
line(TimeMod,MeanDistance,'Color',[0 1-1/11*mod(q-1,11) 1/11*mod(q-1,11)],
'LineWidth', 2);

axis([0 5        0        .2]);
xlabel('Time (s)', 'FontSize', 12);
ylabel('Distance (m)', 'FontSize',12);

hold on;


end
cd('HomeStretch:Erica:Erica.m-files:Video m-files:');
JellyMove2;
ScaledDist=abs(ScaledDist)/100;
DistPlot = figure(1);
subplot(2,2,2); plot(Time,DistLine/100, 'r', 'LineWidth', 2);%must convert to meters


%  cd('HomeStretch:Erica:ModelFigures:');
% print DistPlot.jpeg -f1 -djpeg

% xlabel('Time (s)');
% ylabel('Distance(m)');
%first plot - E = 1000,
```

FreqDep.m - This code generates a scaling relationship for frequency v. size, based on the timing of muscle force production based on Gladfelter's data

```
close all;
clear all;
global Ro
global Tm


HomePath = 'HomeStretch:Erica:Erica.m-files:ModelDevt:';
cd(HomePath);

circ = [.015, .028, .05, .07, .12];%m
Ro = circ./(2*pi);
Tm = [0.15, 0.25, 0.35,          0.4, 0.5];
```

```
% Now lets use a minimization method to find the parameters.
initguess = [1  1        1];
foptions(1) = 0;
foptions(2) = 1.e-6;
foptions(3) = 1.e-6;
foptions(14) = 1000*length(Ro);

[Pfiddle,out] = fmins('freqfmins',initguess, foptions);
guess1 = Pfiddle(1);
intercept = Pfiddle(2);

%Square root dependence
Estimate = intercept + guess1*Ro.^0.5;
%Estimate = guess1*Ro.^0.5;
R = (.002:.001:.03);
TmOut = intercept + guess1*R.^0.5;
CyclePeriod = TmOut + 1.3*TmOut;
freq = 1./CyclePeriod;

a = plot(Ro, Tm, 'k*', R, TmOut, 'k', 'LineWidth', 2);
box('off');
figure;
b = plot(R,freq, 'k', 'LineWidth', 2);
h = findobj('type','line');


OutValsEnd = [intercept       guess1];
```

freqmins.m-

```
%This function contains the least-square minimization routine used to fit Gladfelter's
data to a usable size-freq relationship

function [c] = freqfmins(Pfiddle)

global Tm
global Ro
intercept = Pfiddle(2);
guess1 = Pfiddle(1);

err = Tm-(intercept + guess1*Ro.^0.5);
                                    c = sum(err.^2);
```

BIOGRAPHICAL SKETCH

Erica Goldman was born and raised in theGreat City of New York. While there, she became an accomplished ice skater, Broadway singer (okay, maybe not), and did her first invertebrate research project on starfish, for which she won a Westinghouse prize.

She went off to college at Yale, where she continued thrashing about in the tide pools in her hip waders and studied crayfish and small dudes called hydroids. She also went to Russia and began her career as Science Ambassador by studying wormlike dudes on the bottom of Lake Baikal. She also developed a relationship with the folks at Woods Hole, where she spent a summer studying mollusks.

She then joined the wacky lab headed by Tom Daniel at the University of Washington, where she completed the foregoing project on jellyfish and had frequent seizure-like laughing episodes where she was completely nonresponsive. These paroxysms were prompted by such characters as The Thesis Dummy and the Specter of Impending Doom and by the 4:00 pm latte.

But her graduate career was marked by other notable accomplishments:

- She went off to Antarctica and stomped about in the red suits and sturdy boots and studied pteropods.
- Then she somehow stowed away on the Alvin, where she took fantastic video pictures and studied something about tube worms.
- She created a remarkable portfolio of science writing, culminating in a piece published with *The Sciences*, the late New York Academy of Sciences magazine.

She plans to take a position with *Science* for the next six months before accepting the Knauss Fellowship in Washington DC as a Legislative Fellow.

—JK